THE RELATIONSHIP BETWEEN BLOOD PERFUSION AND THERMAL MEASUREMENTS AT THE SKIN SURFACE

By,

Christopher P.B. Nicholson

A thesis submitted to the University of Dublin for the degree of Doctor of Philosophy

Department of Mechanical and Manufacturing Engineering, Trinity College, Dublin 2

April 2006.
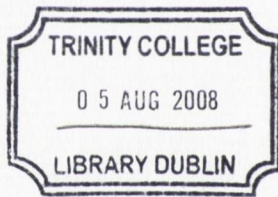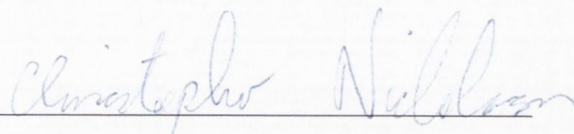
DECLARATION

I, Christopher Nicholson, declare that this thesis is solely my own work except where clearly referenced. I also declare that no part of this thesis has been submitted as an exercise for any other degree at any other university.

I agree that the library may lend a copy of this thesis.

Christopher Patrick Blackwood Nicholson
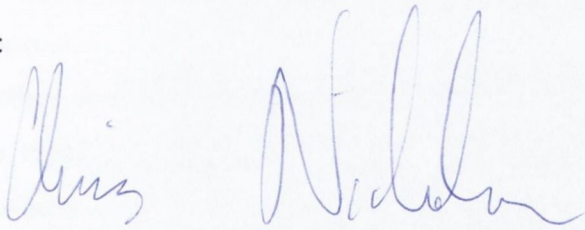
January, 2005.

DECLARATION

This thesis has not been submitted as an exercise for a degree at any other university. Except where stated, the work described therein was carried out by me alone.

I give permission for the Library to lend or copy this thesis upon request.

Signed:

ABSTRACT

Blood perfusion is defined as the volumetric flow rate of blood through a given volume of tissue. Blood perfusion measurements are an important clinical indicator for many medical conditions but to date there is no cost effective and accurate measurement solution available. Among a number of existing perfusion measurement techniques there is a range of thermal methods; these thermal methods offer the prospect of cheap and accurate perfusion measurement devices. The aim of this study is to investigate the relationship between non-invasive surface thermal measurements and the perfusion levels in the various tissues of the lower arm, leg and finger with a view to ultimately developing a practical, non-invasive and cost effective perfusion measurement device.

The most promising thermal technique to date is known as the Forced Convection Approach in which a localised cooling load is applied to a small section of the skin surface using a perfusion probe. The thermal response at the surface is then related to the value of perfusion using a numerical model of the system based on an appropriate bio-heat model. Initial work repeating that of previous researchers identified a number of areas in which experimental and numerical improvements were required. A number of important developments were first made to the experimental procedure. A greater appreciation of the simplifying assumptions and applicability of the model was then developed. A crucial development was the concept of the Possible Perfusion Values curve; this refined approach was then implemented. A further simpler but novel technique, namely the Steady State Perfusion Measurement Technique was also developed based on the PPV methodology.

Results of the study showed the refined technique not to be sensitive enough to allow perfusion measurement on healthy individuals. However it was also shown that it should be much more sensitive at impaired perfusion levels as experienced in many medical conditions. The steady state technique shows promise but needs further investigation on some of its underlying assumptions. Thus, the main contribution of this study is its development of a perfusion measurement methodology for thermal techniques through use of the PPV curve combined with progress made in the critical evaluation of the numerical modelling assumptions.

ACKNOWLEDGEMENTS

CONTENTS

Nomenclature

Symbol	Description	Units
B	bias limit	[-]
C	specific heat capacity	[J/kgK]
c	compliance	[m/N]
C_s	local perfusion correction factor	[-]
d	diameter	[m]
EF	efficiency factor	[-]
h	convective heat transfer coefficient	[W/m^{2}K]
k	thermal conductivity	[W/mK]
k_{pen}	Pennes correction factor	[-]
L	half plane thickness	[m]
p	pressure	[N/m^2]
P	precision limit	[-]
$\dot{q}$	volumetric heat generation	[W/m^3]
q''	heat flux	[W/m^2]
R_c	contact resistance	[°C/W]
t	time	[s]
S_{xy}	standard deviation	[-]
T	temperature	[K]
ΔT	perfusion correction factor	[-]
U	overall heat transfer coefficient	[W/m^2]
v	velocity	[m/s]
V	volume	[m^3]
X_e	equilibrium length	[m]
x,y,z	rectangular coordinates	[m]

Dimensionless Numbers

Symbol	Description	Units
Bi	Biot No.	[-]

Fo	Fourier No.	
Nu	Nusselt No.	[-]
Pr	Prandtl No.	[-]
Re	Reynolds No.	[-]

Subscripts

Symbol	Description
a	artery
atm	atmospheric
b	blood
bas	basal
c	contact
i	initial condition
$meta$	metabolic rate
$metabas$	basal metabolic rate
p	probe
per	perfusion
s	surface
sk	skin
t	tissue
v	venous
∞	free stream conditions

Greek Symbols

Symbol	Description	
α	thermal diffusivity	[m^2/s]
ρ	density	[kg/m^3]
θ^*	dimensionless temperature	[-]
ω	blood perfusion	[m^3/m^3/s]

LIST OF FIGURES

LIST OF TABLES

1 INTRODUCTION

This study is concerned with investigating the relationship between blood perfusion in the tissues of the limbs and thermal measurements at the skin surface with a view to establishing the feasibility of measuring perfusion using this relationship. This chapter will discuss the reasons for the importance of blood perfusion measurements, the applicability of current techniques and the specific objectives of the current study.

1.1 BACKGROUND

Blood Perfusion (ω) is defined as the volumetric flow rate of blood through a given volume of tissue. Li et al. [1] note that despite its clinical significance, there is still no ideal method of measurement. Blood perfusion is an important medical parameter in a wide variety of clinical conditions such as:

- Peripheral vascular disease
- Diabetic arthropathy
- Raynaud's Syndrome
- Buerger's Disease
- Diagnosis and treatment of cancer
- Decision making during and after surgery
- Reconstructive Surgery
- Transdermally administered drugs
- Evaluation of statin treatments

There are various methods for measuring perfusion including laser doppler devices, plethysmographic equipment and even radioactive tracers; however all these methods have associated difficulties of cost, impracticality or an inability to deliver absolute measurements. Further to this there are also a range of potential thermal methods which in contrast offer the possibility of low cost and greater accuracy. There are a number of different methods based on cooling or heating of the tissue. The thermal diffusion probe method requires a heated thermistor to be inserted into the skin. The rate of heat dissipation is then related to perfusion. Another heating method applies a sinusoidally varying heat source to the skin. The phase shift between the skin

temperature and applied heating frequency is then related to perfusion. Finally there are also cooling methods which use either constant temperature cooling devices or apply a constant cooling air flow rate. These are known variously as the induced cooling method and the forced convection approach. These methods infer perfusion by comparing surface thermal measurements from experimental tests with those from a numerical model based on bio-heat transfer theory, which is run for a range of perfusion values. When the experimental and numerical thermal measurements match, the value of perfusion is said to be estimated. The premise of these methods is that for a given set of environmental conditions, limb geometry and tissue properties, the main determinant of surface temperature is the rate at which warm blood enters the tissues of the limb. By establishing the heat required to maintain a particular surface temperature it is therefore theoretically possible to account for the rate at which blood perfuses the various tissues. However, as with any physiological system the process is more complicated as there are various other factors such as the countercurrent re-warming of blood returning to the core. Arkin et al. [2] note that these bio-heat models are not only used for estimation of perfusion but also in analysis of burns [3,4,5], cryosurgery [6,7] hypothermia [8], in measurement of tissue thermal properties [9] and in whole body thermal models.

1.2 RESEARCH OBJECTIVES

The objectives of this study are to:

1. Identify the most promising thermal technique for perfusion measurement
2. To assess the current start of the art in the chosen technique from which to make any necessary experimental and numerical developments
3. To improve upon existing techniques by accounting for the volume geometry using MRI scans.
4. To develop a method of inferring both skin and muscle perfusion from one surface test
5. To evaluate the new model based on the above

This thesis will first discuss the various physiological factors relevant to blood perfusion measurements. It will then describe developments in the modelling of heat transfer in biological systems before outlining the various thermal and non-thermal

perfusion measurement methods that exist. Development work carried out on the chosen method will be described. A full description will be given of the innovations made. Finally the results of the study will be discussed from which conclusions will be drawn.

2 PHYSIOLOGICAL EFFECTS RELATING TO BLOOD FLOW

Blood Perfusion (ω) is defined as the volumetric flow rate of blood through a given volume of tissue or as the microcirculation of blood in tissue. A crude way to show that blood perfuses skin tissue is to depress an area of skin and note the change in colour from white to red, once the pressure is released as the capillaries in the skin refill. The length of time it takes for the blood to refill the depressed area of skin is a crude way of measuring the blood supply to that area of skin tissue. This chapter will discuss; physiological factors relevant to this study such as an overview of the circulatory system, factors affecting local and global blood perfusion, skin and muscle composition and finally experimental methods of altering skin blood flow.

2.1 FUNCTIONS PERFORMED BY BLOOD AND THE CIRCULATORY SYSTEM

Blood has a number of very important functions, which are described by Martini [10] under three headings:

Transport

Blood carries:

- oxygen from the lungs to other tissues. It also carries carbon dioxide back to the lungs to be expelled (exhaled);
- dissolved foods from the gut to different parts of the body;
- waste products to the kidneys to be excreted in urine;
- hormones and antibodies around the body.

Protection

Blood contains:

- platelets and fibrinogen to make it clot, preventing severe loss of blood after injury;
- white blood cells which protect us against infection.

Regulation

Blood helps:

- to keep our body temperature constant by allowing us to retain or lose heat;

- to control the amount of water and other chemicals in different parts of the body.

2.2   OVERVIEW OF CIRCULATORY SYSTEM

Berne et al. [11] gives the following overview of circulation. The cardiovascular system is made up of a pump (namely the heart), a series of distributing tubes (arterial system) and collecting tubes (venous system) and an extensive system of thin walled vessels (capillaries) which link the arterial and venous systems. Large arteries carry blood away from the heart; these vessels then divide into smaller vessels called arterioles before splitting again into capillaries where the exchange of nutrients and waste products between the blood and cells actually takes place. The blood then enters the venous system where it is pumped back to the heart.

The heart consists of two pumps in series, the right ventricle which pumps blood through the lungs for exchanges of O_2 and CO_2 and the left ventricle which pumps blood to all other tissues of the body. Unidirectional flow thorough the heart is achieved by the appropriate arrangement of effective flap valves.

When blood in the left ventricle leaves the heart it enters into the systemic system as shown in Figure 2-1. The first vessel in this system is the aorta. Although cardiac output is intermittent continuous flow to the periphery (namely capillary beds) is accomplished by distention (enlargement due to internal pressure) of the aorta and its branches during ventricular (a chamber of the heart which receives blood from a corresponding atrium) systole (contraction) and elastic recoil of the walls of the large arteries with forward propulsion of the blood during ventricular relaxation (diastole).
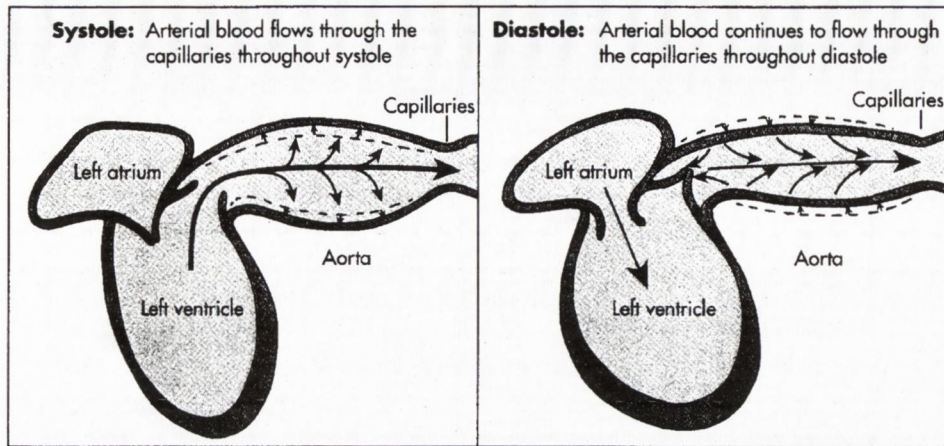
Figure 2-1 (A) When the arteries are normally compliant, a substantial fraction of the stroke volume is stored in the arteries during ventricular systole; the arterial walls are stretched. (B) During ventricular diastole the previously stretched arteries recoil. The volume of blood displaced by the recoil ensures continuous capillary flow throughout diastole. Berne et al. [11]

So while part of the energy released by the cardiac contraction as kinetic energy is dissipated as forward capillary flow during ventricular systole, the remainder is stored as potential energy in that much of the stroke volume is retained by the distensible arteries during systole. During diastole (dilation of cavities of heart during which they fill with blood) the elastic recoil of the arterial walls converts this potential energy back into kinetic energy for distribution through the rest of the system. The compliance of a vessel is a measure of its ability to increase in volume by distension for a given change in internal pressure:

$$c_a = \Delta V_a / \Delta p_a$$

Eq. 2-1

where V_a is arterial volume, p_a is arterial pressure and c_a is arterial compliance. Generally as people age the compliance of their arteries decreases which affects the efficiency of the circulatory system.

As the blood leaves the aorta and continues through the arterial system the branches become narrower and their walls become thinner as they change histologically (in tissue structure and organisation) toward the periphery. This is shown in Figure 2-2, from Berne et al. [11]. The aorta is predominantly an elastic structure, while the

6

peripheral arteries are more muscular and in the arterioles the muscular layer predominates.
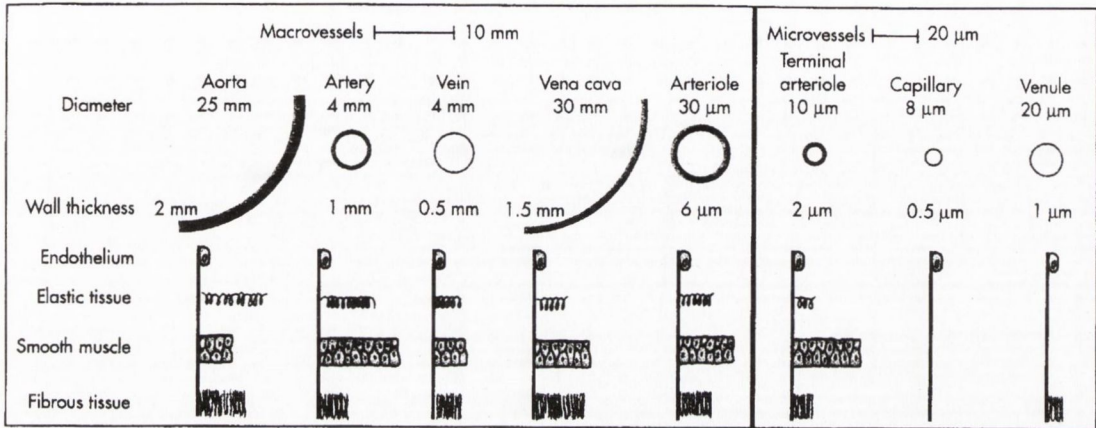
Figure 2-2 Internal diameter, wall thickness and relative amounts of the principal components of the vessel walls of the various blood vessels that make up the circulatory system. (Cross sections are not to scale) Berne et al. [11]

The velocity of blood flow is strongly related to the diameter of the vessel as shown in Figure 2-4. In the aorta and the large arteries blood moves rapidly as the resistance to blood flow is relatively small, and the pressure drop from the root of the aorta to the small arteries is also relatively small (Figure 2-3). However, in the small arteries and arterioles, resistance to blood flow is large, and the pressure drop across these vessels is also large. The greatest resistance is in the arterioles, which are often known as resistance vessels. The degree of contraction in the circular muscle of these small vessels regulates tissue blood flow and aids in controlling the arterial blood pressure. Martini [10] notes that flow is inversely proportional to the resistance and the resistance in turn is inversely proportional to the fourth power of the radius. This is as described by the Hagen-Poiseuille equation. However this equation is only valid for laminar, fully developed, steady flow. Table 2-1 shows blood flow to be laminar for the various vessels of the vasculature with the exception of large vessels such as the aorta.

Vessel	Diameter (mm)	Reynolds Number
Aorta	16-32	1,200-5,800
Large artery	2-6	110-850
Capillary	0.005-0.01	0.0007-0.003
Large Veins	5-10	210-570
Vena Cava	20	630-900

Table 2-1 Reynolds No. for a range of vessel diameters from Arts [12]
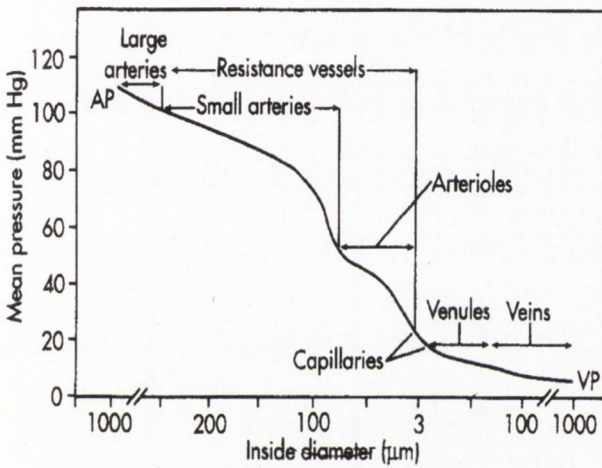
Figure 2-3 Pressure drop across the vascular system in the hamster cheek pouch. AP, mean arterial pressure; VP venous pressure from Berne et al. [11].
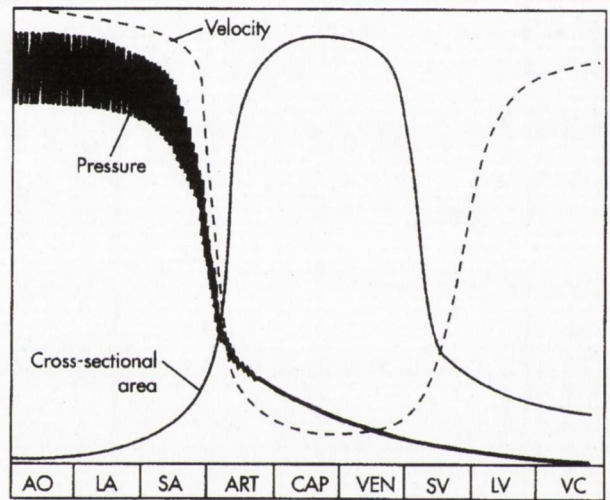
Figure 2-4 Phasic pressure, velocity of flow and cross sectional area of the systemic circulation. AO, Aorta; ART, arterioles; CAP, capillaries; LA, large arteries; LV large veins; SA, small arteries; SV, small veins; VC, venae cava; Ven, venules from Berne et al. [11].

In addition to a sharp reduction in pressure across the arterioles shown in Figure 2-3 and Figure 2-4, flow changes from pulsate to steady. The pulsatile arterial blood flow, which is caused by intermittent cardiac ejection, is damped at the capillary level by the combination of the distensibility of the large arteries and the frictional resistance in the small arteries and arterioles.   Thus the arterial system is said to act as a hydraulic filter. Many capillaries arise from each arteriole. Hence the total cross-sectional area of the capillary bed is very large despite the fact that the cross-sectional area of each capillary is about the diameter of a red blood cell, which is far less than that of each arteriole.

As a result of the large total cross-sectional area, blood flow velocity slows considerably in the capillaries. The velocity of blood flow and the cross-sectional area at each level of the vasculature are essentially mirror images of each other (Figure 2-4). Because the capillaries consist of short tubes with walls only one cell thick and because flow velocity is slow, conditions in the capillaries are ideal for the exchange of diffusible substances between blood and tissue.

On its return to the heart from the capillaries, blood passes through venules and then through veins, of increasing calibre and decreasing number. Most of the blood in the systemic circulation is located in the venous vessels. Conversely, the blood in the pulmonary vascular bed is about equally divided among the arterial, capillary, and venous vessels.

Blood entering the right ventricle from the right atrium is pumped through the pulmonary arterial system at a mean pressure about one seventh that in the systemic arteries. The blood then passes through the lung capillaries where CO_2 is released and O_2 is taken up. The O_2 rich blood returns via the pulmonary veins to the left atrium and ventricle to complete the cycle. The circulatory system is shown in Figure 2-5 below.
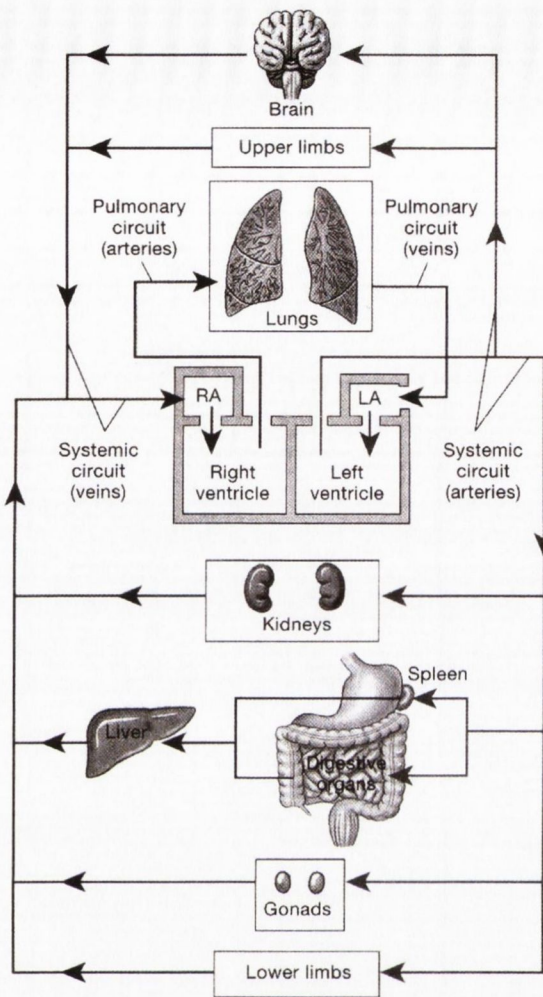
Figure 2-5 An overview of the pattern of circulation from Martini [10]

Capillaries are the functional units of blood circulation. They allow the blood fulfil its main purpose which is to service the cells of the body.

When the blood reaches the capillaries it is still under pressure (Figure 2-4). The many branches help to slow it down but as a result of this pressure and the ultra-thin structure of the capillary itself (since it has no muscle), some plasma and red blood cells are forced out through the capillary walls into the surrounding tissue carrying nutrients, oxygen and water with them.

This fluid, which bathes the cells and into which some of the wastes from the cells will diffuse, is called interstitial fluid. Some of this fluid may diffuse back into the main bloodstream through the capillaries, but most of it does not, since there is no pressure to force it back. Instead it drains into the blind-ending lymph ducts, which

reach into the very deepest tissue. These lymphatic vessels carry lymphocytes, hormones, nutrients and waste products from their tissues of origin back to the venous system.

2.3   FACTORS AFFECTING BLOOD PERFUSION

When analysing blood perfusion measurements it is useful to have an appreciation for factors affecting it, namely: (1) condition of circulatory system (2) the surrounding environment (3) the individual's level of activity (4) the individual's physical state (5) neural stimuli (6) hormonal stimuli (7) tissue type

Condition of Circulatory System

Clearly, if a person's arteries have a restriction due to a blockage and their heart is weak, blood will be pumped less rapidly. Similarly, the heart of a trained athlete can pump up to 30% more blood than an unfit person's can at maximum workload. Wilmore [13] states that it has been found also that athletes who train on a regular basis have a greater number of capillaries in their muscular tissue, so they can supply the cells with blood more rapidly than someone who is unfit.

A deficiency or blockage in the circulatory system can lead to a decreased level of perfusion in a localised area, which is known as ischemia (localised tissue anaemia due to obstruction of the inflow of arterial blood). This condition is a common problem with bed-ridden patients. Herrman et al. [14] discusses how pressure induced ischemia can lead to pressure ulcers and cell death.

The surrounding environment

The body is always striving to maintain haemostasis (the process by which the internal environment is kept within desirable limits) through haemostatic regulation. An example of this is thermo-regulation, which is when heat loss (which occurs primarily at the body surface) is balanced by heat production (in active tissues). Body core temperature is normally stringently controlled by thermoregulatory responses that are triggered by small deviations in core and skin temperature from their normal values. Under normal conditions the metabolic heat production is matched by heat loss, and the core temperature is maintained at approximately 37°C. When the skin and core weighted average temperature is too high vasodilatation and sweating will occur.

When the temperature is too low peripheral vasoconstriction and metabolic responses (non-shivering thermogenesis and shivering thermogenesis) are triggered. Core temperature between the sweating and vasoconstriction thresholds define the inter-threshold range; without drugs this range is just 0.2°C. Thus, the surrounding environment is one of the largest influences on skin blood perfusion as it has such a significant effect on the internal core temperature. When it is cold and one needs to conserve heat for the vital organs in the core, blood flow to the skin and peripheries decreases. The converse is true if the surrounding environment is very warm. Consequently the blood flow to the skin varies depending on the need for loss or conservation of body heat, as noted by Berne et al. [11].

Pitman et al. [15] notes that haemostasis is achieved by a combination of behavioural and physiological responses. In general the behavioural responses have a greater effect (adding or removing clothes) than the physiological responses, which serve as fine-tuning. The physiological response provokes a change in the blood flow to the skin (perfusion).

Martini [10] notes that a visible example of this is the colour one takes on when either hot or cold. Blood contains red blood cells filled with the pigment haemoglobin. Haemoglobin binds and transports oxygen in the bloodstream. When bound to oxygen, haemoglobin is bright red, giving skin a reddish tint as would be the case in a warm environment. Conversely when someone is cold they turn blue and when someone experiences a fright the blood drains from the skin and the person looks 'white'.

If the exposure to cold is prolonged, another slower process occurs. The brain increases the output of thyroid hormone into the blood stream from the thyroid gland in the neck. The thyroid hormone reaches all the cells of the body and increases their metabolic activity which increases heat production.

The individual's current level of activity

From Table 2-2 below it is clear that as one's activity levels increase the energy demands of the muscles increase significantly. To fuel this level of activity the metabolic rate must therefore increase. To achieve this, the individual cells must be

supplied with more oxygen and nutrients which in turn requires an increased blood supply to the area in question.

As so much heat is generated during this period of elevated activity (Doone [16] notes that the body is only about 20% efficient) the blood flow to the skin must increase in order to dissipate as much of this heat as necessary to keep the internal temperature within acceptable limits, again by the process of thermoregulation. From this it is clear that the muscle blood flow can vary by an order of magnitude depending on the exercise level.

Organ	Tissue blood flow (ml/min)		
	Rest	Light Exercise	Strenuous exercise
Skeletal muscles	1200	4500	12500
Heart	250	350	750
Brain	750	750	750
Skin	500	1500	1900
Kidney	1100	900	600
Abdominal viscera	1400	1100	600
Miscellaneous	600	400	400
Total cardiac output	5800	9500	17500

Table 2-2 Table showing distribution of blood during exercise, from Martini [10]

The individual's physical state

The healthier the person the lower will be their resting heart rate and the more compliant their arteries and so their overall capacity to pump blood through the capillaries will increase. However, illness can also lead to a temporary increase in blood flow. Thus, if one had a fever the body will attempt to lose as much heat as possible by increasing skin blood flow and initiating sweating. Further to this many of the medical conditions outlined in Section 1.1 will also lead to local or global variations in blood perfusion.

Neural stimuli

Martini [10] notes that the nervous system is responsible for adjusting cardiac output and peripheral resistance in order to maintain adequate blood flow to vital tissues and

organs. As an example of the influence of neural stimuli, when there is a sudden drop in temperature the nerves will sense this and cause a rapid decrease in blood flow to that area to conserve heat in the core of the body. This halting of the blood flow takes 'seconds rather than minutes' as described by Luckwill [17].

Hormonal stimuli

The endocrine system provides both short-term and long-term regulation of cardiovascular performance through release of hormones. These would tend to have a slower effect than neural stimuli as it takes time for the released hormone to be distributed around the body but their effects can last a much longer time. There are many hormones which play a part in cardiovascular regulation, such as antidiuretic hormone (ADH); which causes peripheral vasoconstriction that elevates blood pressure in response to a decrease in blood volume or an increase in the osmotic concentration of the plasma. EPO is a hormone which is realised at the kidneys if the blood pressure declines or if the oxygen content of the blood becomes abnormally low. This hormone stimulates red blood cell production and maturation, elevating the blood volume and improving the oxygen-carrying capacity of blood. Other hormones would which can effect blood perfusion are Angiotensin II and Atrial Natriuretic Peptide.

Tissue Type

In most tissues such as muscle for instance, the main aim of the circulatory system is to supply the tissue with blood in amounts commensurate with the local requirements for O_2 and nutrients while also removing waste products. However Berne [11] notes that for the skin the O_2 and nutrient requirements are quite low thus making thermo-regulation the domination determinant of perfusion in skin tissue.

2.4 THE INTEGUMENTARY SYSTEM (SKIN)

The skin of the human body is an organ comprising of the cutaneous membrane and accessory structures (i.e. hair, nails and exocrine glands). Martini [10] states that the integument makes up approximately 16% of the body weight. Its main functions are to:

1. form a protective layer over the body to help prevent injury and disease
2. keep moisture in the body (water retention)

3. synthesise vitamin D$_3$
4. regulate body temperature
5. excrete waste through integumentary glands
6. detect pressure, pain and temperature stimuli

Humphries [18] notes that when faults occur with this organ, they are detectable by signs of blemishes, changes in colour, flexibility, elasticity, sensitivity etc. as opposed to other organs, which can be damaged without externally visible effects. These signs may indicate dysfunction in other systems. Changes in skin colour and temperature are one of the first signs of blood occlusion in the body extremities.

The integument does not function in isolation. It is fed with an extensive network of blood vessels and sensory receptors that monitor touch, pressure and pain provide valuable information to the nervous system. However for this study of most interest is the blood supply system and the thermal properties and composition of the sub-layers of the skin. The integumentary system has two major components, the cutaneous membrane and the accessory structure (including hair, nails, glands etc). The cutaneous membrane consists of the epidermis *(epi-, above)* and the dermis (an underlying area of connective tissues). Below the dermis the loose connective tissue of the subcutaneous layer separates the integument from the deep fascia (connective tissues that create the internal framework of the body) around muscle tissue and other organs including bones. Generally the sub-cutaneous layer is not considered part of the integument.

The main arteries and veins supplying the skin are located in the sub-cutaneous layer along its border with the reticular layer of the dermis as shown in Figure 2-6. This network is known as the cutaneous plexus. Arterioles supply the tissue in this layer and in the integument above it. Capillary beds supply the hair follicles, sweat glands and other structures in the dermis. On reaching the papillary layer, these small arteries form another branching network, the papillary plexus, which provides arterial blood to capillary loops that follow the contours of the epidermis-dermis boundary.
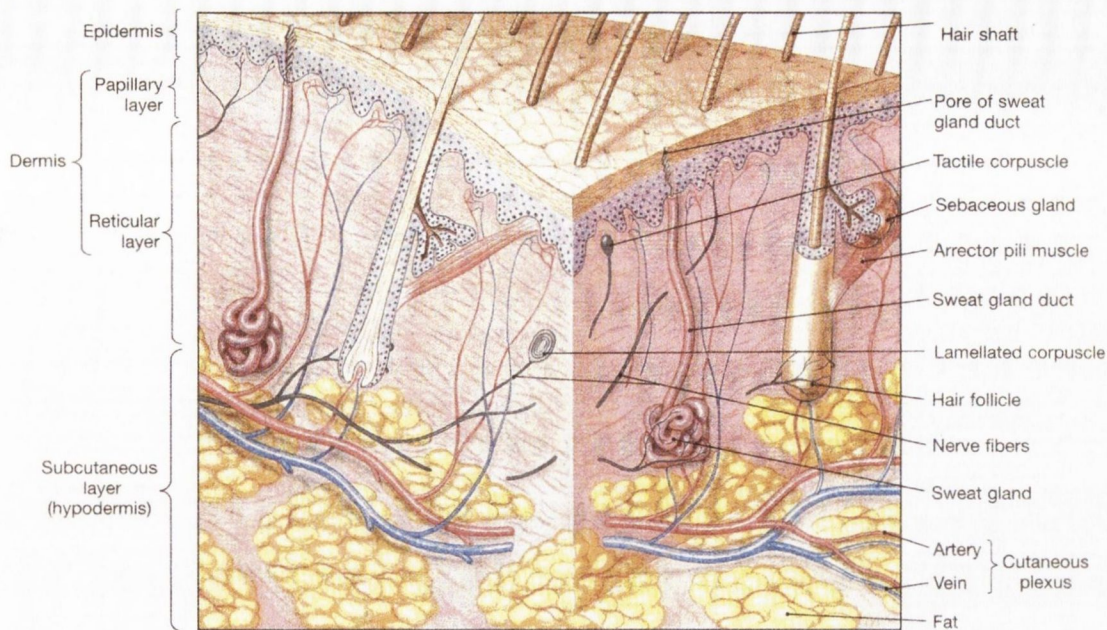
Figure 2-6 Composition of skin, from Martini [10]

Epidermis

This outermost layer of the skin varies in thickness from 0.08mm to 0.5mm (for the thick skin on the palms and soles of the feet). The skin is a stratified structure and is generally considered to have 5 distinct sub layers. The top sub layer is the stratum corneum, which is made up of dead keratinocytes cells that contain keratin, a protein that protects your skin from harmful substances, such as chemicals, and infections by viruses, bacteria and fungi. Stratum corneum cells continuously flake off through washing or other friction and are then replaced by new cells from the lower sub layers. This process makes your skin a dynamic organ that's constantly being replenished.

Also present are melanocytes, which produce the dark brown pigment melanin that gives colour to the skin and hair. The more melanin that's produced, the darker the skin. Langerhans' cells form part of the immune system, helping to protect your body against infection. Both melanocytes and Langerhans' cells are concentrated at the basal layer of the epidermis. Pennes [19] notes that the epidermis loses water to the environment at an average rate of 500ml per day, through insensible perspiration, which is not a result of sweat glands. In contrast sensible perspiration can vary from 0-4L/hour.

16

Dermis

The dermis lies between the epidermis and the subcutaneous layer. Sejrsen [20] notes that it is a highly vascular layer of tissue, which varies in thickness from 0.5mm over the eyelids to 4mm on the back with an average thickness of 1.2mm between the wrist and elbow. It includes strong white fibres called collagen and elastic yellow fibres called elastin which are woven together in a dense bed to give your skin strength and elasticity. Blood vessels, muscle cells, nerve fibres, lymph channels, hair follicles, oil glands and sweat glands run throughout the dermis.

Capillary beds supply the hair follicles, sweat glands, and other structures in the dermis. On reaching the papillary layer, these small arteries form another branching network, the *papillary plexus*, which provides arterial blood to capillary loops that follow the contours of the epidermis-dermis boundary.

Subcutaneous tissue

This layer contains the supply blood vessels and nerves for the skin, as well as the roots of the oil glands and sweat glands. It holds in body heat and cushions the internal organs against injury. Constriction of the blood vessels in this layer controls the blood supply to the skin. The thickness of the layer varies from person to person and from location to location on the body.

2.5 MORPHOLOGY OF THE BLOOD CIRCULATION IN THE LIMBS

Martini [10] describes the morphology of blood vessels in the arms and legs in the following manner.

2.5.1 Upper arm

Arterial System

The Ascending Aorta begins at the aortic semilunar valve. This supplies the Brachiocephalic trunk which in turn supplies the right subclavian artery. After leaving the thoracic cavity and passing across the superior border of the first rib, the subclavian is called the axillary artery. This artery crosses the axilla to enter the arm, where it gives rise to humeral circumflex arteries which supply structures next to the

head of the humerous. Distally it becomes the brachial artery which supplies blood to the rest of the upper limb. As it approaches the coronoid fossa of the humerus the brachial artery divides into the radial artery which follows the radius and the ulnar artery which follows the ulna to the wrist. These arteries supply blood to the forearm. At the wrist they fuse to form the superficial and deep palmar arches which supply blood to the hand and to the digital arteries of the thumb and fingers.

Venous System

Veins are more variable than arteries in their branching patterns; however they do exist in symmetric form in the body. Complementary arteries and veins usually run alongside each other. The main difference between the arterial and venous systems is that in the peripheral limbs, arteries are usually located in deep tissue, where they are protected by muscle and bone, whereas there are two sets of peripheral veins, one located superficially and one deep. The reason for this is control of body temperature. When it is hot, blood flows in the superficial veins where it can be cooled and vice versa for cold weather.

The venous system of the forearm can be describes as follows. The digital veins empty into the superficial and deep palmar veins of the hand which are interconnected to form the palmar venous arches. The superficial veins empty into the cephalic vein, the median antebrachial vein and the basilica vein. The deep palmar veins drain into the radial vein and the ulnar vein. After crossing the elbow these veins fuse to form the brachial vein. As the brachial vein continues toward the trunk it receives blood from the basilica vein before entering the axilla as the axillary vein. The Axillary and Cephalic vein then join the subclavian vein which in turn fuses with the superior vena cava.

2.5.2 Lower Leg
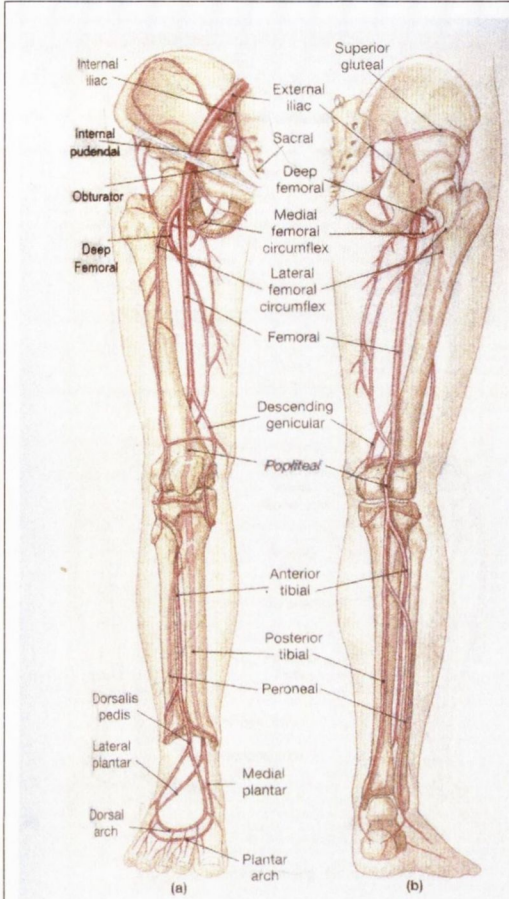
Figure 2-7 Arteries of the leg, from Martini [10]
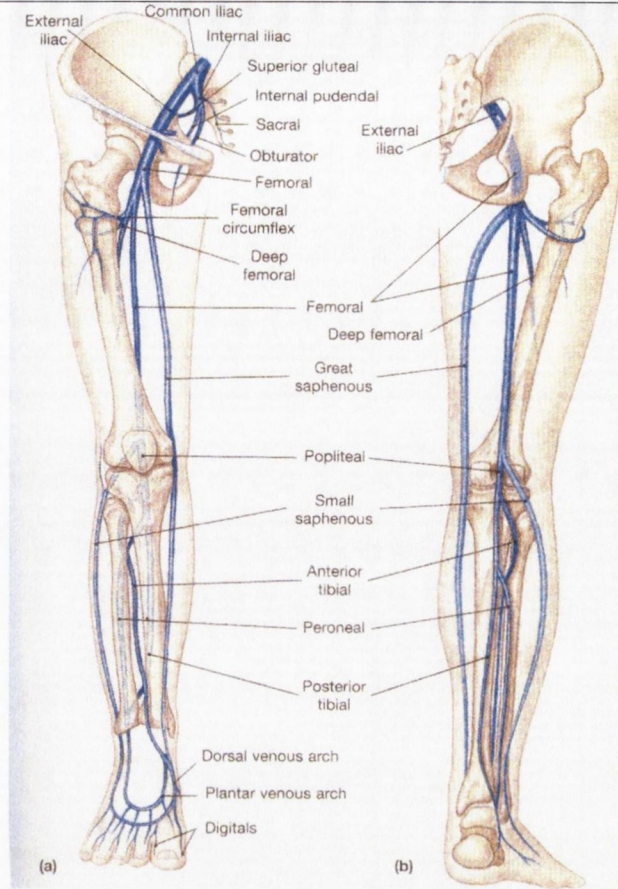
Figure 2-8 Veins of the leg, from Martini [10]

Arteries of the lower leg

The important arteries of the leg are given in Figure 2-7. The main artery supplying the lower leg is the popliteal which is itself supplied by the femoral artery. This artery derives from the descending geniculary artery at the knee, which supplies the area around the knee joint. The popliteal splits into the posterior and anterior tibial arteries just below the knee. The posterior tibial artery supplies the peroneal artery while the anterior tibial artery descends between the tibia and fibula to supply the foot.

Veins of the lower leg

Blood enters the leg through the planter network, which supplies the anterior tibial vein, the posterior tibial vein and the peroneal vein. The leg is further drained by the great and small saphenous veins. The great saphenous vein runs along the medial

aspect of the leg and drains into the femoral vein near the hip. The small saphenous runs along the posterior and lateral aspects of the calf muscle and enters the popliteal vein at the knee.

2.6   EXPERIMENTAL METHODS OF ALTERING SKIN BLOOD PERFUSION

When carrying out experiments it is very useful to be able to induce a variation in blood perfusion. The ability to detect a change in the measured variable provides some degree of validation of the measurement technique.

- Certain drugs are known to affect blood flow. For instance, sodium nitroprusside causes blood vessels to dilate and increases blood flow to the heart. Acetycholine causes blood vessels to dilate and slows heart rate and LNMMA decreases blood flow by blocking the production of nitric oxide.
- Influence of varying levels of restricting pressure produced by inflating a pressure cuff proximal to the measuring site
- Varying the atmospheric temperature and hence core body temperature. To achieve this, testing can be conducted in a temperature-controlled environment.
- Increasing muscular activity
- Through inducing cold shock
- Influence of deep breathing exercises
- Altering the insulation provided by the body's clothing

2.7   SUMMARY

This chapter has described the functioning of the vascular distribution system, the composition of the skin, morphology of the blood circulation in the limbs but most importantly the various factors affecting blood perfusion which are vital for interpreting the results from testing in later sections.

3 MODELLING OF HEAT TRANSFER IN BIOLOGICAL TISSUE

This chapter will examine various methods of modelling heat transfer within biological tissue. There will be a particular emphasis on Pennes' [19] 1948 study, including criticism of his work. This study is the seminal work in this field. A number of new bio-heat models have since been developed for particular applications or to address some of Pennes' simplifying assumptions. Various other thermally significant factors are discussed. Finally justification is given for the decision to continue with a modified version of Pennes original bio-heat equation.

3.1 PENNES BIO-HEAT EQUATION

Pennes [19] developed and validated his benchmark equation for relating blood flow to thermal effects in tissue over a period from 1947 –1948. The Bio-heat Equation was derived through the application of heat transfer theory for homogenous, isotropic conductors:

$$(\rho C)_t \frac{\partial T_t}{\partial t} = k_t \nabla^2 T_t + (\rho C \omega)_b (T_a - T_v) + \dot{q}_{meta} \qquad \text{Eq. 3-1}$$

where T is temperature, ρ density, c the specific heat, k the thermal conductivity, ω the blood perfusion and $\dot{q}_{meta}$ the volumetric heat generation due to metabolism. Subscripts t, b, a and v refer respectively to the tissue, the blood, the arterial blood and the venous blood. This equation represents an energy balance within the tissue. The left hand term accounts for the rate of change of thermal energy of the tissue. The terms on the right account for the heat transfer due to conduction through the tissue, convective heat transfer due to perfusion and internal heat generation due to metabolism respectively.

A number of assumptions are inherent in the analysis of Pennes [19]:

- Material (i.e. tissue) is assumed to be an homogenous, isotropic conductor

- Since the cross section of the proximal forearm is almost perfectly cylindrical, the general differential equation of heat flow is used in cylindrical coordinates.
- The rate of heat production by skin and subcutaneous fat is assumed to be negligible.
- The thermal conductivity is taken as uniform throughout the arm.
- The rate of perfusion is considered uniform.
- The temperature of the blood on leaving the tissue is assumed to be equal to the tissue temperature.
- The variation in micro vascular circulation is neglected.
- Heat transfer between arteries and veins is assumed to be negligible.
- It is assumed that the blood reaches thermal equilibrium in the capillary beds i.e. the blood enters the capillary beds at the arterial temperature and leaves at the temperature of the tissue.

A number of these assumptions have since been proven to be incorrect and will be discussed in the remainder of this chapter. As discussed in Section 2.2 the flow in arteries with a diameter of less than 4mm can be considered to be laminar over the range of physiological flow rates. Holman et al. [21] shows the Nusselt No. to be constant for fully developed laminar flow in a pipe. This implies that the heat transfer coefficient is substantially constant which would suggest that heat transfer will not change with perfusion. However this premise is based on consideration of a single vessel in isolation, whereas Pennes' approach is based on a macroscopic perspective. Pennes [19] assumed that the heat deposited in the tissue by the warm blood entering to be proportional to the difference between the arterial and local tissue temperature. As it can be shown that the blood always reaches thermal equilibrium with the tissue (see Section 3.3) it follows that the level of heat deposited into the tissue volume is indeed proportional to the perfusion level.

To validate the bio-heat equation a series of stringent temperature measurements were performed by Pennes [19] on live subjects. These consisted of surface measurements, both longitudinally down the arm as shown in Figure 3-1 and also radially around the circumference. Various internal measurements were made of the temperature of the blood as it entered the arm as shown in Figure 3-2 and of the temperature profile

through the arm as shown in Figure 3-3. Finally the effect of circulatory occlusion on surface temperature measurements was investigated.
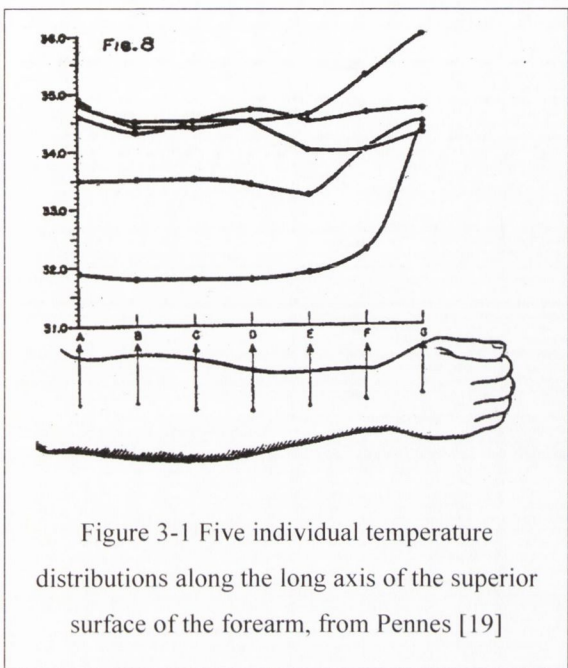
Figure 3-1 Five individual temperature distributions along the long axis of the superior surface of the forearm, from Pennes [19]
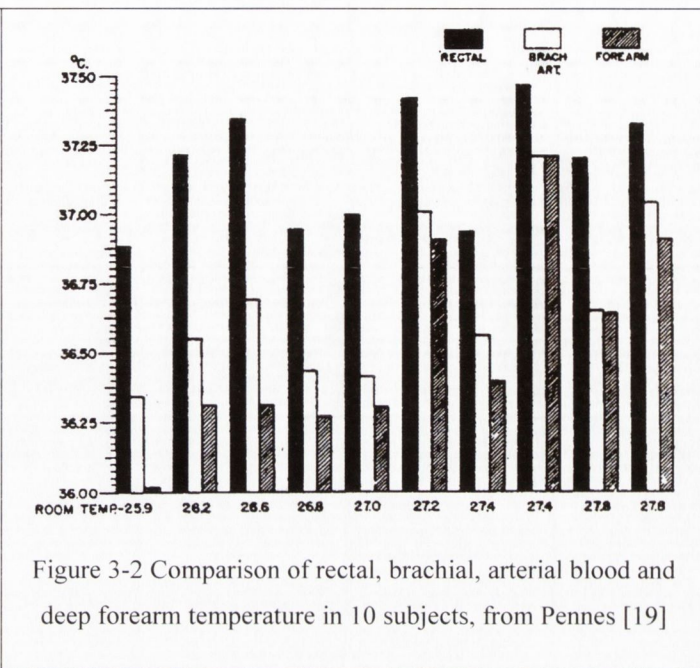
Figure 3-2 Comparison of rectal, brachial, arterial blood and deep forearm temperature in 10 subjects, from Pennes [19]

Pennes compared temperature distributions calculated using the Bio-heat equation through the cross section of the arm for various perfusion and metabolic rates with average experimental results, as shown in Figure 3-3.

Pennes [19] notes the experimental curve was most closely approximated when the blood flow was assigned values from 0.0002/s to 0.0003/s. These values correspond closely to the range of 0.00025/s to 0.0005/s found by Barcroft and Edholm [22] using plethysmographic measurements on the forearm. In the 26 years following its publication Pennes [19] paper was cited an average of 1.7 times per year. Since 1990 the paper has averaged 25 citations annually.

°C

Mean experimental
results (bold line)

$\omega_{computed}=0.0003/s$

$\omega_{computed}=0.00025/s$

$\omega_{computed}=0.0002/s$

Depth in cm
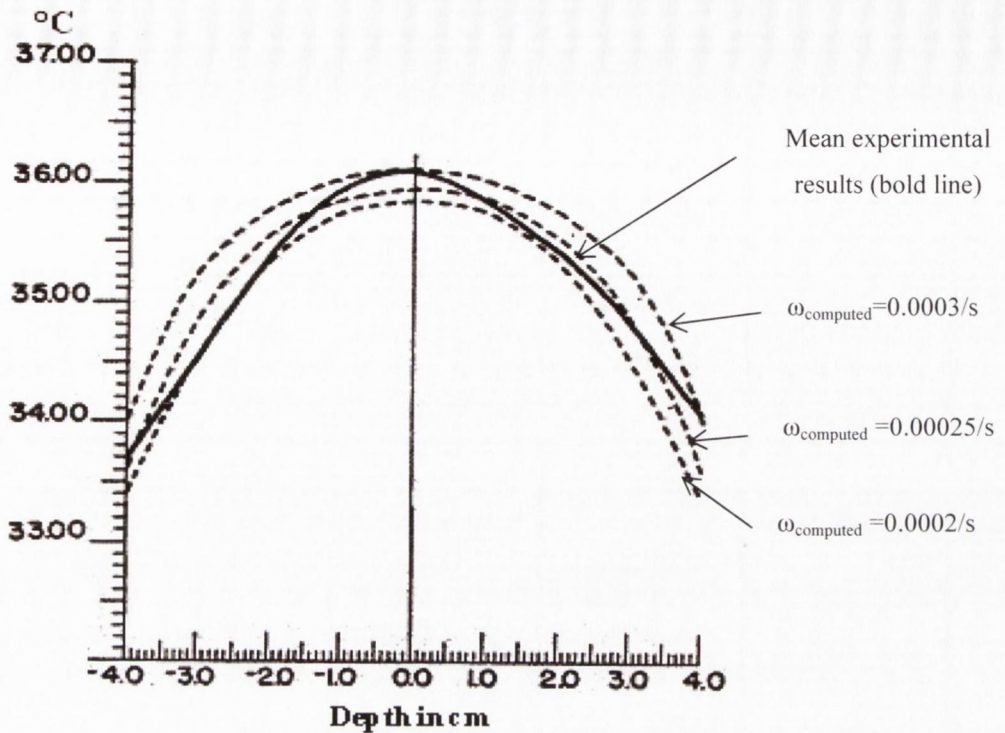
Figure 3-3 Pennes [19] comparison between the recorded mean experimental temperature readings
(solid line) and the theoretical temperature values computed using the Bio-heat equation for various
perfusion and metabolic rates (dashed line)

In a review paper written by Wissler [23] fifty years after the original publication of
Pennes' 1948 paper it is noted that there were a number of discrepancies in the Pennes
[19] analysis and in some of the constant values he used, such as the thermal
conductivity of the tissue, blood flow levels and the use of a constant arterial
temperature. By underestimating the magnitudes of the conduction and blood flow
terms in the energy balance by comparable amounts (one-half to two-thirds) it was
found for a steady state analysis that the errors are essentially offsetting and as Wissler
shows the correct parametric values do not yield substantially different temperatures.
In his conclusion he notes that the experimental data reported by Pennes 'will
probably be as good as we will ever have'.

3.2   THERMAL EQUILIBRIUM LENGTHS FOR BLOOD VESSELS

Pennes' assumptions about the isotropic nature of the composition and thermal
properties of the arm are clearly incorrect but can be addressed with modern
numerical methods, as discussed in Chapter 5. His assumptions about where the heat

exchange between blood and tissue occurs and whether the blood leaves the tissue at the temperature of the tissue are more difficult to evaluate. Chen and Holmes [24] were among the first to examine these assumptions.

They carried out a study on the equilibrium lengths of vessels with their surrounding tissue, where the equilibrium length (X_e) as defined by Eq. 3-2 is a measure of the length required for the blood temperature in an individual vessel to equilibrate with the local tissue temperature. This is illustrated by Figure 3-4. With this information one can estimate the heat loss from the major supply arteries, as well as the calibre of the vessels in the micro-circulation where temperature equilibration with tissue actually occurs.
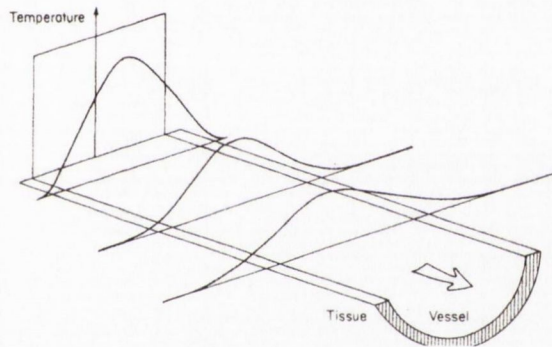
Figure 3-4 Schematic view of the axial and transverse variation of blood temperature in an ideal vessel, from Chen and Holmes [24]

$$X_e = \frac{d}{4}\frac{\rho_b c_b \upsilon}{U} \qquad \text{Eq. 3-2}$$

In Eq. 3-2, v is the mean blood velocity in the vessel, d is the blood vessel diameter, c the specific heat capacity and U is the overall heat transfer coefficient, based on the blood vessel lumen (which is the bore of a blood vessel). Chen and Holmes [24] state that in general the blood velocity in a vessel is roughly proportional to the radius, which indicates that the equilibration length X_e is very sensitive to vessel radius. This is evident in the estimates of X_e shown in Table 3-1. It is seen that the equilibration lengths for the larger arteries and veins are in the range of metres, indicating that, in general, the blood in these large vessels is not thermally equilibrated

with the solid tissues. On the other hand the equilibrium lengths for precapillary arterioles, capillaries and venules are generally of the order of microns, indicating that in these vessels the blood temperature is essentially equal to the solid tissue temperature. Thus Pennes assumption that thermal equilibration takes place only in the capillary bed is shown to be incorrect.

j	Vessel	% Vascular Volume	r_j (μm)	X_{ej} (m)	l_j/X_{ej}
1	Aorta	3.30	5000	190	0.002
2	Large artery	6.59	1500	4	0.05
3	Arterial branch	5.49	500	0.3	0.3
4	Terminal branch	0.55	300	0.3	0.3
5	*	1	175	0.009	1
6	Arteriole	2.75	10	5×10^{-6}	400
7	Capillary	6.59	4	2×10^{-7}	6000
8	Venules	12.09	15	2×10^{-6}	800
9	Terminal vein	3.30	750	0.1	0.1
10	Venous branch	29.67	1200	0.3	0.3
11	Large vein	24.18	3000	5	0.04
12	Vena cava	5.49	6250	190	0.002

Table 3-1 Estimates of X_e from Chen and Holmes [24]

It is useful to examine the ratio of the vessel length (l) to equilibrium length (X_e) for different generations of the vessels, as shown in the last column of Table 3-1. This ratio is a direct measure of the ability of blood to equilibrate its temperature with the solid tissue before it flows into a vessel of the next generation. Of most interest from this analysis is the vessel in which thermal equilibrium actually occurs, i.e. where the vessel to equilibrium length is equal to one. The analysis shows that this occurs between the Arterioles (j=6) and terminal branches of the arterial system (j=4). An entry (j=5) is made to indicate the approximate diameter of a vessel between the terminal branch arteries and the arterioles where the vessel to equilibrium length

equals one. It is seen that a vessel with l_j and X_{ej} equal to unity would have a diameter of perhaps 0.2mm to 0.5mm. A corresponding diameter on the venous side would be about 0.3mm to 0.1mm, although this vessel is not shown in Table 3-1.

Figure 3-5 shows the blood temperature with reference to the tissue temperature as the blood traverses the systemic vasculature.
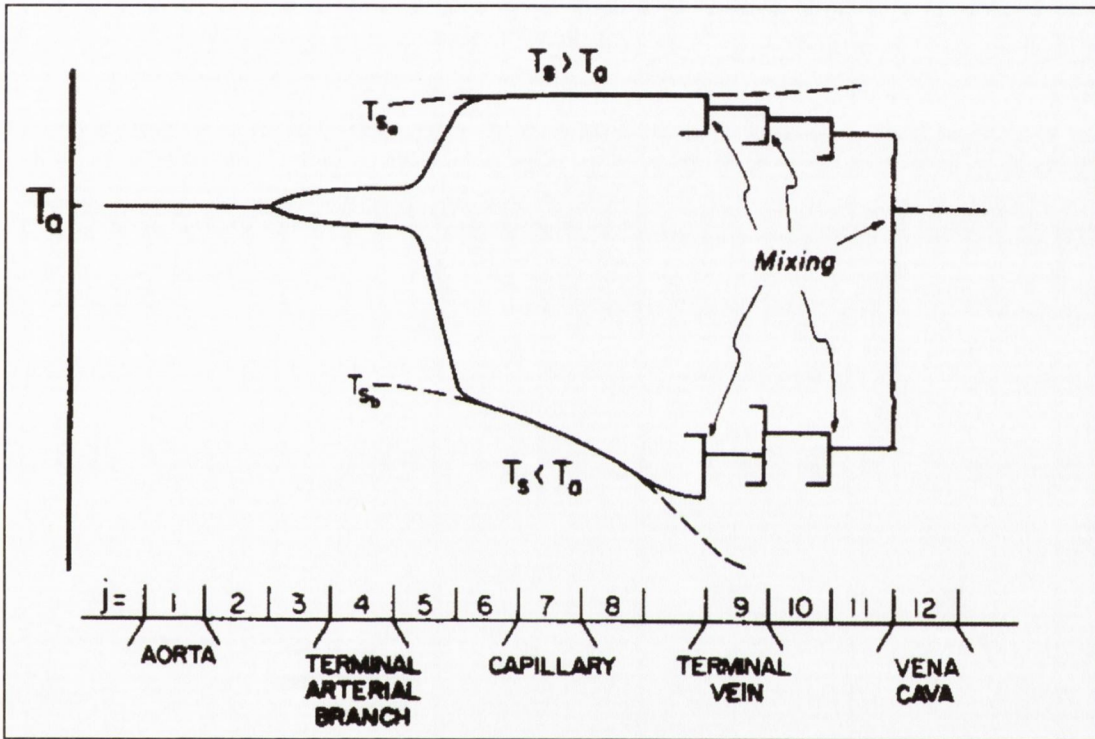
Figure 3-5 Schematic representation of the blood temperature as the blood traverses the systemic circulation (j=1:12). From Chen and Holmes [24]

As blood leaves the heart and travels in the large arteries, its temperature remains essentially constant at T_a with little equilibration taking place. Some temperature equilibration will occur between blood and tissue as blood is distributed to warmer ($T_s > T_a$) or cooler ($T_s < T_a$) structures via arterial and terminal arterial branches. However most of the temperature equilibration occurs as the blood passes through vessels whose diameter is between that of the terminal arterial branch ($j=4$) and that of the arteriole ($j=6$). As blood reaches the latter, T will essentially be at the solid tissue temperature. Beyond this point, T_b faithfully follows T_s through its spatial and temporal variations until the blood reaches the terminal veins. At this point the blood temperature ceases to equilibrate with the tissue and remains virtually constant except

27

as it mixes with other blood of different temperatures at venous confluences. Finally the cooler blood from peripheral structures and warmer blood from internal organs mix within the vena cave and the right atrium and ventricle. Following thermal exchange in the pulmonary circulation and remixing in the left heart, the blood attains the same temperature it had at the start of the circuit.

In their study Chen and Holmes [24] demonstrated Pennes assumption that the temperature equilibration occurred in the capillaries to be incorrect. This provoked renewed interest in the development of further bio-heat models.

3.3 ALTERNATE TISSUE HEAT TRANSFER MODELS

Models are often divided into one of two categories, namely: continuum models or vascular models. Pennes' model is one of the few true continuum models. The vast majority of models account for at least some of the venous system, thus making the distinction between whether they are continuum or vascular dependent on the size of the vessels they consider.

Wulff [25] and Klinger [26] addressed the isotropic nature of Pennes' perfusion term. Bazett et al. [27] initially presented the counter-current structure from observations of large arteries and veins in human limbs. The first major quantitative analysis was presented by Mitchell and Myers [28]. It was then followed by the work of Keller and Seiler [29] who presented a one dimensional steady-state continuum model for heat transfer through the tissue of peripheral regions, combining the effects of tissue conduction, convection by blood flow, vascular heat exchange and tissue metabolism. The effective conductivity of the non-isothermal region was determined under various flow conditions. It was shown that the minimum effective conductivity is the thermal conductivity of the tissue and the maximum is the geometric mean of the conductivity and the capillary perfusion rate. They also provided for some level of countercurrent heat exchange between veins and arteries.

Chen and Holmes [24] model is one of the most developed and builds on their analysis of the significance of blood vessel size on thermal equilibration length as described in the previous section. The blood vessels are divided into two categories,

large vessels, each of which is treated separately, and small vessels that, in view of their small size and large number, are treated as part of the continuum that also includes the tissue. They then separated the heat transfer between the small blood vessels and tissue into three modes. The first mode reflects the equilibration of blood temperature, initially at that of a large vessel, with tissue temperature. The second mode relates to already thermally equilibrated vessels and deals with the part of heat transfer that takes place when the flowing blood convects heat across a tissue temperature gradient. The third mode describes the thermal contribution due to the small temperature fluctuations of nearly equilibrated blood along the tissue temperature gradient. In view of the time lag between the temperatures of the tissue and of the closely following blood, this mode of heat transfer is proportional to the tissue temperature gradient and depends on the local micro-vascular structure. Attempts to apply the Chen and Holmes model (CH) model for the evaluation of temperature distributions within the pig kidney cortex were met with some success as shown by Xu [30] and Xu et al. [31].

Wren [32] notes that as continuum models are generally based on heat conduction it is a simple matter to adapt modelling programs to them. Roemer and Dutton [33] built on Chen and Holmes' work to present a complete derivation of a general, volume-averaged tissue convective energy balance equation. However it has yet to be solved as it requires a large amount of physiological information.

The next significant model to be developed was the 1985 Weinbaum and Jiji [34] model. It is described by Weinbaum et al. [35] as follows: "A new model equation for micro-vascular blood-tissue heat transfer was developed which took a more fundamental physical approach in relating the local blood-tissue energy exchange to the local micro-vascular geometry and flow in the skeletal muscle. It was found that in this tissue the predominant mode of heat transfer was the net heat loss to the tissue from the incomplete countercurrent exchange that took place between the paired vessels. The new model derived to account for this heat transfer mechanism showed that the thermal effect of the blood perfusion could be described in terms of an effective thermal conductivity tensor k_{ijeff} which was proportional to the square of the local Peclet number and dependent on the direction of the vessel axes relative to the local macroscopic tissue temperature gradient."

The Weinbaum-Jiji equation has several limitations in the derivation of the expression for k_{ijeff}

1. it requires that the thermal equilibration between the artery-vein pairs does not depart significantly from nearly perfect counter-current exchange
2. it involves a detailed description of the branching micro-vascular geometry.

The Weinbaum-Jiji equation, therefore, cannot be applied without modification outside the peripheral tissue region for which it was first developed and even there the criterion for validity of the equation can be violated at high flow rates. Limitation 2 requires that detailed anatomical studies be performed to estimate the vessel number density, size, and artery-vein spacing for each vessel generation.

While the models above were developed to be more physiologically realistic, this requirement for greater physiological information often makes them impractical or even impossible to apply generally. Therefore models were developed that could be more easily applied. In their 1994 paper, Brink and Werner [36] use a previously developed highly descriptive 3-D model of the vasculature (Brink et al. [37]) to 'correct' Pennes perfusion source term by introducing a very simple efficiency function as described by Eq. 3-3. The 3-D model has a very high computational cost with a run time of 30 hours on a supercomputer (all be for a 1994 vintage computer) while a model incorporating the correct factor can easily be run on a PC in a matter of minutes.

$$\dot{q}_{per} = EF(\omega, r).(C\rho\omega)_b(T_a - T_v)$$ Eq. 3-3

The efficiency function was found to depend on both radial position and flow rate. However they found for the radial variation that it is sufficient to define only an inner and an outer muscle layer as shown in Figure 3-6.
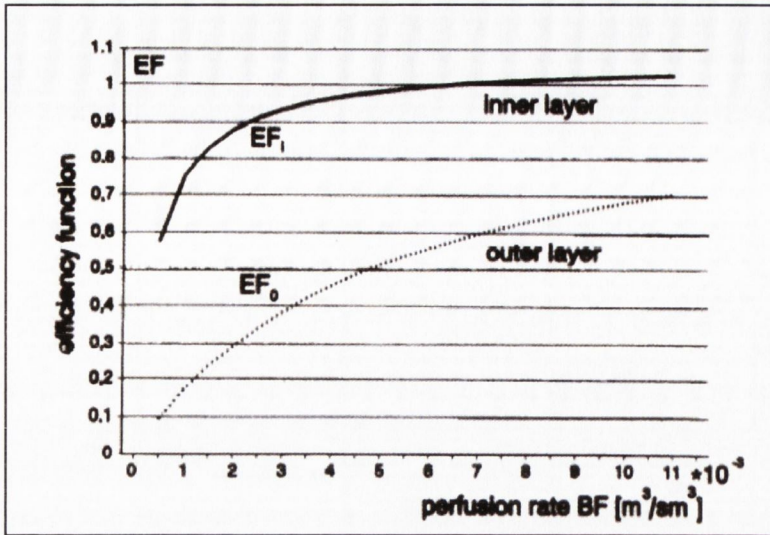
Figure 3-6 Efficiency function for various flow-rates and tissue locations from Brink and Werner [37]

For the skin Brink and Werner [37] state that 'Pennes classical equation does not seem to need substantial correction'. They conclude that when the Efficiency function is combined with Pennes' Equation the results are very good compared with the 3-D model and also compare more favourably with Pennes' experimental data than Pennes original model.

In 1994 Baish [38] proposed a probabilistic statistical model to predict the probability that the temperature at a point would take on a particular value from some statistical information on the vascular geometry and blood flow. Baish [38] notes that an ideal thermal model of perfused tissue should include every blood vessel in its actual position with its blood flow accurately known. The temperature at every point in the tissue and the blood vessels could then be calculated numerically by solving the coupled convection-conduction problem. However limits on current imaging techniques make it impossible to generate such a model. Van Leeuwen et al. [39] note that if magnetic resonance angiography (MRA) imaging is used to build a suitable representation of the patient's vasculature, only vessels with a diameter above 600μm can be reconstructed and included in the model, with 1000μm being a more realistic lower limit.

For the statistical model a theoretical vascular structure is generated using an algorithm developed by Gottlieb [40]. A new analytical technique to calculate the rate

of heat flow into each vessel, the temperature at every point along the vessels and the temperature at any point in the tissue was then developed and a statistical comparison made between the results from the proposed model and those from Pennes equation. With Pennes' solution large-scale gradients are avoided as the blood acts evenly and efficiently. With Baish's [38] solution the largest vessels in the tissue produce local heterogeneity in the temperature field under conditions for which the Pennes equation predicts a uniform temperature. However when the temperatures at many points in the tissue are sampled, a statistical measure shows that for over 3000 points in the model (Figure 3-7) virtually all are clustered near the mean value (similar to that predicted by Pennes). The largest deviations are due to a few large arteries.
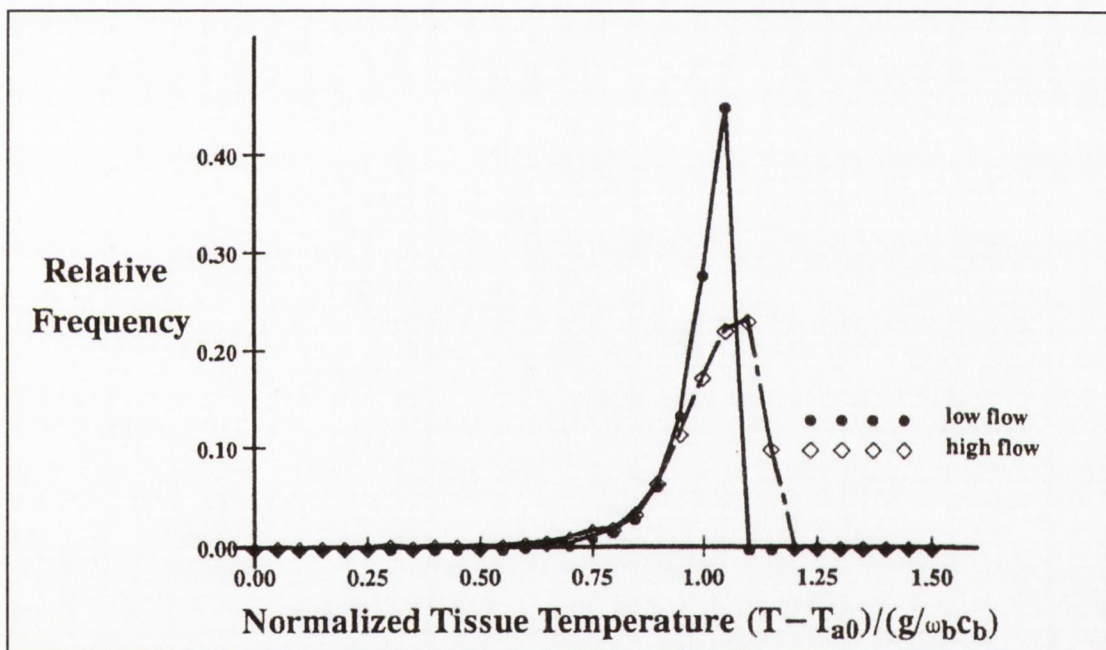
Figure 3-7 Histogram of the tissue temperature over the entire organ for two flow rates, m=0.01gm/s and m=0.02gm/s from Baish [38]

Thus the mean temperature is very accurately predicted by the Pennes equation, provided that the supply artery and return vein are far apart.

In a two paper series Weinbaum et al. [35] and Zhu et al. [41] address the question of venous return temperature and arterial supply temperature. Their work focuses on a basic anatomical structure common to all skeletal muscle tissue as identified by Myrhange and Erikson [42] and shown in Figure 3-8 in which they assume primary

vascular heat transfer occurs. This structure is shown to occur in a repeating pattern throughout the muscle. The counter currently occurring secondary vessels (s) in the tissue cylinder are fed by the primary vessels (P) which in turn are fed from the larger supply arteries and veins (SAV's).
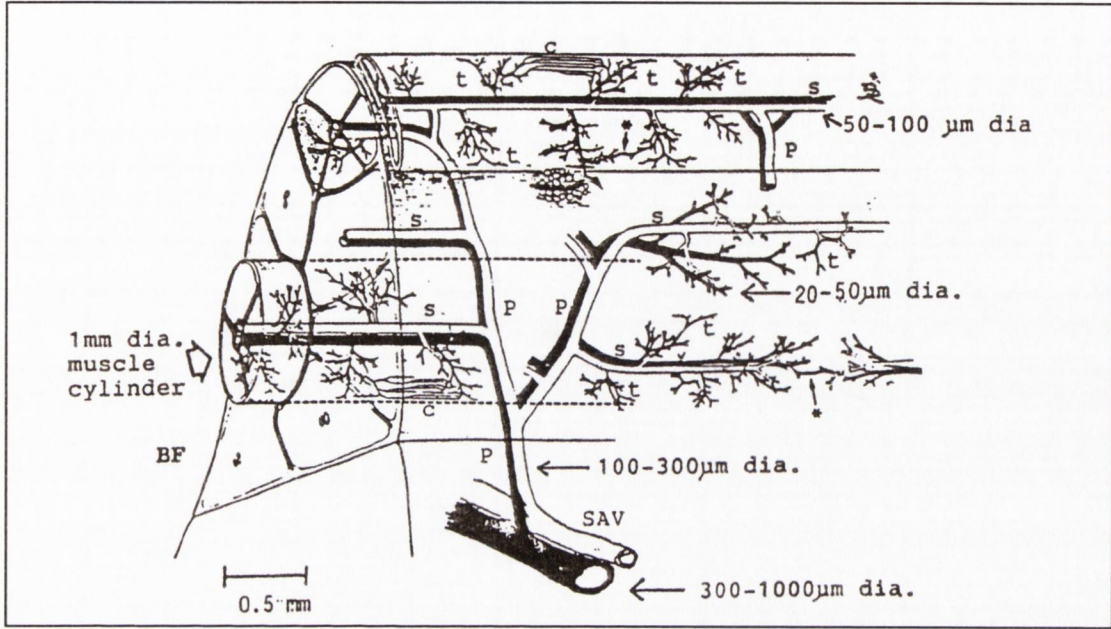
Figure 3-8 Macro and micro-vascular, arrangement as identified by Myrhange and Erikson [42]

The thermal equilibration of the returning blood in the s vein was rigorously analyzed to determine the venous blood temperature leaving the tissue cylinder. This led to a modified Pennes bio-heat equation with a new perfusion source term containing a correction factor, which can be used to predict average tissue temperature distribution in muscle tissue regions containing vessels less than 300µm in diameter.

$$\dot{q}_{per} = \Delta T (C\rho\omega)_b (T_{abo} - T_t)$$ Eq. 3-4

where C, ρ, ω are the specific heat, density and perfusion rate of blood, ΔT is the correction coefficient, T_{abo} the inlet arterial temperature from the P vessel and T_t the tissue temperature. It has been shown that for most muscle tissues that the correction coefficient varies between 0.6 and 0.8 suggesting that there is a 20 to 40 percent re-warming of the vein due to counter current heat transfer between the closely aligned artery and vein pair in the s vessel-tissue cylinder.

In the second paper of the series Zhu et al. [41] examine the temperature of the Supply Artery and Vein vessels (SAV's). These temperatures are necessary in order to establish the entrance arterial temperature to the S vessels tissue cylinder (T_{abo}) as required by Eq. 3-4. They assume due to the short length of the P vessel (which supplies the S vessel from the SAV) that any thermal equilibrium in them may be neglected. The temperature of the SAV vessels depends not only on the interaction between the countercurrent SAV vessels but also on the local tissue temperature distribution. A central question in analyzing the countercurrent equilibration in the SAV vessels is to determine how much thermal energy leaving the artery returns to the countercurrent vein and how much is lost to the surrounding tissue. It was found that at least 77% of the thermal equilibration is achieved in the SAV artery before it enters the S vessel tissue cylinder for normal physiological conditions, which contradicts their initial assumption that the tissue cylinder surrounding the 'S' vessels is the primary heat exchange unit. The model predicts that for a human limb 40% of the heat lost from the SAV arteries and their branches is recaptured by their countercurrent vein. In a related experimental study He et al. [43] conclude that the experimentally measured temperature differences in an isolated rat limb generally agree with the theoretical predictions from Zhu et al. [41].

3.4 WHOLE BODY THERMAL MODELS

Whole body thermal models have been developed by a range of researchers. Stolwijk and Hardy [44] produced one of the first theoretical studies on temperature regulation in man. Ferreira et al. [45] states that human thermal models must have two components, namely a passive element and a temperature control system. The body is first divided into a series of segments which may be described by the application of heat and mass balances to the tissue control volume. The second part is the temperature control system which is responsible for the maintenance of body temperature within strict limits. These models also account for effects such as sweating and shivering. Huizenga et al. [46] developed a model to predict human thermal comfort in non-uniform or transient thermal environments such as those experienced by automobile occupants or in air conditioned buildings. Hegarty et al. [47] examined changes and their effects induced in the human thermoregulatory system under the influence of general anesthesia. Models have been developed to

devise warming procedures for hypothermic patients. Van Leeuwen et al. [48] note that patient temperature during and after surgery is a parameter strongly affecting morbidity. Clinicians want to be able to optimize patient temperature corresponding to the nature and phase of the procedure in order to minimize risk of morbidity and complications. Lower temperatures can confer benefits, chief among them is protection against cerebral ischemic damage, but hypothermia also carries profound adverse effects such as shivering, myocardial ischemia and bleeding disorders.

3.5 PERTURBATIONS IN TISSUE PERFUSION

Deng and Liu [49] state that although generally taken as a constant, blood perfusion is in fact a transient value even under a physiological basal state. This is due to external perturbation and the self-regulation of a biological body. They quantified the relations between blood perfusion and temperature fluctuations in living tissue using Pennes Bio-heat Equation.
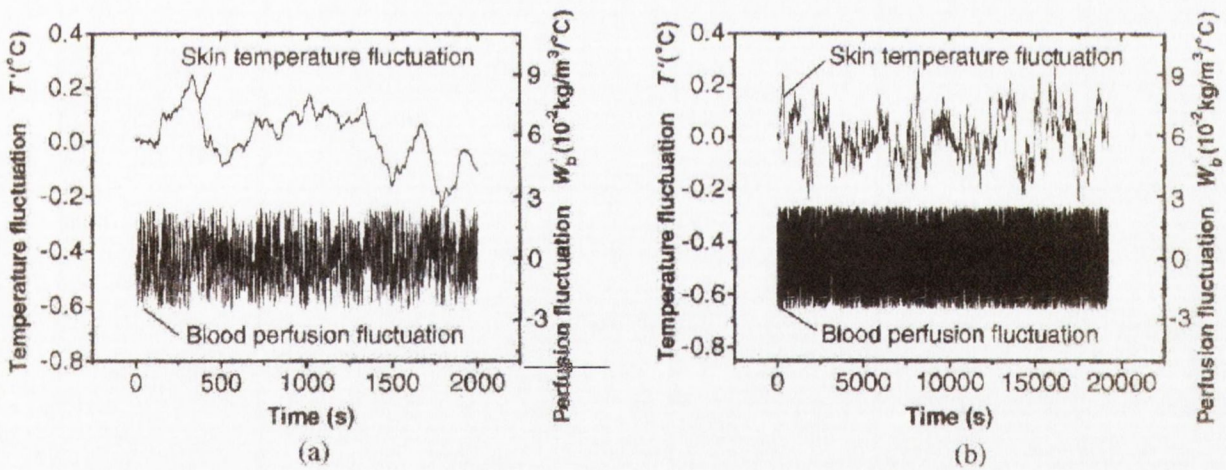
Figure 3-9 (a,b) Temperature fluctuations die to pulsative blood perfusion $\omega_{bas} = 0.0005(/s)$ Deng and Liu [49]

To simulate this perturbation they superimposed onto the basal perfusion rate of 0.0005/s a randomly varying perfusion level of a much lower magnitude. From these results they concluded that a small perturbation in blood perfusion results in an observable temperature fluctuation in the living tissues. Thus one cannot expect to ever attain perfectly steady temperature readings at the skin surface.

Craciunescu and Clegg [50] note from their study on the effect of pulsatile blood flow on temperature distribution that it is reasonable to assume a non-pulsating blood velocity for the purposes of estimating bio heat transfer. Randall et al. [51] note that vascular perfusion is not uniform in space or time, nor is there sufficient blood in the body to simultaneously perfuse the entire vascular bed. Instead the vasculature is continuously shunting blood through one region of tissue and then another. This process is mainly under the control of the autonomic nervous system and is further modulated by local metabolic needs. Essentially the vasculature is a hyper-reactive organ capable of varying the blood supply to local tissue sites by as much as an order of magnitude within a few seconds. Even at rest, modulation of tissue perfusion occurs in the form of vasomotion. Cui and Barbenel [52] note that local skin temperature is determined principally by the level of tissue blood perfusion, metabolic activities, the thermal properties of the tissue and the local environmental conditions.

3.6 VARIATION OF PERFUSION AND METABOLIC RATE WITH TISSUE TEMPERATURE

Rai and Rai [53] note that for all practical purposes the level of tissue metabolism is directly related to the tissue temperature as a function of the basal metabolic rate. This is known as the Q10 effect and is described by Eq. 3-5:

$$\dot{q}_{meta} = \dot{q}_{metabas}(2)^{(T-37)/10} \qquad \text{Eq. 3-5}$$

where $\dot{q}_{meta}$ is the rate of metabolic heat generation, $\dot{q}_{metabas}$ is the basal rate of metabolic heat generation and T the tissue temperature. It states that for a tissue temperature drop of 10°C there results a halving of the heat production.

A number of models exist which relate tissue temperature to skin perfusion. Stolwijk's model [54] relates perfusion to the metabolic heat production (Q10 effect)

$$\omega_{sk} = \dot{q}_{metabas} \cdot 2^{(T_{sk}-T_{sk,0})/10} \qquad \text{Eq. 3-6}$$

$$\omega_{sk} = \dot{q}_{metabas} \cdot 2$$

where $\dot{q}_{metabas}$ is the basal metabolic rate, T_{sk} the skin temperature and $T_{sk,0}$ the basal skin temperature. Fiala [55] incorporates an extra term (C_s) to represent vasoconstriction. The C_s term describes the reaction of local skin blood flow to variations in mean skin temperature of the whole body. This of course requires measurements to be made over the whole body surface, which is not the aim of this study.

$$\omega_{sk} = \frac{\dot{q}_{metabas}}{1 + C_s} \cdot 2^{(T_{sk} - T_{sk,0})/10}$$

Eq. 3-7

The relationship between tissue temperature and perfusion is further discussed in section 4.1.1.

3.7 VARIATION IN THERMO-PHYSICAL PROPERTIES

A full table of tissue thermal properties is given in Appendix A 1. There is a reasonable agreement on tissue thermal properties presented in the literature; however the values used were taken predominately from Fiala et al. [55]. It has been shown by Draper and Boag [56] and Wilson and Spence [57] that there is a variation in the thermal properties of tissue with tissue hydration levels and perfusion levels. An evaluation of the significance of these variations is included in Section 6.5.3.

3.8 SUMMARY

Since Pennes' paper was published in 1948 a number of the assumptions made in the derivation of the bio-heat equation have been shown to be incorrect. To address these deficiencies more physiologically realistic models were developed, often for specific applications such as detection and treatment of cancer by hyperthermia. However, many of these models require large amounts of anatomical data and their complicated formulations make them either difficult or impossible to solve. This encouraged a trend for the development of more easily applicable bio-heat formulations.

The central question is therefore whether to persist with Pennes simple formulation or to adopt one of the more complicated models. A number of researchers have

addressed this question. Nelson [58] notes that validation of the Pennes model has been confirmed by a range of studies and that despite its simplicity the model has shown consistency with observations when applied to perfused phantoms (i.e. mock ups of limbs) and to simulating temperature fields in the human brain. Arkin et al [2] note that, even though it is evident that Pennes' interpretation of vascular heat transfer falls short of describing the actual thermal equilibration process, the Pennes' model predicts realistic tissue temperature in perfused kidneys as long as the measurements are made reasonably far away from large blood vessels. Wilson and Spence [57] also support use of the Pennes' bio-heat equation. They state that while other formulations can be used in specific tissue regions, they are too complicated to apply generally. Basch's [38] statistical analysis showed the mean temperature to be accurately predicted by Pennes equation.

Therefore this review of the relevant literature suggests that the best approach is to use Pennes' equation while incorporating a correction or efficiency factor, as proposed by Baish [38] and Brink and Werner [36] to account for counter current re-warming of the vein. Further justification for this approach is that the vessels identified by Chen and Holmes [24] as the sites of thermal equilibrium are still very numerous in their occurrence, making the assumption of uniform heat generation reasonably realistic. This approach gives an easily applicable and realistic representation of perfused tissue heat transfer. In defence of Pennes, it is not often noted that he in fact included such a term (k) in his original formulation to account for incomplete heat exchange between blood vessel and tissue. This can be seen in Eq. 3-8. However, he assumed this term to be equal to zero and so it is not included in the standard expression, represented by Eq. 3-1.

$$\dot{q}_{per} = (\rho C \omega)_b (k_{pen} - 1)(T_v - T_a) \qquad \text{Eq. 3-8}$$

38

4 EXISTING METHODS OF MEASURING BLOOD PERFUSION

A range of thermal and non-thermal techniques for measuring blood perfusion will be outlined in this chapter. Some of these methods are used in commercial systems while others represent past or ongoing research concepts.

4.1 THERMAL METHODS

Various thermal methods have been developed where the skin is either heated or cooled. In heating one can relate the power needed to heat the tissue to the perfusion while in cooling the heat flux or temperature change at the skin surface can be related to the perfusion.

4.1.1 Introduction to Forced Convection Approach (FCA)

The forced convection approach, the basis for which is Pennes [19] bio-heat equation, relates blood perfusion to surface measurements of heat flux and temperature made during cooling of the skin. Figure 4-1 and Figure 4-2 show typical results for predicted skin temperature and heat flux from the numerical model developed during this study. Cooling is used to mitigate the lack of strong quantitative heat flux signals under natural convection and to increase the sensitivity of the perfusion measurement. Michener et al. [59] notes that in the forced convection approach this is achieved by applying an air or water jet flow to the skin. Such tests are dependent on a large number of variables such as the convective heat transfer coefficient, the design of the cooling system, the contact pressure and numerous physiological effects, as outlined in chapter 2. O'Reilly [60] notes that the results from the forced convection approach indicate good heat flux sensitivity and measurement repeatability.

Figure 4-1 and Figure 4-2 show temperature and heat flux responses for various perfusion values during a numerical simulation of a forced convection test. Cooling of the skin starts at $t=0s$ and continues until $t=120s$. The initially high heat flux values are due to a large difference between skin and cooling air temperature. This

causes a rapid drop in skin temperature which in turn reduces the temperature difference and hence the rate of heat loss.
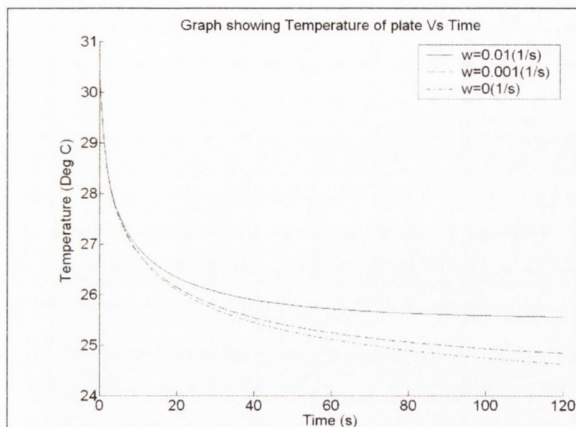
Figure 4-1 Effect of variation of perfusion on temperature curve
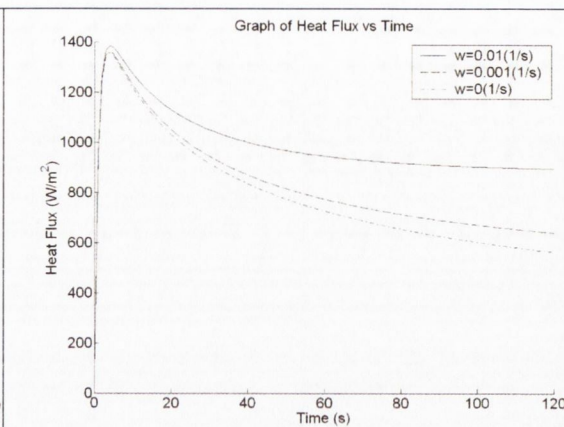
Figure 4-2 Effect of variation of perfusion on heat flux curve

As it is well established that two of the main determinants of perfusion are the ambient and tissue temperature it is logical to question the validity of a technique which deliberately varies the skin temperature and local convective heat transfer conditions. However it is thought that the zone in question is so small that the signal sent from the nerves in this area (when they undergo a change in temperature) is not large enough to effect a change in the global or local blood flow to this area, Bell [61].

4.1.2 Previous perfusion studies carried out with FCA

Most of the work using this technique has been carried out at Virginia Polytechnic Institute and State University under the supervision of Dr T.E. Diller. The first study was conducted by Michener et al. [59] in 1991. Tests were carried out using a water-cooled probe with a temperature and heat flux sensor on its base. A 2-D numerical model was developed to provide predictions of the transient heat flux and the sensitivity of the probe to the tissue perfusion using Pennes standard assumptions. All boundaries of the tissue control volume were defined as insulated except for the boundary under the probe.

Testing was carried out on two dogs. A vasodilating drug was used to increase the perfusion and a pressure cuff to reduce it. The experimental and numerical results

reported by Michener et al. [59] compared reasonably well with one another. It was noted that the effect of perfusion becomes more evident towards the end of a test as is also apparent in Figure 4-2. While the tests qualitatively matched the analytical predictions, due to uncertainties with parameters such as the contact resistance it was not possible to arrive at quantitative values of perfusion. It was found that the greater the contact resistance the less sensitive the test became to a variation in perfusion.

This work was continued by O'Reilly et al. [60]. A new probe was developed and testing was carried out on human subjects. However, the computer model was merely updated to account for the new model geometries. The new probe featured many improvements, including the use of compressed air for cooling. The air initially flows into a mixing chamber and then through an array of 0.8mm diameter holes giving 16 jets which impinged on and cooled the copper base plate which was held in contact with the skin. This is shown in Figure 4-3 below. Testing was carried out on the forearm and lasted about 60 seconds.
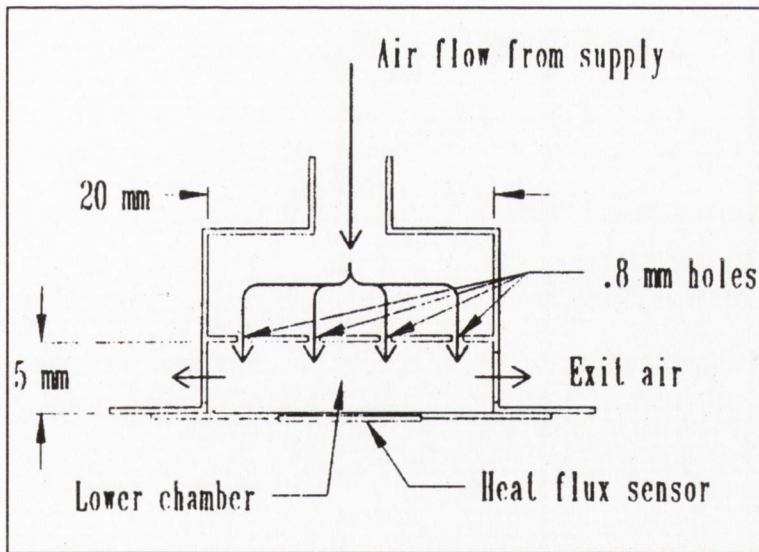
Figure 4-3 Blood perfusion probe, from O'Reilly [60]

The analytical results of O'Reilly et al. [60] indicate that the value of contact resistance is the dominant factor early in the test. Matching the initial experimental and numerical peaks gives the value of contact resistance to be used in the model. Using this value for contact resistance, O'Reilly [60] then varied the value of perfusion till the decay parts of the curve also matched. This is discussed further in

Section 6.4.2. Again it was found that by 60 seconds into the test, perfusion had established itself as the key factor.

Although heat flux curves predicted by the program were found to match well with experimental data the same was not true of predicted and experimental temperature curves. The predicted temperature curves from the numeric model tended to decrease much more rapidly than the experimental curves. This was thought to be due to the off centre location of the thermocouple which was due to the large size of the heat flux sensor.

Scott et al. [62] and [63] carried out the final study to date in this area using the same probe and computer model as used by O'Reilly et al. [60]. The main objective was to evaluate the measurement sensitivity and to develop a systematic methodology for the estimation of cutaneous blood perfusion from the heat flux and temperature measurements. Scott et al. [62] and [63] found that the sensitivity coefficients for both heat flux and temperature are high with respect to contact resistance and are relatively low with respect to blood perfusion, which is the exact opposite of what is desired. This suggested that parameters such as cooling time could be optimised to provide higher sensitivity with respect to blood perfusion. They found, there was an improvement in the sensitivity coefficients for blood perfusion with respect to temperature after the air flow was stopped at 60 seconds and while the skin was re-heating.

It was also found by Scott et al. [62] that, the sensitivity of perfusion with respect to heat flux is small at the beginning of the experiment while the sensitivity of the contact resistance is much larger. This supports the findings of O'Reilly et al. [60] and suggests that when analysing results more consideration should be given to readings nearer the end of the measurement interval.

4.1.3 Thermal Diffusion Probe

Newman et al. [64] carried out their study in 1995, in a continuation of work started by Balasubramaniam and Bowman [65] in 1977. The basis of the method is straightforward: a self heated thermistor is either placed on the tissue surface or inserted into the tissue volume and is heated to a small fixed temperature increment

(2-4°C) above the baseline temperature of the tissue. The electrical heating power necessary to maintain the temperature elevation is related to tissue perfusion by a mathematical model, which describes the probe-tissue thermal interactions. Perfusion is then inferred by attributing it to the enhanced ability of perfused tissue to transport heat above that due solely to conduction.

However, the limitation to this technique is that the entire range of physiologically realistic values of blood perfusion represents only a 4% variation in effective conductivity (i.e. perfusion enhanced conductivity). Newman et al. [66] also note that intrinsic thermal conductivity is a dynamic parameter, which changes over time with the level of tissue hydration. This introduces a level of uncertainty to the theory underpinning the method.

Initial *in-vivo* studies were conducted by inserting a thermistor into the skin and muscle of a rabbit's epigastric flaps. The site was then subjected to repeated arterial occlusions. While the results look promising (Figure 4-4) a major difficulty with the approach is its invasive nature, which leads to discomfort, tissue trauma and possibly local tissue infection. This may be less of a problem in surgical procedures where already there would be significant trauma.
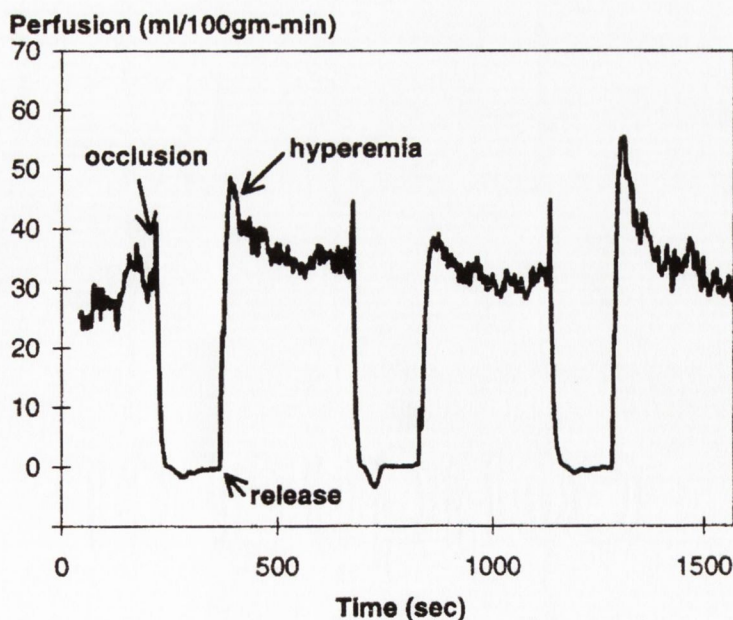
Figure 4-4 Invasive thermal probe measurements in a rabbit epigastric flap supplied by an isolated pedicle and subjected to repeated arterial occlusions. Newman et al. [64]

4.1.4 Sinusoidal Heating Method

Liu and Xu [67] found, when applying an intentionally varying sinusoidal heating load to the skin surface, that there was a correlation between perfusion and the phase shift between the heating curve (lines 2 and 3 in Figure 4-5) and the skin temperature (line 1 in Figure 4-5). The relationship is described in Eq. 4-1:
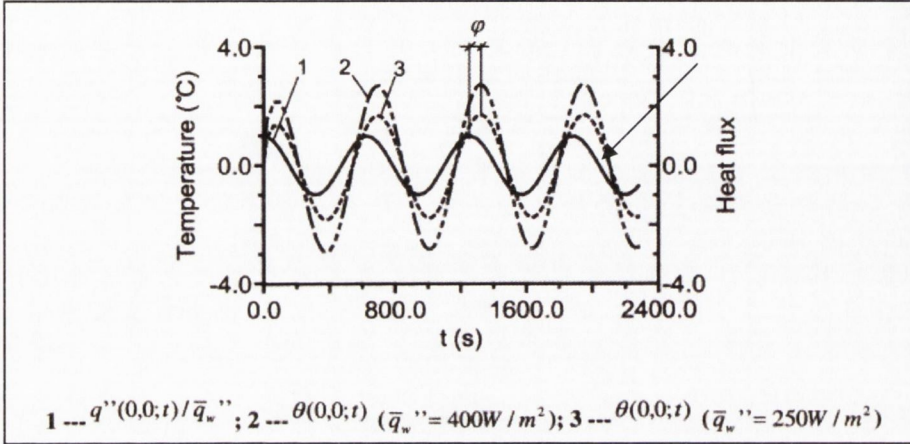
Figure 4-5 Transient temperature and heat flux at the skin surface point (0,0) for a perfusion level of 0.0005/s and a heating frequency of 0.016/s from Liu and Xu [67]

$$\omega_b = -\frac{\rho C \varsigma}{t(2\varphi).\rho_b C_b} \qquad \text{Eq. 4-1}$$

where density (ρ_p), specific heat capacity (C) and heating frequency (ς) of the probe are related to time (t), phase shift (φ), density (ρ_b) and specific heat capacity of the blood (C_b). The disadvantages of the phase shift method are that testing times are relatively long (up to 30 minutes) and the experimental set-up used to generate the sinusoidally varying heating load is rather cumbersome. Also, as with any heating method, there is always the risk of overheating the tissue which could cause tissue damage.
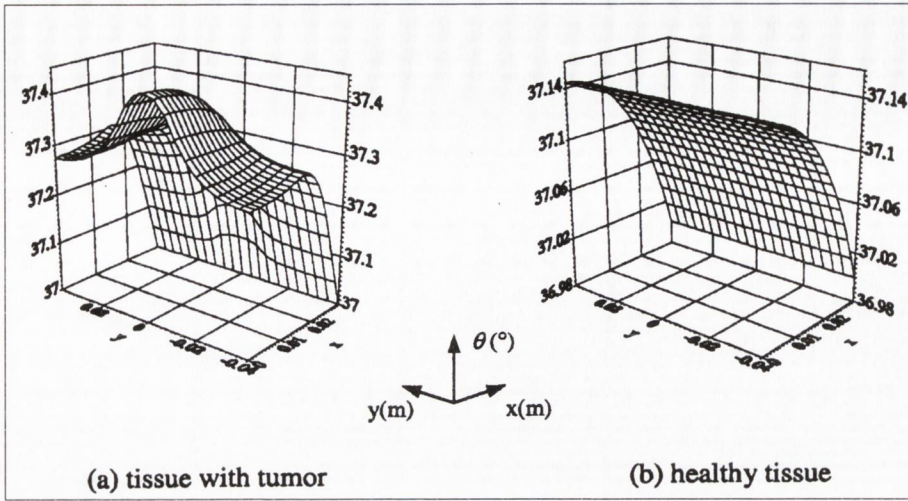
Figure 4-6 Steady state skin temperature distributions, from Lui and Xu [67]

In the same study Lui and Xu [67] then used steady state temperature readings to identify tissue tumour sites. Figure 4-6 shows the predicted change in steady state skin temperature distribution (due to different levels of blood perfusion and metabolic heat generation) present at a tumour site when the measurement region is covered by an insulating material. Given the small magnitude of temperature difference, high-resolution thermal sensors or infrared thermometry are required for this application. To improve sensitivity, forced convection can be applied to the skin (Figure 4-7). This part of the study is therefore similar to that of Michener [59], O'Reilly [60] and Scott [62].
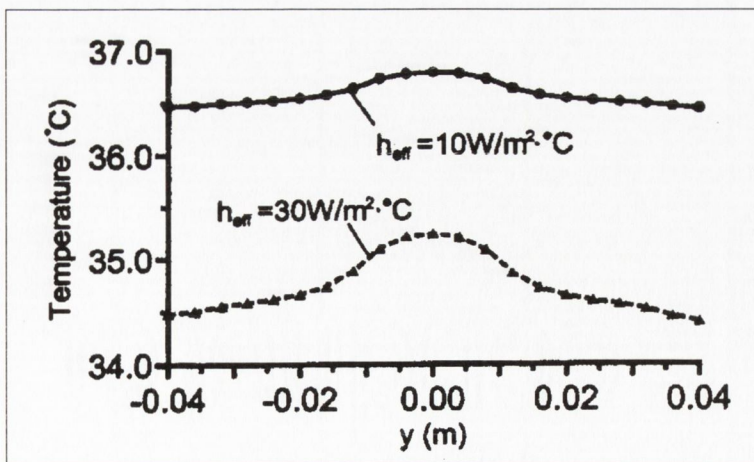
Figure 4-7 Numerical comparison of temperatures at the skin surface (tissue with a tumour) under different convection coefficients, Lui and Xu [67]

4.1.5 Wilson and Spence's Induced Cooling method

Wilson and Spence [57] used a cold metal block to induce cooling in their study. Their work is therefore similar in concept to that of Michener [59], O'Reilly [60] and Scott [62], only differing in the cooling method. A transient 1-D finite difference bio-heat model incorporating five tissue layers was developed. They related perfusion to surface temperature readings rather than surface heat flux readings as in the forced convection approach. Figure 4-8 shows results from the model after 15s of cooling from the block (curve B). Curve A is the initial steady state solution. Curves C and D are tissue profiles after 10s and 100s reheating respectively under laboratory conditions.
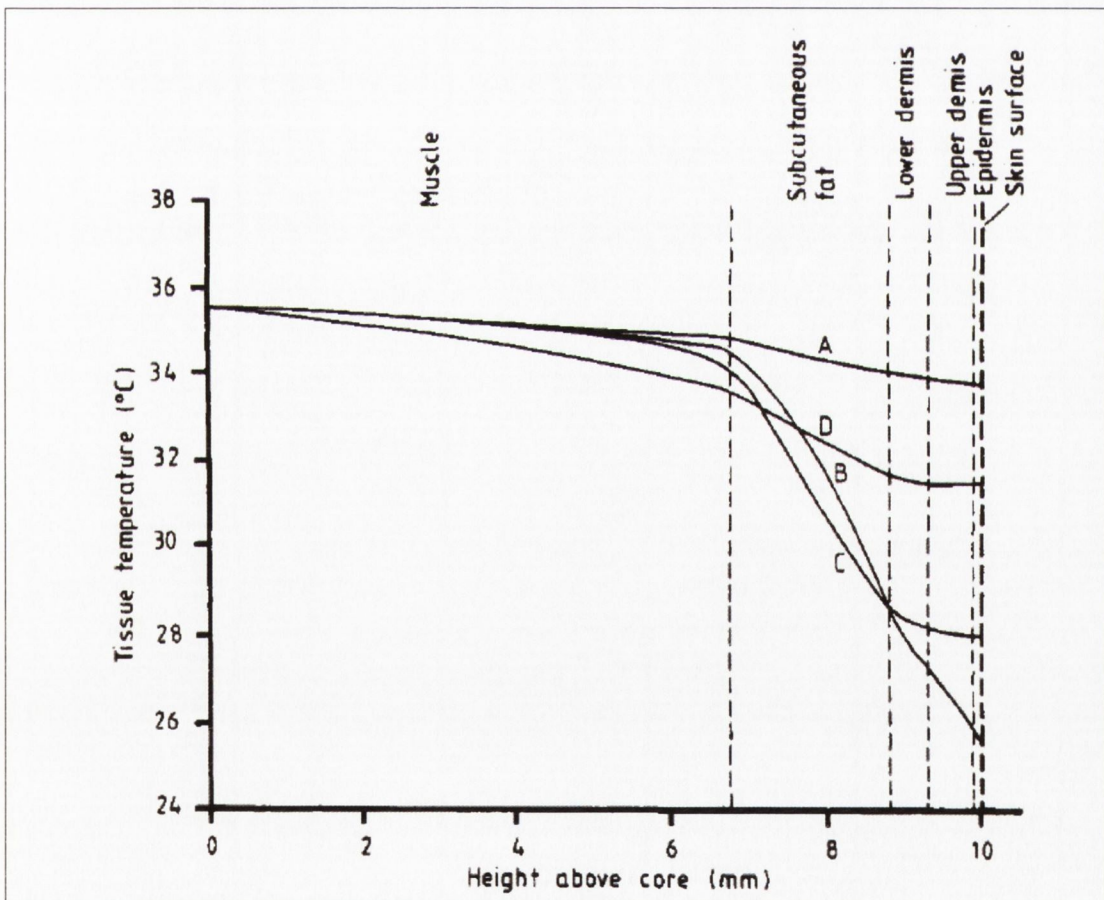
Figure 4-8 Predicted tissue temperature profiles before and after transient cooling, from Wilson and Spence [57]

For estimation of perfusion they focus on the re-heat part of the test. They found the initial slope of the surface reheat curve, up to roughly 30s post cooling to be mainly a function of tissue thermal properties rather than perfusion. Subsequently the surface temperature reheat curve becomes a function of dermal perfusion, with the optimum

dependence of the reheat curve on dermal perfusion occurring around 100s post-cooling. Figure 4-9 shows reasonable correlation between non-dimensionialised experimental and numerical results but Wilson and Spence [57] conclude that further investigations must be carried out to determine the value of dynamic temperature measurements for measuring dermal perfusion.
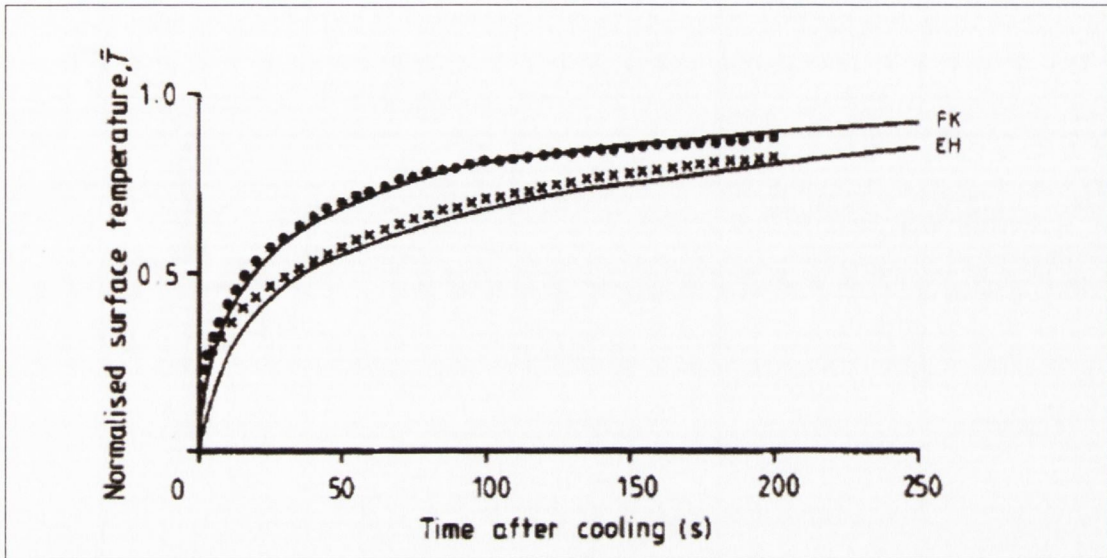
Figure 4-9 Comparison of experimental --- and theoretical ••• normalized reheat rates for subjects FK and EH, from Wilson and Spence [57].

4.2   Non-thermal Methods

Rådegran [68] presents a comprehensive review of present techniques for measuring blood flow in human subjects and offers advice as to when each is most suitable. The most commonly used techniques are listed below.

4.2.1 Radioactive tracers

Technetium-99m serum albumin can be used as a radioactive tracer to detect absolute blood flow, however it has the obvious drawback of introducing a radioactive substance to the patient. Sadaba et al. [69] used it successfully in a recent study to assess the function of the hand after harvesting of the radial artery for myocardial revascularization.

4.2.2 Plethysmography

This is one of the most common and accepted methods of measuring total limb blood flow. A pressure cuff is placed on the limb in question (for the forearm it is placed

47

above the elbow). The cuff is inflated above diastolic pressure but below the systolic, allowing blood to enter the limb but not leave. The cuff incorporates a very small diameter flexible tube containing mercury. The arm swells as the blood enters (but cannot leave) so the tube lengthens. The change in length is proportional to the change in resistance of the tube (which is measured using a wheatstone bridge). The rate of change in length of the mercury filled tube can then be used to work out a rate of change in volume of the arm which is equal to the rate at which the blood is entering for the first few seconds before the back pressure increases. The cuff is then deflated and the blood is allowed to flow again. After about 20 seconds the cuff may be inflated again. This process can be carried on almost indefinitely.

This method is very well accepted and used in many blood flow studies. However, it only measures the total inflow of blood to a limb and so one cannot use it to isolate the level of perfusion to the individual tissues.

4.2.3 Laser Doppler

Perhaps the most successful method to date is the Laser Doppler approach. While this method is currently being used, its disadvantages are its high cost and the fact that it can only detect changes in perfusion and is not able to measure absolute values.

Light is transmitted to the tissue via a fibre-optic probe. When this light hits moving blood cells, it undergoes a change in wavelength (Doppler shift). The magnitude and frequency distribution of these changes are directly related to the number and velocity of blood cells, i.e. the blood perfusion. Measurements obtained from laser Doppler flowmeters are intrinsically of a relative nature. Although such measurements are proportional to perfusion, the factor of proportionality will be different for different tissues.

The term commonly used to describe blood flow measured by the laser Doppler technique is 'flux': a quantity proportional to the product of the average speed of the blood cells and their number concentration (often referred to as blood volume). This is expressed in arbitrary 'perfusion units' (PU). When a larger volume of tissue is stimulated to vasodilate or vasoconstrict, or where for example a healing process

results in increased blood flow, the measured blood flow changes in the small tissue volume are generally taken to be representative of the larger volume.

In a Laser Doppler blood flow Imager (LDI) the low intensity laser beam is scanned across a tissue surface in a raster fashion using a moving mirror. Thus both large and small areas can be scanned.

4.3   CONCLUSION

There are a number of possible approaches for measuring blood perfusion. The laser Doppler method suffers from the fact that it can only give relative and not absolute measurements of blood perfusion. Various heating methods exist but these have an associated risk of damaging the tissue due to overheating and some methods are based on invasive procedures, which cause discomfort to the patient and give rise to the risk of infection. The thermal probe proposed by Newman [66] is very sensitive to very small variations in thermal conductivity. The phase shift approach developed by Liu and Xu [67] has merit but the tests take up to thirty minutes to run which makes them impractical in a clinical environment. Wilson and Spence's [57] approach is, in essence, very similar to the Forced Convection Approach. It is felt that cooling by forced convection offers greater control than contact with a cooled metal block which would also give rise to more uncertain skin contact resistance.

As yet no one approach has been able to deliver a practical, cost effective and accurate solution for the problem of measuring blood perfusion in skin tissue. However of all the approaches the forced convection approach seems the most promising. It is safe, quick, cheap, non-invasive and no more restrictive to the patient than a standard electrode. In theory it should also give absolute measurements without the need for no-flow calibrations. This confirmed the initial decision to pursue the forced convection approach.

A number of issues were identified in the studies carried out at Virginia Tech, which need further investigation. These include development of a more comprehensive model with improved boundary and initial temperature profiles. A multi layer model is also required. Improvement of the probe strapping method is necessary, to decrease the level of contact resistance, which has been found to decrease the sensitivity of

readings to perfusion levels. Experimental verification of the results with other methods is also required along with optimisation of cooling times and cooling loads.

Thus the decision was made to focus on a refined implementation of the forced convection approach, with the issues described above being addressed. The next chapter describes the development of the various numerical models, for use in conjunction with experimental measurements obtained from a blood perfusion probe.

5   Numerical Model

5.1   Introduction

The aim of computer modelling is to accurately represent the experimental procedure in order to allow a value of perfusion to be estimated. The model outputs a temperature map of a representative area of the arm by solving the bio-heat equation with appropriate boundary and initial conditions. Both transient and steady state models were developed and will be discussed. Numerical techniques are used as the geometry and boundary conditions are too complicated to allow solution using analytical methods. To estimate the perfusion level in the tissue the value of perfusion is altered in the model until the numerical and experimental surface temperature readings match. This chapter will discuss the various modelling programs used, the theory of operation underpinning them and the merits and disadvantages of each. Specific details about their application will be dealt with in the subsequent chapters. Both steady state and transient two-dimensional (2-D) models were used. A three-dimensional (3-D) model was developed to test the 2-D assumption.

Finite Difference Scheme implemented in MatLab

The first model was a finite difference solution written and implemented in MatLab specifically for this study. At the time this approach offered the greatest flexibility for dealing with the bio-heat equation. While the model became quite sophisticated over the period of its development it was restricted to simple rectangular 2-D or 3-D meshes. When it became necessary to model the curvature of the arm it was decided to use a commercially available package with the necessary meshing abilities rather than developing custom code in MatLab. Nonetheless, much valuable work was made using the finite difference model and thus is described here.

Finite element modelling using Ansys and FemLab

Initially Ansys was employed as it was readily available, but while the geometry and boundary conditions could easily be incorporated there were no suitable elements for dealing with the perfusion term. An element was needed which could handle internal generation as a function of tissue temperature.

However at this time a new version of FemLab was released incorporating the bio-heat equation. This allowed the complex geometries to be modelled in 2-D and 3-D for both steady-state and transient situations.

5.2 FINITE DIFFERENCE METHOD

The finite difference approach is a well established numerical method which has been applied to a wide range of heat transfer problems. A numerical technique calculates the temperatures at discrete points (nodes) which are generally spaced at regular increments across a domain. A differential equation such as the Conduction Heat Equation (Eq. 5-1) must be re-written in terms of finite difference approximations, which approximate differential increments in the temperature between nodes. The smaller the node spacing the more closely the true temperature distribution will be represented. A brief description of finite difference formulations is given in this and subsequent sections but a full description is available in any standard text such as Holman [70] and Incropera and DeWitt [71].

The Bio-heat equation is very similar in form to the Conduction Heat Equation (Eq. 5-1), when the perfusion and metabolism terms are treated as a type of internal generation as shown in Eq. 5-2.

$$\frac{\partial^2 T}{\partial x^2} + \frac{\partial^2 T}{\partial y^2} + \frac{\partial^2 T}{\partial z^2} + \frac{\dot{q}}{k} = \frac{1}{\alpha}\frac{\partial T}{\partial t} \qquad \text{Eq. 5-1}$$

$$\dot{q} = \dot{q}_{per} + \dot{q}_{meta} \qquad \text{Eq. 5-2}$$

or, by expanding the perfusion term,

$$\dot{q} = (\rho C \omega)_b (T_a - T_v) + \dot{q}_{meta} \qquad \text{Eq. 5-3}$$

52

5.2.1 Two-Dimensional steady-state problems

The first step is to develop a solution for a 2-D steady state problem. The appropriate form for a steady state 2-D system with internal generation (such as the bio-heat equation) would be:

$$\frac{\partial^2 T}{\partial x^2} + \frac{\partial^2 T}{\partial y^2} + \frac{\dot{q}}{k} = 0$$

Eq. 5-4

A meshing algorithm is required to select points at equal intervals (m,n) across the domain, as shown in Figure 5-1, to which the finite difference formulation may be applied.
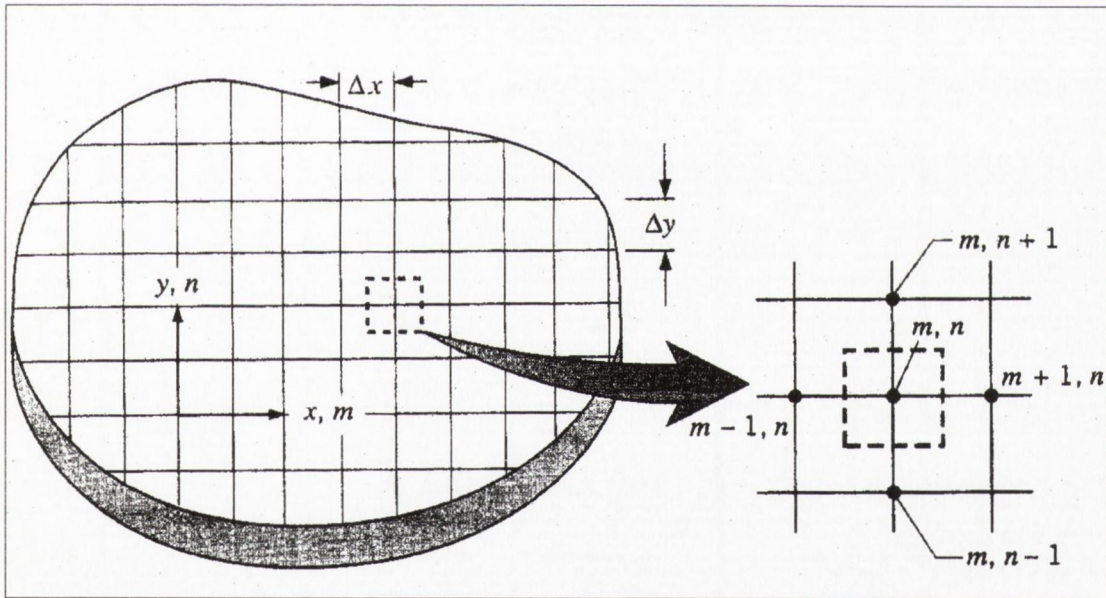
Figure 5-1 Mesh with individual node from Incropera and DeWitt [71]

Once the nodes are chosen it is necessary to reduce the appropriate form of the heat conduction equation (in this case Eq. 5-4) to the finite difference form of the equation. For example, for an internal node in a mesh with internal generation, where $\Delta x = \Delta y$ we obtain:

$$T_{m,n+1} + T_{m,n-1} + T_{m+1,n} + T_{m-1,n} + \frac{\dot{q}(\Delta x)^2}{k} - 4T_{m,n} = 0$$

Eq. 5-5

Hence for the *m,n* node the heat equation is reduced to an approximate algebraic equation. This form of the heat equation may be applied to any interior node that is equidistant from its four neighbouring nodes.

One can also write suitable equations for

- Convective boundary nodes
- Exterior corners with convective boundaries
- Insulated boundaries
- Interior nodes near curved boundaries

Solution of finite difference equations

Once the nodal network has been established and an appropriate finite difference equation has been written for each node, the temperature distribution may be determined. The problem reduces to one of solving a system of linear, algebraic equations. The nodal equations may be written as:

$$
\begin{aligned}
a_{11}T_1 + a_{12}T_2 + \cdots + a_{1n}T_n &= C_1 \\
a_{21}T_1 + a_{22}T_2 + \cdots\cdots\cdots &= C_2 \\
a_{31}T_1 + \cdots\cdots\cdots\cdots\cdots &= C_3 \\
\cdots\cdots\cdots\cdots\cdots\cdots\cdots\cdots & \\
a_{n1}T_1 + a_{n2}T_2 + \cdots + a_{nn}T_n &= C_n
\end{aligned}
$$

Eq. 5-6

where $T_1, T_2, \cdots, T_n$ are the unknown nodal temperatures. By using matrix notation

$$
[A] = \begin{bmatrix}
a_{11} & a_{12} & \cdots & a_{1n} \\
a_{21} & a_{22} & \cdots & a_{2n} \\
a_{31} & a_{32} & \cdots & a_{3n} \\
\cdots & \cdots & \cdots & \cdots \\
a_{n1} & a_{n2} & \cdots & a_{nn}
\end{bmatrix}
\quad
[C] = \begin{bmatrix}
C_1 \\
C_2 \\
\cdot \\
\cdot \\
C_n
\end{bmatrix}
\quad
[T] = \begin{bmatrix}
T_1 \\
T_2 \\
\cdot \\
\cdot \\
T_n
\end{bmatrix}
$$

Eq. 5-7

$$
[A][T] = [C]
$$

Eq. 5-8

The solution can then be found by finding the inverse of A such that

$$[T] = [A]^{-1} [C]$$

Eq. 5-9

As the matrix contains a large number of zero elements and so is quite sparse, a Gauss Seidel iteration method is very efficient at solving the problem quickly.

Some precautions

It is important to verify that a numerical solution has been correctly formulated by performing an energy balance on a control surface about the nodal regions whose temperatures have been evaluated. Even when the finite-difference equations have been properly formulated and solved, the results may still represent a coarse approximation to the actual temperature field. This behaviour is a consequence of the finite spacing between nodes and of finite-difference approximations to Fourier's law of conduction. The mesh size should be reduced to the point where reducing it further has no significant effect. Such grid independent results will provide an accurate solution to the physical problem provided the equations themselves can accurately represent the physical process. Another method used to verify the system of equations is to compare the results with a simpler analytical solution.

5.2.2 Transient solution to heat equation

With the Forced Convection Approach a transient solution is necessary to model the change of skin temperature with time on application of the cooling load. The 3-D heat equation with internal heat generation is:

$$\frac{\partial^2 T}{\partial x^2} + \frac{\partial^2 T}{\partial y^2} + \frac{\partial^2 T}{\partial z^2} + \frac{\dot{q}}{k} = \frac{1}{\alpha} \frac{\partial T}{\partial t}$$

Eq. 5-10

Again there are various procedures for determining the time dependence of the temperature distribution within a solid during a transient process. Depending on complexity the following methods may be used:

- The lumped capacitance method (negligible temperature gradients)
- Exact solutions (not used in this study)

55

- Numerical (Finite difference) methods

The lumped capacitance method

This is the simplest method for solving transient heat conduction problems. It works by assuming that the internal temperature variation in space is negligible and in effect that the temperature distribution within the body is uniform at any instant in time. Such systems are obviously idealised as a temperature gradient must exist in a material if heat is to be conducted into or out of the material.

This approximation is only reasonable when the surface convective resistance is large compared with the internal conduction resistance (as with the copper base plate on the probe). Such analysis may be expected to yield reasonable estimates when the following condition is met:

$$Bi = {h\Delta x}/{k} << 0.1$$

<div align="right">Eq. 5-11</div>

where Bi is the dimensionless number known as the Biot number, Δx and k are the thickness and the thermal conductivity of the plate and h is the convective heat transfer coefficient. The Biot Number plays a fundamental role in transient conduction problems that involve surface convection effects. It gives the ratio between the temperature drop in the solid and the temperature difference between the solid surface and the fluid.

Transient finite difference method for 2-D Heat Equation

If the temperature gradients within the solid are no longer negligible then spatial effects must be considered. As before the perfusion and metabolism terms are included as forms of internal generation in the heat equation. The solution to these partial differential equations provides the 2-D variation of temperature with both time and the spatial coordinates.

$$\frac{\partial^2 T}{\partial x^2} + \frac{\partial^2 T}{\partial y^2} + \frac{\dot{q}}{k} = \alpha \frac{\partial T}{\partial t}$$

<div align="right">Eq. 5-12</div>

It can be shown that the temperature depends on the following factors:

$$T = T(x, y, T_i, T_\infty, L, k, C, \rho, h, \dot{q}) \qquad \text{Eq. 5-13}$$

where x and y are the distances from the half plane thicknesses, t time, T_i the initial temperature, T_{atm} ambient temperature, L the half plane thickness, α the thermal diffusivity, h the convective heat transfer coefficient and $\dot{q}$ the rate of internal heat generation. These in turn can be re-cast in the following dimensionless groups

$$\theta^* = f(x^*, y^*, Fo, Bi) \qquad \text{Eq. 5-14}$$

where θ^* is dimensionless temperature

$$\theta^* = \frac{T_t - T_a}{T_\infty - T_a} \qquad \text{Eq. 15}$$

The Fourier Number (Fo) can be physically interpreted as the ratio of heat transferred by conduction and the rate of change of energy storage. Hence the Fourier number provides a measure of the relative effectiveness with which a solid conducts and stores thermal energy. Dimensionless spatial coordinate (x^*, y^*) are defined where (L) is the half plane thickness. This generalization greatly simplifies the presentation and utilization of transient solutions; the dimensionless variables are used extensively in the model's implementation.

Solution of transient problems by finite difference methods

Both *explicit* and *implicit* forms of finite-difference approximations are available for transient conduction problems. The explicit form is easy to implement but must conform to certain stability criteria. The implicit method is more cumbersome to implement but benefits from being unconditionally stable and more numerically efficient. Both methods were implemented but ultimately the implicit method was chosen.

Discretization of the Heat Equation (Implicit Method)

The difference equation may be written by computing the space derivatives at the $p+1$ time increment.

$$\frac{\partial^2 T}{\partial x^2} \approx \frac{T^{p+1}_{m+1,n} + T^{p+1}_{m-1,n} - 2T^{p+1}_{m,n}}{(\Delta x)^2} \qquad \frac{\partial^2 T}{\partial y^2} \approx \frac{T^{p+1}_{m,n+1} + T^{p+1}_{m,n-1} - 2T^{p+1}_{m,n}}{(\Delta y)^2}$$

Holman [70] describes such an arrangement as a backward-difference formulation because the time derivative moves backward from the times for heat conduction into the node. The implicit form of the finite difference formulation (of the bio-heat equation) for an interior node is then:

$$T^p_{m,n} = (1+4Fo)T^{p+1}_{m,n} - Fo(T^{p+1}_{m+1,n} + T^{p+1}_{m-1,n} + T^{p+1}_{m,n+1} + T^{p+1}_{m,n-1}) + \frac{\dot{q}\alpha\Delta t}{k} \qquad \text{Eq. 5-16}$$

This backward-difference formulation does not permit the explicit calculation of the temperature T^{p+1} in terms of T^p. Rather, a whole set of equations must be written for the entire nodal system and solved simultaneously (using Gauss Seidel iteration for example) to determine the temperature T^{p+1}. Thus this method produces an implicit formulation for the future temperatures in the transient analysis. Relative to the explicit method the implicit formulation has the important advantage of being unconditionally stable, i.e. the solution remains stable for all space and time intervals. This means that there are no restrictions on Δx and Δt.

The obvious disadvantage of the implicit method is the larger number of calculations for each time step. For problems involving a large number of nodes however the implicit method may result in less total computer time expended for the final solution because the stability requirements may mean that very small time increments have to be imposed in the explicit method. Much larger time increments can be employed with the implicit method, thus speeding the solution.

5.3   Solution of bio-heat equation using FemLab

FemLab was developed for modelling a wide range of scientific and engineering problems based on partial differential equations (PDE's) which are solved using finite element methods. In its basic configuration FemLab allows the user define their own PDE's but specific modules are also available for application areas such as structural mechanics, electromagnetics and heat transfer. Within the heat transfer module there are three application modes, including one for heat transfer in biological tissue using Pennes' bio-heat equation. This section will describe the solution steps in solving a problem using the bio-heat application mode from drafting of the geometry, mesh generation, prescription of boundary conditions, through to solution of the problem and post-processing of the results. A screen capture of FemLab is shown in Figure 5-2 below.
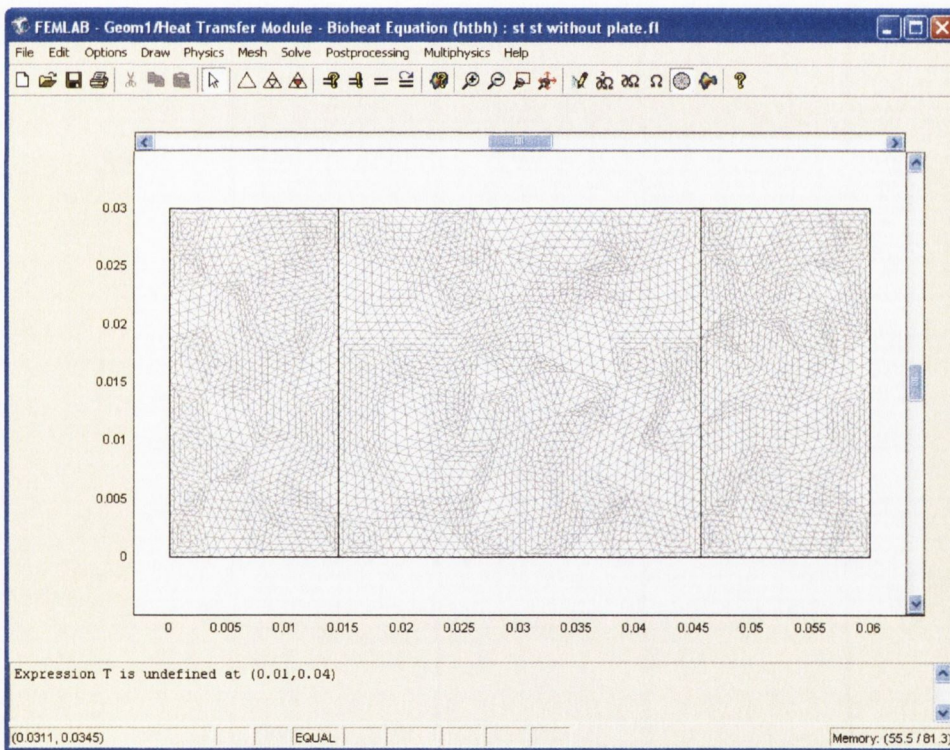
Figure 5-2 Screen capture from FemLab

Rao [72] describes the finite element method as follows. In the finite element method, the actual continuum or body of matter is represented as an assemblage of subdivisions called finite elements. These elements are considered to be interconnected at specified joints called nodes or nodal points. The nodes usually lie

on the element boundaries where adjacent elements are considered to be connected. Since the actual variation of the field variable (such as temperature) inside the continuum is not known, we assume that the variation of the field variable inside a finite element can be approximated by a simple function. These approximating functions (also called interpolation models) are defined in terms of the values of the field variables at the nodes. When field equations (like equilibrium equations) for the whole continuum are written, the new unknowns will be the nodal values of the field variable. By solving the field equations, which are generally in the form of matrix equations, the nodal values of the field variable will be known. Once these are known, the approximating functions define the field variable throughout the assemblage of elements.

The solution of a general continuum problem by the finite element method always follows an orderly step-by-step process. For a heat transfer problem the procedure can be stated as follows.

1. Idealisation
2. Interpolation
3. Defining element characteristic matrices and vectors
4. Assembly of element matrices and vectors and derivation of governing equations
5. Solution for nodal temperatures

5.3.1 Generation and visualisation of model

FemLab provides all the capabilities of a simple drafting package for generation of simple geometries. However it also allows the user to import geometry files from drafting and solid modelling packages such as AutoCAD or SolidWorks. For 2-D CAD geometries the standard DXF file format is used. If the DXF geometries contain small gaps that make it impossible to create a valid 2-D solid or extremely short edges which lead to very dense meshes the user can apply repair tolerance settings when importing the file that automatically close small gaps and/or join the short edges.

3-D geometric models may be imported using the IGES format, a neutral standard for exchanging geometric models among CAD systems. This process does not always work flawlessly as the IGES format uses the lowest-common-denominator approach

to describe a geometric model, which means that some information is generally lost. Further, the IGES format allows certain geometric models to have different representations, some of which are less compatible with the receiving system than others. Generally these difficulties can be overcome by drawing the object in a different sequence or by using different mating methods.

A number of visualization tools are available for viewing the completed geometry. It is possible to zoom and orbit around the model and also to apply advanced lighting and rendering techniques to create specialized visualizations, although these capabilities were not particularly required in this study.

5.3.2 Model Set-up

To set up a model the following must be defined: an equation set, material properties, boundary, interface and initial conditions. A new model may be created by customizing pre-defined equations or writing new PDE's. However as explained the bio-heat equation has already been defined in the heat transfer module. The material properties and boundary conditions are inputted into the relevant edit fields as shown in Figure 5-3 and Figure 5-4 respectively. An edit field can contain numerical values, mathematical and local functions, and any constants, expression or interpolation functions that have been defined.

Boundary conditions define the interface between the model geometry and its surroundings. For thermal models it is possible to apply constant temperature, insulated, or heat flux boundary conditions. In each case the appropriate equation is displayed as shown in Figure 5-4. One of the following interface conditions must be set on the interior boundaries: temperature continuity, heat flux discontinuity or constant temperature.

For the bio-heat equation FemLab only offers Lagrangian elements although the user can select the order of the element. The recommend default is to use quadratic elements. This reduces the number of elements required when compared to using linear elements but is more that sufficient to accurately handle the changing temperature gradients found in forced convection testing.

Subdomain Settings - Bioheat Equation (htbh)

Equation

$\nabla \bullet (-k \nabla T) = \rho_b C_b \omega_b (T_b - T) + Q_{met} + Q_{ext}$, T= temperature

Subdomain selection

```
1
2
```

☐ Select by group
☑ Active in this domain

Physics | Init | Element

Thermal properties and heat sources/sinks

Library material: [▼]   [Load...]

Quantity	Value/Expression	Description
δ_{ts}	1	Time-scaling coefficient
⦿ k (isotropic)	Thermal_cond(T)	Thermal conductivity of tissue
○ k (anisotropic)	0.5 0 0 0.5	Thermal conductivity of tissue
ρ	1069	Density of tissue
C	3700	Specific heat of tissue
ρ_b	1069	Density of blood
C_b	3700	Specific heat of blood
ω_b	0.00001*t+0.0005	Blood perfusion rate
T_b	36	Arterial blood temperature
Q_{met}	200	Metabolic heat source
Q_{ext}	0	Spatial heat source

[OK]   [Cancel]   [Apply]

Thermal
conductivity
as a function
of
temperature

Time varying
perfusion
level

Figure 5-3 Sub-domain settings dialog box from FemLab

Boundary Settings - Bioheat Equation (htbh)

Equation

$\mathbf{n} \bullet (k \nabla T) = q_0 + h(T_{inf} - T)$

Boundary selection

```
1
2
3
4
5
6
7
```

☐ Select by group
☑ Interior boundaries

Boundary sources and constraints

Boundary condition: [Heat flux ▼]

Quantity	Value/Expression	Description
q_0	0	Inward heat flux
h	h_free+((h_forced-h	Heat transfer coefficient
T_{inf}	21	h_free+((h_forced-h_free)*flc2hs(t-30,2))
T_0	0	Temperature

[OK]   [Cancel]   [Apply]

Equation
describing
boundary
condition

Heavyside
step function
for smoothing
sudden
change in
convective
heat transfer
coefficient

Figure 5-4 Boundary settings dialog box from FemLab

5.3.3 Meshing

The next stage is to mesh the model. For a 2-D geometry, it is possible to choose between generating an unstructured mesh consisting of triangular elements or a mapped mesh consisting of quadrilateral elements. However to use a mapped quadrilateral mesh, it is necessary that the geometry is 'rectangular' in shape, therefore unstructured meshes were generally used. A 3-D mesh is either generated as an unstructured mesh containing tetrahedral elements or by extruding or revolving a 2-D mesh.

FemLab offers the user control over a large number of mesh parameters which determine the global and local mesh density. All mesh parameters prescribe a maximum allowed mesh element size. The size of a local mesh element must not be larger than the minimum prescribed local element size determined by all mesh parameters. The maximum element size is by default $1/15^{th}$ that of the length of the longest parallel distance to an axis in the geometry. The element growth rate determines the maximum rate at which the element size can grow from a region with small elements to a region with larger elements. The default value is 1.3, that is, element size can grow by 30% from one element to another. The mesh curvature factor determines the size of boundary elements compared to the curvature. This controls how accurately the triangular elements can describe a curved boundary. Alternatively predefined settings can be used to generate a range of mesh densities from fine to course. Parameters may be applied to individual sub-domains or boundaries if locally high gradients are expected.

Two refinement methods are available to improve the quality of the mesh, namely regular or longest. The regular refinement method divides each element into four while the longest refinement method bisects the longest edge of each element. An on screen selection maybe made to apply refinement to only certain selected elements.

The mesh statistics dialog box gives statistical data for the current mesh including information such as the number of elements and the minimum element quality. All these capabilities allow a user generate and optimise a mesh that is both

computationally efficient and of high quality. Figure 5-5 shows the effect of a variation in the parameters listed above on a sample domain.
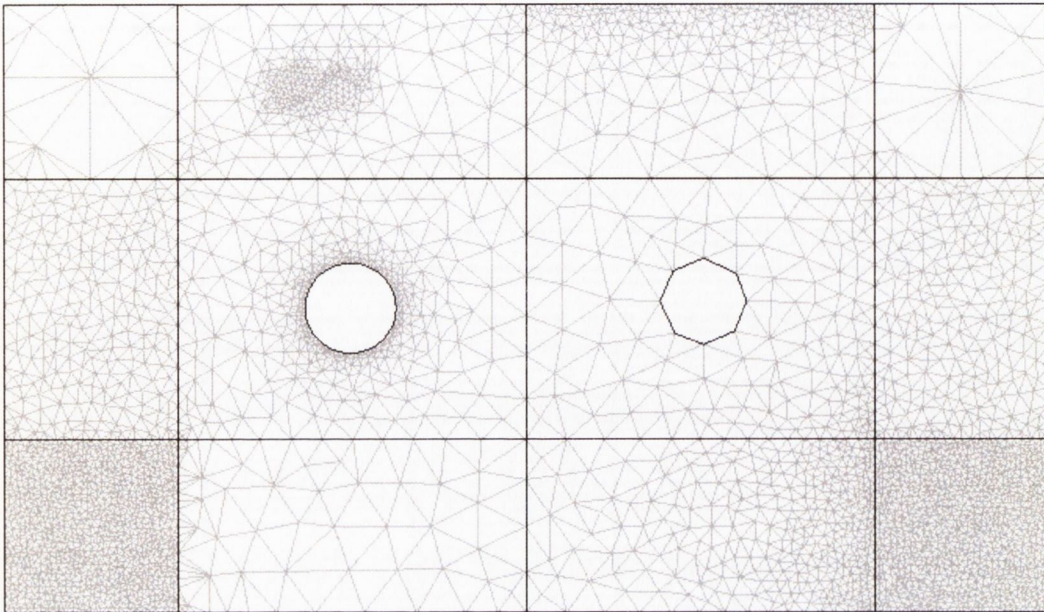
Figure 5-5 Effect of variation of a range of mesh parameters in FemLab

Solution of model

All FemLab solvers break down each problem into one or several linear systems by approximating the given problem with a linearized problem. The equations and boundary conditions formulated by the application modes are collected into one large system of PDE's. In this process, the equations and boundary conditions are also converted to the selected solution form which can be coefficient form, general form or weak form. The bio-heat application mode uses the coefficient form which is written as

$$d_a \dot{u} + \nabla.(-c \nabla u - \alpha u + \gamma) + \beta.\nabla u + au = f \qquad \text{Eq. 5-17}$$

where u is the variable to be solved for, d_a is the mass coefficient, c the diffusion coefficient, α the conservative flux convection coefficient, γ the conservative flux source term, a the absorption coefficient and f the source term. δ_{ts} is included as a

time scaling factor. Eq. 5-17 is formulated using the following terms and coefficients shown in Table 5-1 below.

Term/Coefficient	2D	3D
d_a	$\delta_{ts}\rho C$	$\delta_{ts}\rho C$
c	$\begin{bmatrix} k_{xx} & k_{xy} \\ k_{yx} & k_{yy} \end{bmatrix}$	$\begin{bmatrix} k_{xx} & k_{xy} & k_{xz} \\ k_{yx} & k_{yy} & k_{yz} \\ k_{zx} & k_{zy} & k_{zz} \end{bmatrix}$
a	$\rho_b C_b \omega_b$	$\rho_b C_b \omega_b$
f	$\rho_b C_b \omega_b T_b + Q_{ext} + Q_{met}$	$\rho_b C_b \omega_b T_b + Q_{ext} + Q_{met}$

Table 5-1 Coefficients for the coefficient form of the bio-heat equation in FemLab

The boundary conditions are assigned using Eq. 5-18 and coefficients from Table 5-2.

$$\mathbf{n}.(c\nabla u + \alpha u - \gamma) + qu = g - h^T \mu \qquad \text{Eq. 5-18}$$

Type	q-term	g-term	h-term	r-term	Description
q	h	$q_0 + h*T_{inf}$	0	0	Heat Flux
$q0$	0	0	0	0	Thermal insulation/ symmetry
T	0	0	1	T_0	Temperature
dq	h	$q_0 + h*T_{inf}$	0	0	Heat flux discontinuity
$cont$	0	0	0	0	Continuity

Table 5-2 Available boundary conditions in FemLab

The user can alter the coefficients as required using the sub-domain settings box shown below in Figure 5-6.
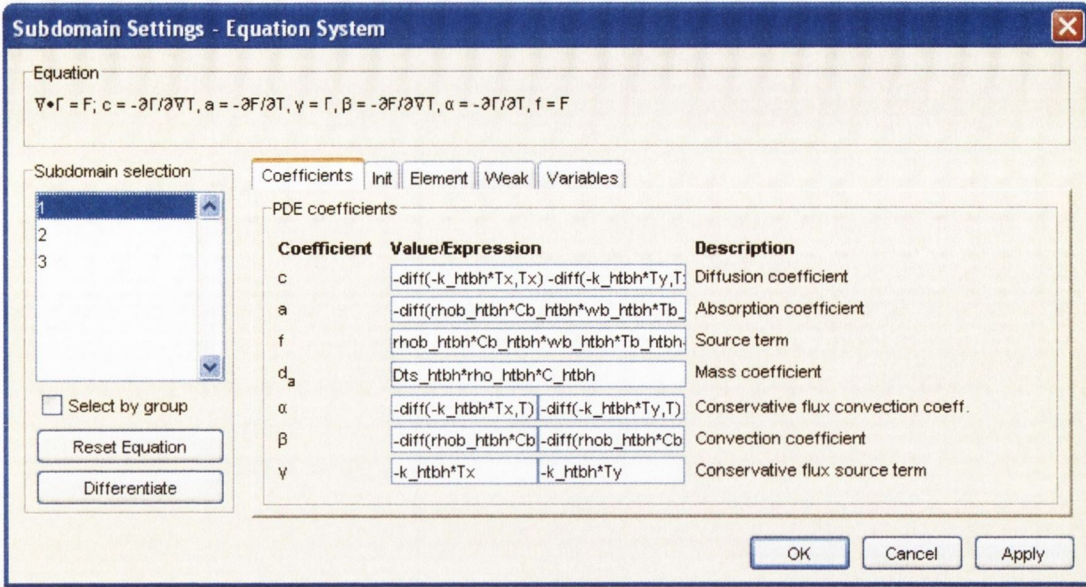
Figure 5-6 Sub-domain settings dialog box from FemLab

The model is now ready to be solved. Both steady state and transient solutions non-linear solvers are available. For both solvers the user can set the convergence criteria and the maximum number of iterations before failure. Further settings are available for highly non-linear problems. The non-linear solver uses an affine invariant form of the damped Newton method as described by Deuflhard [73]. An adaptive solver refines the mesh during the solution process. The time-dependent solver is used for both linear and non-linear PDE problems. The user can set time steps, the error at each integration step, and the output times for the solution variables which can be independent of the time steps taken by the solver.

5.3.4 Postprocessing

FemLab provides numerous post processing and visualization tools for creating surface plots, slice plots, iso-surface plots, contour plots, streamline plots and principle stress/strain plots. For transient solutions animations are also available. It is possible to integrate variables such as temperature or heat flux over specific volumes or sub-domains. All post-processing data can be exported to a text file for storage or external analysis. For 3-D analysis it is possible to take a sectional view through the geometry.

5.3.5 Analysing model convergence and accuracy

To verify the model it is important to conduct a convergence test to determine if the mesh density is sufficient. This is done by running the model and then refining the mesh before running it again. The solution should converge to a stable value as the mesh is refined. Alternatively adaptive mesh refinement automatically adds mesh elements to resolve those areas where the mesh quality is low.

5.3.6 MatLab interface

FemLab generates MatLab scripts for all commands issued using the Graphical User Interface (GUI). This allows the user to take advantage of the power of MatLab as a programming language to automate a complicated solution and data analysis process. This feature was used extensively.

5.4 SUMMARY

The finite difference model is used throughout Chapter 6 while FemLab is used in Chapters 7 and 8 where there is a requirement to handle more sophisticated geometries.

6 PERFUSION MEASUREMENT FROM FORCED CONVECTION APPROACH

6.1 INTRODUCTION

As described in Section 4.3 it was decided to pursue development of the Forced Convection Approach by building on the work of previous researchers in the US and by Vard [74] and O'Donovan [75] in this research group. The principle of operation of this approach is once more briefly outlined here. A localised cooling load is applied to the skin of the forearm using a perfusion probe (as shown in Figure 6-1), which results in a temperature drop of the underlying tissues. The value of perfusion has been shown to have an appreciable effect on the rate of temperature decay. A numerical model of the process is used to estimate the value of perfusion from an experimental test. This is done by varying the level of perfusion in the numerical model until the numerical and experimental temperature responses match. At the onset of the project there was a probe available from previous research carried out by Vard [74] and O'Donovan [75] as shown in Figure 6-1. (Dimensions of probe used in this study are included in Appendix A 5.)
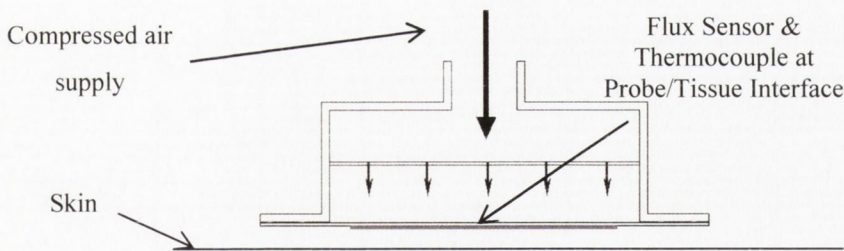
Figure 6-1 Schematic of original probe as designed by Vard [74]

Following preliminary testing a new probe and data acquisition system were developed which addressed limitations in the original design. Sensors were calibrated and uncertainty levels established. Development work was then carried out on the numerical and experimental aspects of this approach. Testing was then conducted on human subjects. This chapter will address all of these topics.

6.2   BLOOD PERFUSION PROBE

The purpose of the probe is to apply a cooling load to the skin surface. To achieve
this, the probe must:

1. be held evenly and firmly to the limb
2. present a flush base so as not to disrupt local blood flow
3. provide an even and controllable level of cooling
4. incorporate the necessary heat flux and temperature sensors.

The copper plate is employed to perform two of these functions, namely to ensure that
the sensors are held in a central and repeatable location and to guarantee a very
defined area of cooling.

The principle of operation of the new probe is the same as those designed by Vard
[74] and O'Reilly [60], albeit with a number of improvements. A schematic of the
new probe is shown in Figure 6-2; more detailed drawings are included in Appendix
A 5. Compressed air (at a temperature lower than that of the skin) enters a mixing
chamber before passing through an array of holes in the bottom of the chamber, which
give rise to a series of impinging jets. These jets impinge on a copper base plate in
which is embedded a combined heat flux and temperature sensor. The plate and
sensor lie in contact with the skin.
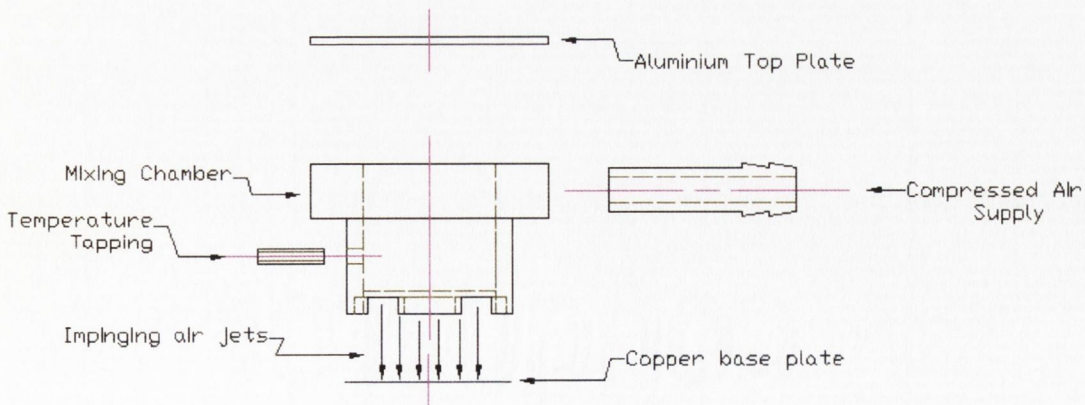
Figure 6-2 Exploded view of blood perfusion probe used in this study

Design of copper plate and strapping method

In developing a new strapping method the aim was to hold the copper plate firmly and evenly to the arm while avoiding any areas of high pressure that might disrupt localised blood flow, as had been experienced with the probe designed by Vard [74]. The solution chosen used a standard blood pressure cuff and a number of flexible tufnol sheets (with a thickness of 0.4mm and thermal conductivity of 0.37W/m°C, cut to a size of 150mm square). The copper plate was machined from a 50mm diameter copper bar. Prior to being parted from the bar a 0.4mm deep step was machined into the bar from the outside in, to a diameter of 31mm. The copper plate was then parted from the bar with a final thickness of 0.8mm. The plate was then machined to accept the heat flux sensor so that it presented a flush base to the arm thus avoiding any localised pressure concentrations.

A circular hole of diameter 31mm was cut in the centre of the first tufnol sheet. The plate sits into this hole but because of the outer step it cannot pass through it. The second sheet was designed to act as a spacer and has a 50mm hole cut in it equal to the outer diameter of the bar (i.e. 50mm). It was placed on top of the first sheet and glued in position. The third sheet has a hole of equal diameter to that of the first and serves to trap the plate in position between the first and last sheets. The copper plate now lies flush with the first tufnol sheet, as shown in Figure 6-3.
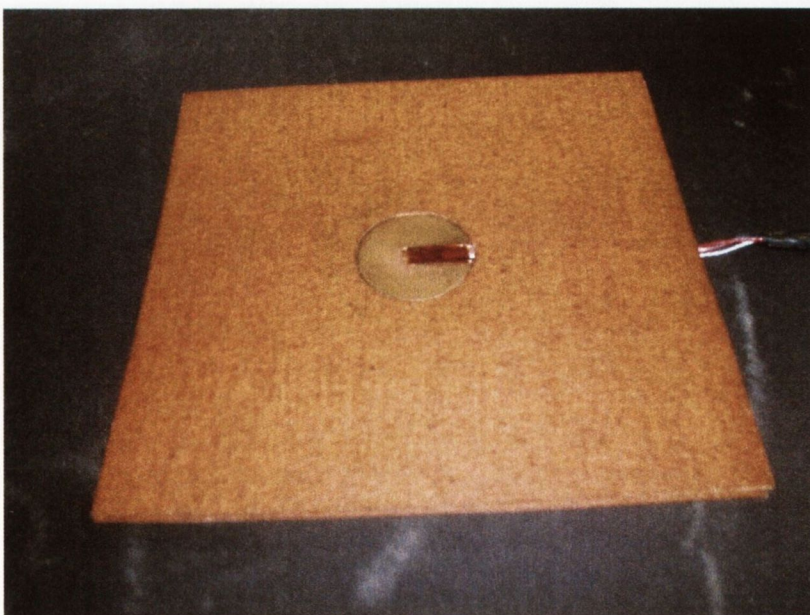
Figure 6-3 Photo showing copper plate and heat flux sensor lying flush with the tufnol sheet

70

A hole of 31mm was cut in a blood pressure cuff. The tufnol sheets were then glued to the cuff and the probe glued to the top of the copper plate. When the cuff is placed on the arm and inflated it presses the tufnol and plate against the skin. This leads to a firm but even pressure being applied. The influence of cuff inflation pressure is addressed in section 6.4. This arrangement is shown in Figure 6-4. The cuff also serves to insulate the skin adjacent to the probe so only the small area of the copper plate touching the skin is significantly cooled.

A disadvantage of this method is that it takes up to 15 seconds to position the probe on the arm during which time cooling of the skin occurs. Michener et al. [59] avoided this difficulty by manually holding the probe in contact with the skin during the test. While solving the time associated aspect of the placement problem this approach has a major disadvantage as it gives an uneven level of contact pressure and hence contact resistance during the test and so was not used in this study. This issue is discussed further in Chapter 7.

Figure 6-4 Cuff and probe located on the arm

Optimisation of cooling area

The larger the area that one cools the larger the signal that will be sent from the nerves on the arm and so the greater the chance the blood flow will be affected, Bell [61]. O'Reilly et al. [60] noted that there was a significant error in his study due to the fact that the thermocouple was located significantly off centre (in order to accommodate the heat flux sensor in this central location). By making the probe in this study

71

slightly larger this effect was reduced to a point where it was felt that there was a good compromise between thermocouple location and overall surface area. The various plate areas are given in Table 6-1 below.

Paper	Surface area of plate	Open flow area
O'Reilly[60]	400 mm^2	2.0%
Vard [74]	900mm^2	1.6%
Nicholson	755mm^2	3.0%

Table 6-1 Summary of probe dimensions from various studies

Another primary design consideration was to ensure uniform cooling of the copper base plate by the jet array. To achieve this, the probe was designed with a greater open flow area (as shown in Table 6-1). There are 45 jets of 0.4mm diameter spaced at 3.13mm intervals in a rectangular matrix. Ashforth-Frost and Jambunathan [76] have shown that the maximum Nusselt number occurs at a distance of approximately 110% of the potential core length which is equivalent to a jet diameter to plate spacing of 6.5. This coincides with the location where the enhanced heat transfer due to increased turbulence intensity more than compensates for the loss of centre line velocity.

6.3   INSTRUMENTATION AND CALIBRATION

This section will discuss the sensors used, their characteristics, and their calibration. All measurements were taken, displayed and logged with a data acquisition system. An uncertainty analysis is made in accordance with guidelines set down by the ASME Journal of Heat Transfer [77]. The uncertainty is made up of the precision (*P*) and bias error (*B*) as described in Eq. 6-1.

$$U = [B^2 + P^2]^{1/2}$$

Eq. 6-1

Coleman and Steele [78] define the bias error as the fixed or constant component of the total error and the precision error as the random component, or un-repeatability of the error. Combined as in Eq. 6-1 this gives the uncertainty which can be viewed as the total experimental error. For this study a 95% confidence level is used. For the

precision limit this is the interval about a nominal result that the experimenter is 95% confident that a measurement will lie when made under the same conditions and using the same equipment as a series of prior measurements. The bias error is assigned with the understanding that the experimenter is 95% confident that the true value of the bias error, if known, would be less than B. Typically the bias error is virtually eliminated during the calibration. The ASME guidelines assume all distributions to be Gaussian which implies that a confidence level of 95% is equal to two standard deviations.

Data Acquisition Set-up and LabView program

A PC based data acquisition system was employed. This consisted of a National Instruments PCI 6034E data acquisition card used in conjunction with a powerful data acquisition, control and analysis package know as LabView. A LabView program was written to capture, filter, save and display the measurement data in real time. It also allows the user to input a range of test parameters such as candidate name to be saved with the data for future reference. The program can control a digital output on the card which in this study was used to operate a solenoid which opened and closed a valve in the compressed air supply line, allowing precise programmable control of the cooling time.

The PCI 6034E is a 16-bit card capable of sampling in the MHz range, although in this study the highest sample rate required was in the kHz range. It allows 8 or 16 channels to be acquired simultaneously, depending on whether differential or single ended channels are used. The choice of acquisition board was determined mainly by the low magnitude of the signal from the heat flux sensor (typically μV before amplification). After amplification by a factor of 1000, this allowed for a theoretical resolution of approximately $1W/m^2$, however due to a high noise to signal ratio this was not achieved in practice. This issue is discussed further in a following section which deals specifically with the calibration of the heat flux sensor. Later in the study a laptop and a portable 16bit PCMCIA DAQ card (PC-516) with 4 differential or 8 single ended channels was used to facilitate testing in external locations.

Thermocouples

Thermocouples were used to measure both skin and ambient temperatures. In this study the cold junction temperature is taken at the data acquisition connector block (to

which the thermocouples are connected). The temperature of this junction is measured by an onboard thermistor. LabView can then automatically calculate a thermocouple temperature. T-type thermocouples (copper/constantan junction) were used in this study. They have a sensitivity of $46\mu V/°C$ and a recommended temperature range that should not exceed –25°C to 100°C.

Calibration was carried out using a heated water bath with temperature control and a Resistance Temperature Detector (RTD) temperature probe as a reference. The RTD calibration certificate (included in Appendix A 2) shows the uncertainty of the probe to be 0.165°C at 25°C. The thermocouples and RTD probe are immersed in the water bath which has a heating element and an agitator to ensure constant water temperature. Bath temperature was varied from 20°C to 50°C and allowed to equilibrate fully before any measurements were taken. The results of the calibration are shown in Figure 6-5 to which a linear regression is applied, as described by Eq. 6-2.

$$T_{RTD} = 0.97695 T_{therm1} + 1.57$$

<div align="right">Eq. 6-2</div>
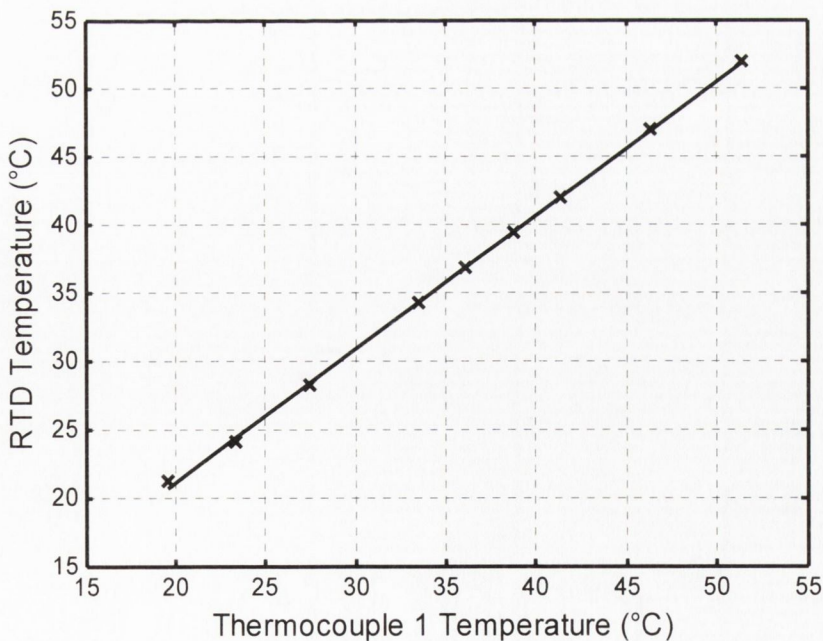
Figure 6-5 Calibration results for thermocouple 1

Next, the uncertainty of the data from the associated linear regression is calculated. To establish the precision error it is necessary to estimate the standard deviation (S_{xy}) of the data from the regression curve. Bendat and Piersol [79] express this in Eq. 6-3.

74

$$S_{xy} = \left[\frac{1}{N-2} \left(\sum_{i=1}^{N} (y_i - \bar{y})^2 - \frac{\left[\sum_{i=1}^{N} (x_i - \bar{x})(y_i - \bar{y}) \right]^2}{\sum_{i=1}^{N} (x_i - \bar{x})^2} \right) \right]^{1/2}$$ Eq. 6-3

x_i and y_i are defined as arbitrary values within the range of the calibration data. $\bar{x}$ and $\bar{y}$ are the mean of the respective x and y components of the data and N is the number of data points plotted. As stated before a 95% certainty level corresponds to two standard deviations, as defined in Eq. 6-4.

$$U_{precision} = 2 \times S_{xy}$$ Eq. 6-4

There is also an uncertainty associated with the regression fit, which Bendat and Piersol [79] quantify using Eq. 6-5

$$U_{regression} = S_{xy} t \left[\frac{1}{N} + \frac{(x_0 - \bar{x})^2}{\sum_{i=1}^{N} (x_i - \bar{x})^2} \right]^{1/2}$$ Eq. 6-5

where t is a factor defined by the number of data points plotted. Three sensors were calibrated for which the measurement and regression uncertainties are given in Table 6-2 below. In all cases the regression uncertainty is low. For the measurement uncertainty the typical operating temperature was assigned as 300K and the bias error was taken as 0.2°C which the uncertainty associated with the RTD reference probe. The results are shown to be in the expected range.

Sensor	Regression Uncertainty	Measurement Uncertainty
Micro-Foil embedded thermocouple	0.08%	0.26%
T-type 1	0.06%	0.23%
T-type 2	0.09%	0.29%

Table 6-2 Measurement and regression uncertainty

Heat Flux Sensor

A microfoil heat flux sensor was used to measure the heat flux flowing from the body to the plate or to the surroundings. Such sensors work on the principle that a heat flux flowing through the sensor can be related to the temperature difference across a thin piece of insulating material within the sensor, as described by Eq. 6-6. The insulating material is usually kapton and the temperature difference is measured using thermocouples, or more usually thermopiles in order to increase the magnitude of the signal. This arrangement is then sandwiched between two further layers of thin material for protection.

$$q'' = \frac{k(T_2 - T_1)}{\Delta x}$$
Eq. 6-6

The heat flux sensor used in this study was an RdF micro foil heat flux sensor (product no. 27036-3) with a sensitivity of $0.317\mu V/W/m^2$ and a response time of 0.4s (for which a calibration certificate is included in Appendix A 3). The heat flux signal is amplified 1000 times by a differential amplifier (Omega Omni-Amp III) before being read by the data acquisition system as described above. The sensor also incorporates a T-type thermocouple for temperature measurements as shown in Figure 6-6; this thermocouple was calibrated in the manner described by Eq. 6-3 to Eq. 6-5. The uncertainties are listed in Table 6-2.
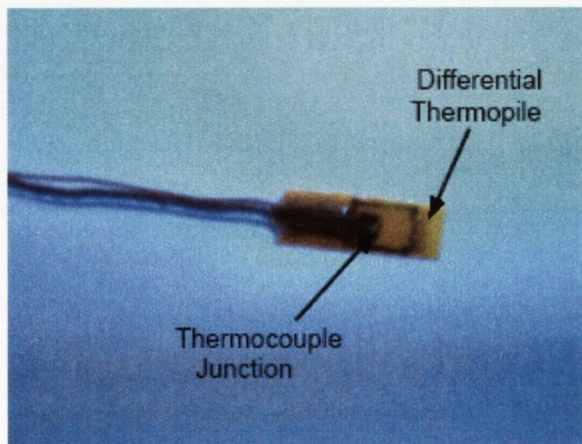
Figure 6-6 Photograph of type of Micro-foil heat flux sensor used in this study

The heat flux sensor was calibrated against a correlation developed by Shadlesky [80] for stagnation point heat transfer, that defines the heat transfer at the stagnation point

of an impinging air jet to be constant and independent of the nozzle to impingement surface spacing for a specific range of parameters. Several other studies, including one by Liu and Sullivan [81], have also shown this to be true. An experimental set-up developed by O'Donovan [82] for a study on fluctuating heat transfer to an impinging air jet was used for this calibration. The correlation is described by Eq. 6-7

$$q'' = \frac{0.585 \, \mathrm{Pr}^{0.4} \, \mathrm{Re}^{0.5} \, k \Delta T}{D}$$

Eq. 6-7

where Pr is the Prandtl number, Re the Reynolds number, k the thermal conductivity of air, D the nozzle diameter and ΔT the temperature difference between the plate and the impinging air jet. The results of this calibration are shown in Figure 6-7 where the calculated heat flux is plotted against the voltage from the sensor. The relationship between the heat flux and the voltage is shown to be linear. The fit between the data and the linear regression was good and so the uncertainty of the linear regression is small. The resulting calibration constant derived from the slope of the graph is $2.78 \times 10^6 \mathrm{W/m^2/V}$; which is similar to the manufacturer's value of $2.47 \times 10^6 \mathrm{W/m^2/V}$. The intercept value is comparable to the voltage under a zero flow condition, which is the heat transfer due to natural convection and radiation to the surroundings. The precision limit of the calibration compared to the linear regression was found to be +/- $36 \mathrm{W/m^2}$. However this high precision limit is thought to be mainly due to uncertainties associated with the parameters used in the calculation of heat flux from the correlation shown in Eq. 6-7 as under steady state conditions the fluctuation in the heat flux reading is only +/-$3 \mathrm{W/m^2}$. Table 6-3 shows typical heat flux values for free and forced convection conditions with the corresponding % uncertainty for both the high and low precision limits.

	Typical heat flux	+/-$36 \mathrm{W/m^2}$	+/-$3 \mathrm{W/m^2}$
Free convection	$80 \mathrm{W/m^2 {}^\circ C}$	45%	3.75%
Forced convection	$500 \mathrm{W/m^2 {}^\circ C}$	7.2%	0.6%

Table 6-3 % Uncertainty values for heat flux sensor for various heat fluxes and precision limits

A precision limit of +/-$36 \mathrm{W/m^2}$ results in a large % uncertainty at low heat flux values as experienced under free convection conditions while at higher heat flux values as

experienced under forced convection, the % uncertainty is much less significant. The high precision limit thus represents a worst case scenario with the actual uncertainty expected to be very much closer to the lower limit.
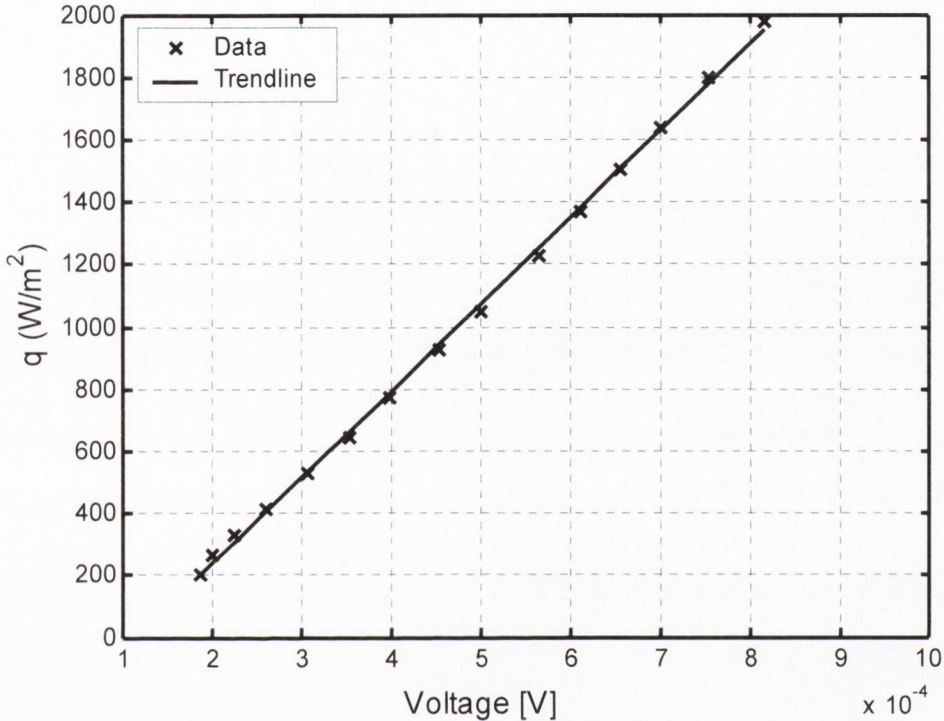
Figure 6-7 Calibration curve for RdF microfoil Heat Flux sensor

Thermistors

The thermocouples that were used in the initial project stages were replaced by thermistors which have superior sensitivity, lower susceptibility to drift and better interchangeability. The thermistor is a temperature sensitive resistor although unlike thermocouples, they do not exhibit a linear relationship with temperature. This can be seen from the resistance/temperature profile in Figure 6-8. BetaTherm precision 10K3A1B thermistors were used. The manufacturer states that each device will match the published resistance-temperature characteristics within ±0.1°C over a temperature range from 0°C to 70°C. Compared to thermocouples, the only drawback of thermistors is that they have a reduced temperature range; this was not a limiting factor in this study.
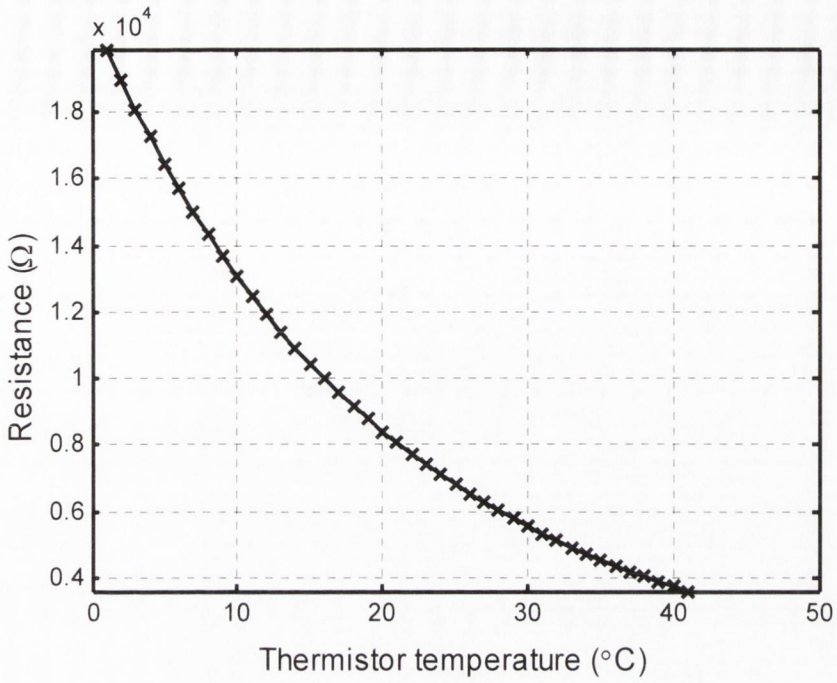
Figure 6-8 Resistance/Temperature profile for BetaTherm 10K3A1B thermistors

The thermistors were calibrated in the same manner as the thermocouples. In all eight thermistors were set-up and calibrated. The results of the calibration for thermistor 1 are shown in Figure 6-9 below.
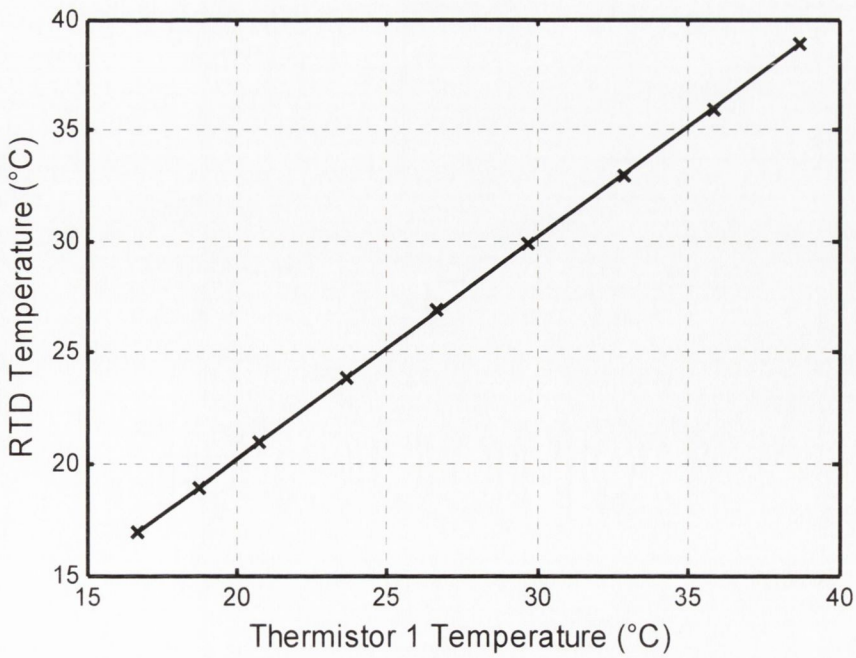
Figure 6-9 Calibration curve for Thermistor 1

The calibration graphs for the remaining thermistors are not shown; instead the precision limit and % uncertainty calculated from the linear regression for each thermistor is listed in Table 6-4. The precision limit was calculated from the uncertainty of the data to the associated linear regression as before. The % uncertainty was calculated for a typical operating temperature of 300K and includes a bias error of 0.2°C to account for the uncertainty associated with the RTD reference probe.

	1	2	3	4	5	6	7	8
Precision Limit (°C)	±0.12	±0.12	±0.12	±0.13	±0.12	±0.11	±0.12	±0.12
% Uncertainty	0.11%	0.11%	0.11%	0.11%	0.11%	0.10%	0.11%	0.11%

Table 6-4 Precision and % uncertainty for all 8 thermistors

The thermistors are shown to have a % uncertainty that is less than half that of the thermocouples.

Amplifier

An Omega Omni-Amp III DC signal amplifier with a gain of 1000 was used to amplify the voltage signal from the microfoil heat flux sensor. Even with amplification the signals are of very low magnitude and are therefore very susceptible to noise. All leads were shielded and grounded, however the level of noise was still found to be high. A spectrum analysis revealed a significant level of noise on the signal, particularly at 50Hz. It was considered that the AC power supply for the amplifier might be responsible for this. Figure 6-10 shows how the amplified heat flux signal improved when the AC supply was replaced by a 9V battery. However as the batteries discharged the level of amplification was found to change with time. The next solution was to use a DC power supply. This approach introduced some noise at 50Hz which was removed using a simple RC Low Pass Filter with a cut off frequency of 15Hz, as shown in Figure 6-11.
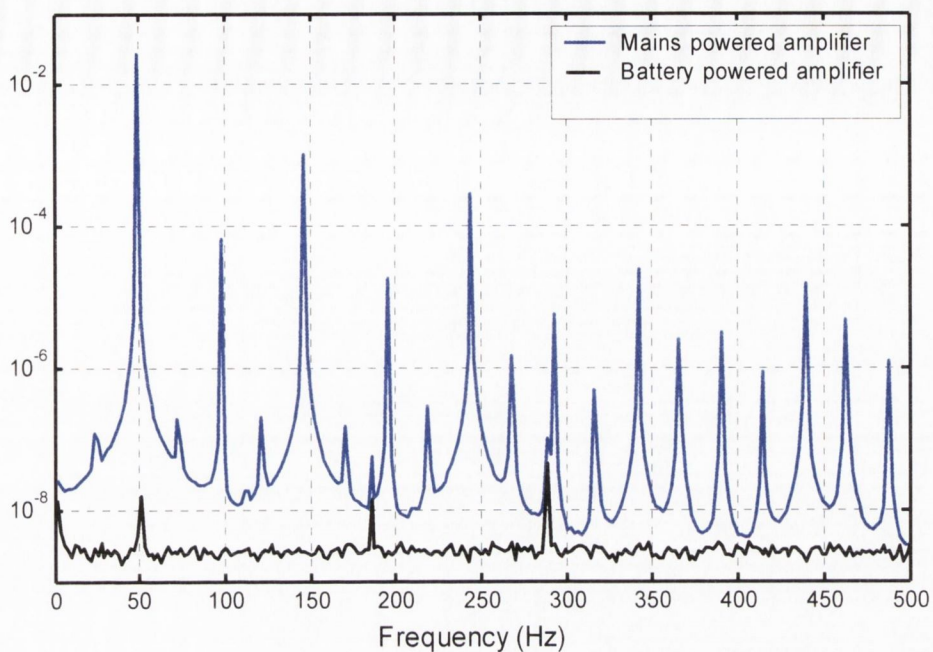
Figure 6-10 Spectrum analysis of mains powered and battery-powered amplifier
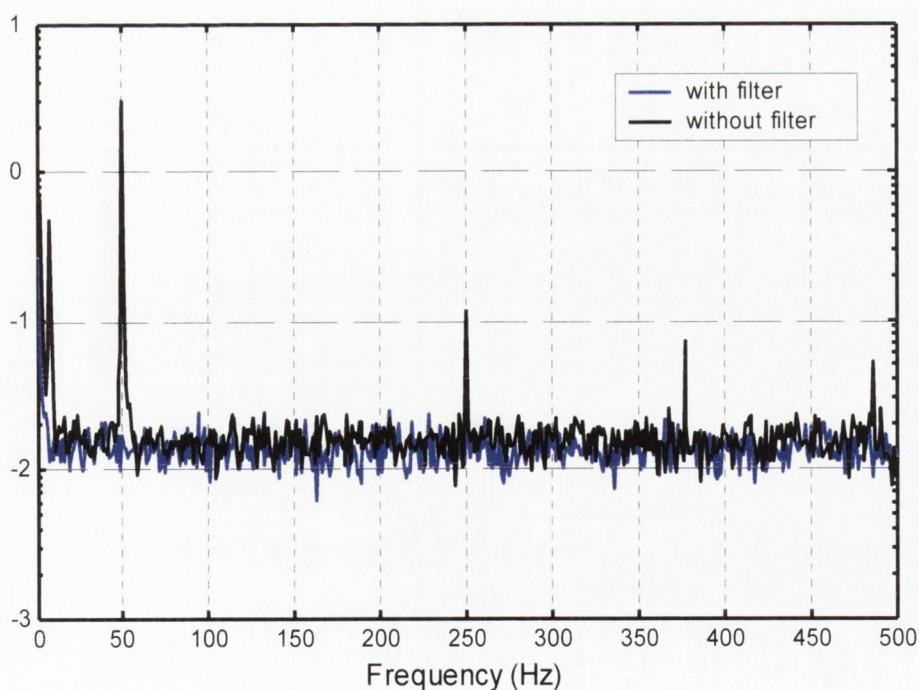
Figure 6-11 Spectrum analysis of signals from DC powered amplifier with and without low pass filter

The gain and common mode rejection ratio (CMRR) of the amplifier were re-calibrated on an annual basis, using a high precision voltmeter, a DC power supply and a series of high precision resistors to step down the voltage. The 'CMRR'

potentiometer is set for minimal AC output. The DC offset is set to zero using the 'Zero' potentiometer. The gain is then adjusted using the 'x1000' potentiometer such that the input is amplified 1000 times.

Flow meter

An Alicat Scientific Precision Gas Flow Meter was used to measure the mass flow rate of compressed air passing through the probe. The meter generates an output voltage proportional to the flow rate of air which can be read by the data acquisition system. The meter was calibrated by the manufacturer up to a flow rate of 400 Standard Litres Per Minute (SLPM). The uncertainty in the calibration certificate is stated as +/- 1% of the full scale reading which is equivalent to +/- 4SLPM which is more than sufficient accuracy for this study. The calibration certificate for the air flow meter is included in Appendix A 4.

Uncertainty in calculated parameters

Finally the uncertainty in the convective heat transfer coefficient must be calculated. Coleman and Steele [78] note that when a measurement, r, is a function of a number of other measurements, the uncertainty of the measurement, U_r, is a function of the uncertainties of the constituent measurements as described by

$$r = r(X_1, X_2, \ldots, X_j)$$

Eq. 6-8

The uncertainty in the convective heat transfer coefficient is therefore

$$\frac{U_h}{h} = \sqrt{\left(\frac{U_q}{q}\right)^2 + \left(\frac{U_{T_f}}{T_f}\right)^2 + \left(\frac{U_{T_s}}{T_s}\right)^2}$$

Eq. 6-9

The uncertainty of the temperature measurement has been shown to be small when compared to the heat flux uncertainty. Thus the uncertainty in the convective heat transfer coefficient is virtually the same as that for the heat flux measurement for which uncertainty values are listed in Table 6-3 for both free and forced convection conditions. As before the uncertainty is highest under free convection conditions but again is expected to be much lower than the worst case scenario reported.

6.3.1 Summary of calibration

All uncertainties were calculated using a 95% confidence level. The uncertainty values for the thermistors and thermocouples were consistent with the manufacturer's claims. During the simultaneous calibration of all 8 thermistors used, the largest temperature difference between the thermistors at one measurement point was found to be only 0.06°C. This implies very good relative accuracy between the thermistors. The high precision limit calculated for the heat flux sensor was thought to be mainly related to uncertainties associated with the parameters used in the calculation of the heat flux in Eq. 6-7. The true uncertainty is expected to be very much lower. The uncertainty of the convective heat transfer coefficient is predominately due to the uncertainty of the heat flux reading. The effect of the measurement uncertainties on perfusion estimation is discussed in later sections.

6.4   SET-UP TESTS

The objective here was to establish the best set-up and procedure for testing whereas later tests were aimed at obtaining data for the estimation of blood perfusion. Tests were conducted to measure the free stream temperature, convective heat transfer coefficient and contact resistance between the plate and the arm. Issues relating to repeatability and placement time of the probe were also investigated.

6.4.1 Free-stream temperature measurement

The free-stream temperature of the cooling air is measured using a temperature tapping in the probe mixing chamber as shown in Figure 6-2. However, as the air exits the chamber through the jet array, its pressure drops and it was expected that there would be an associated temperature drop. To measure this, the plate was placed on an insulated surface and readings of the chamber and plate temperature were taken for various flow rates, as shown in Figure 6-12.
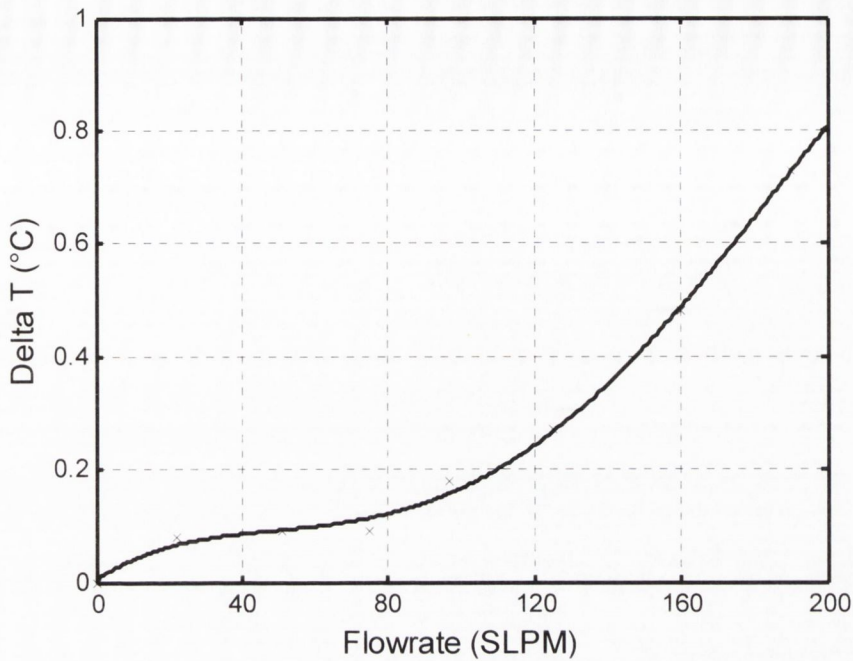
Figure 6-12 Difference between chamber and impinging jet temperature at various flow rates

From Figure 6-12 it can be seen that at low flow rates, (i.e. < 80SLPM) the temperature difference is only 0.1°C, while at higher flow rates it increases up to a maximum of 0.7°C at 190SLPM. This result was used as a correction factor for each test.

6.4.2 Determination of heat transfer coefficients

The objective was to determine the convective heat transfer coefficient between the base plate and the cooling jet array as a function of air flow rate, such that the air flow rate could be pre set before a test to deliver the desired cooling load. For convenience preliminary tests were conducted with the plate and probe sitting on an electrically heated hot plate (Stuart SB-162) rather than on the arm. The convective heat transfer coefficient was determined by dividing the measured heat flux by the temperature difference between the impinging air and the plate, results for which are shown in Figure 6-13. Initially the value increases rapidly with increasing flow-rate from a natural convection level until about 50SLPM, at which point the rate of increase becomes less rapid. The air flow rate is set using a throttle valve and an air flow meter. The choice of air flow rate for testing under the forced convection approach is discussed in subsequent sections.

In order to model the plate using the lumped capacitance approach as described in section 5.2.2 the Biot number must not exceed 0.1. For the dimensions of the plate this limits the convective heat transfer coefficient to a value below $12,500\text{W/m}^2\text{°C}$. As the maximum value used in testing is only $300\text{W/m}^2\text{°C}$ it is safe to apply this simplification.
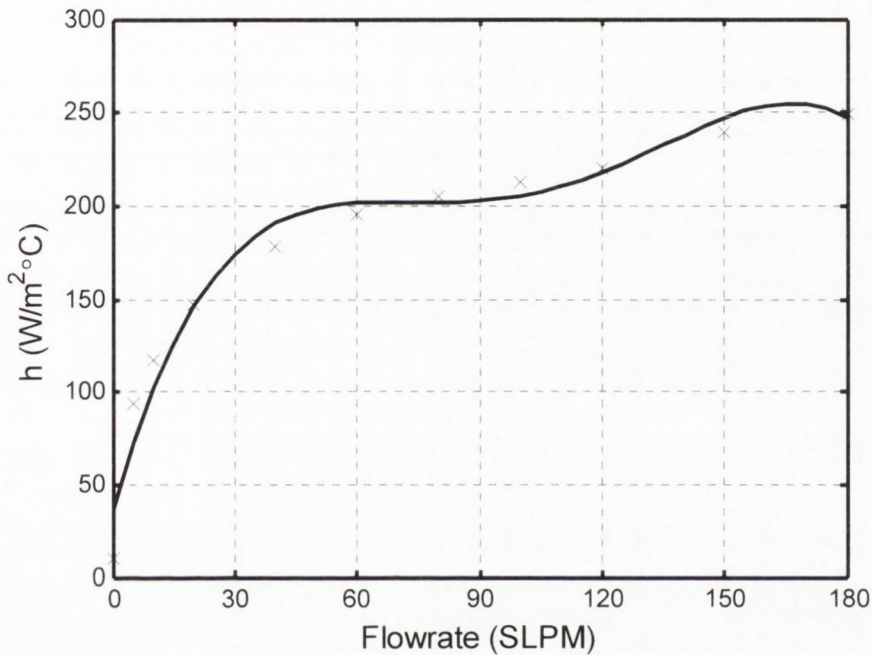
Figure 6-13 Magnitude of convective heat transfer coefficient on the copper base plate for various flowrates

6.4.3 Contact Resistance tests

Contact resistance arises when imperfect contact is made between two surfaces (in this case the skin and plate) due to microscopic roughness, resulting in entrapment of air in the voids between the surfaces. This leads to a discontinuous temperature profile across the boundary. Contact resistance can be expressed as the difference in surface temperature of the interfacing solids divided by the heat flux flowing through the contact area as described by Eq. 6-10.

$$R_c = \frac{\Delta T}{q''}$$

Eq. 6-10

O'Reilly et al. [60] found the thermal contact resistance between the skin and plate to vary between $0.0075\text{-}0.0090\text{m}^2\text{°C/W}$. Analytical results from the same study showed

85

that the initial peaks in the heat flux readings are significantly increased by a decrease in contact resistance as shown in Figure 6-14.
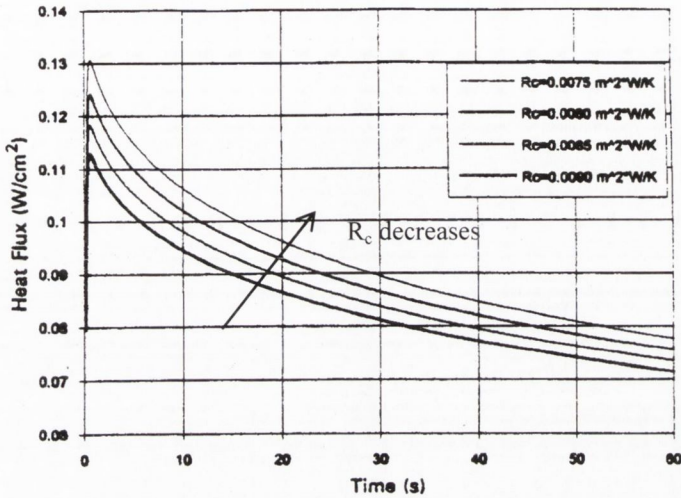
Figure 6-14 Analytical prediction of contact resistance effect on heat flux (ω_b=0.002/s) from O'Reilly et al. [60]

As this is an important parameter, tests were conducted to measure the thermal contact resistance between the skin and the probe for various cuff pressures. This was achieved through simultaneous measurement of the skin temperature, plate temperature and the heat flux flowing between them, results for which are shown in Figure 6-15.
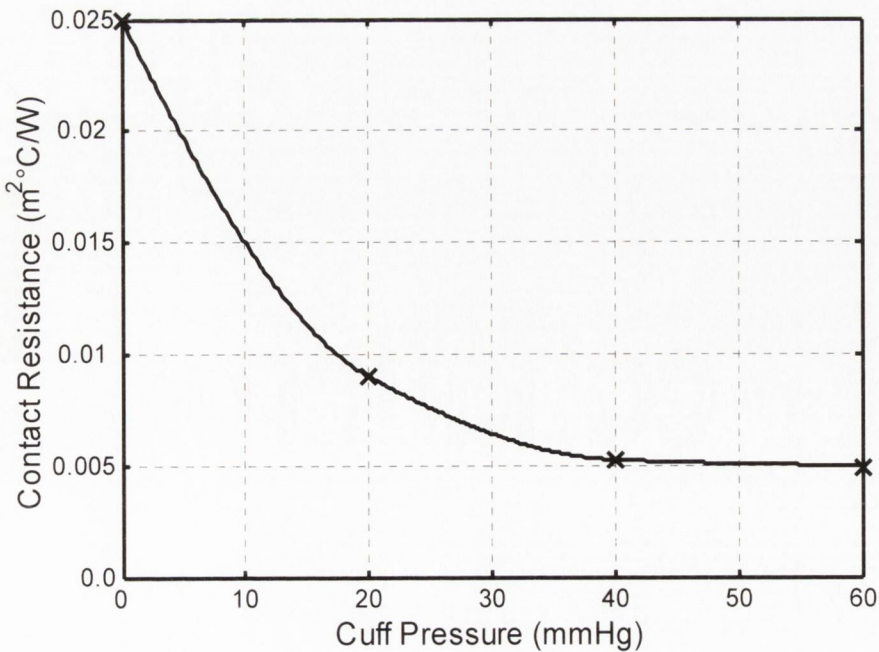
Figure 6-15 Contact Resistance between base plate of probe and skin surface

At a cuff pressure of zero the probe is simply resting on the arm. Between 0-20mmHg the magnitude of contact resistance decreases rapidly as the cuff pressure increases. At these low pressures the probe is only loosely held to the arm thus explaining the high resistance. Between 20-40mmHg contact improves and so the contact resistance further decreases. At 40mmHg the probe is firmly held to the arm and any increase in cuff pressure does little to reduce the contact resistance. It was found that pressures exceeding 50mmHg begin to impede blood flow. As the decreases in contact resistance between 40-60mmHg is very small there is no benefit in exceeding 50mmHg and so a strapping pressure of 45mmHg was chosen. At 45mmHg the contact resistance is $0.005m^2°C/W$, which is lower than that reported by O'Reilly et al. [60], indicating an improved strapping technique.

6.4.4 Probe equilibrium time

As illustrated in Figure 6-16, O'Reilly et al. [60] found that the tests where the probe was placed on the arm just before the test began had a better-defined peak than those where the probe was left on the arm for a longer period, which had lower and broader peaks. The approach taken in this study was to try and alter the initial temperature of the tissue to as small an extent as possible by using a short placement time. It was found that the probe could be situated and inflated within 15 seconds. If the probe was not correctly positioned in this time the test was abandoned. This issue is discussed further in Chapter 7.
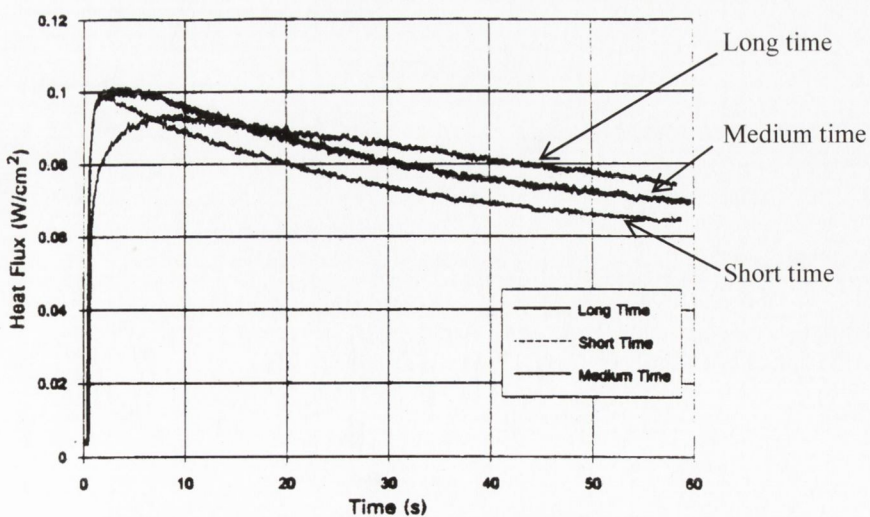
Figure 6-16 Effect of initial equilibration time on experimental heat flux. Short Time 10s before start, Medium time 30-60 s before start, long time till equilibrium reached before start, from O'Reilly et al. [60]

87

6.4.5 Investigation of repeatability of tests

If the test conditions can be made repeatable such that room temperature, compressed air supply temperature, initial probe temperature, probe position and flow rate are held constant from test to test it makes the value of perfusion the only varying term. This makes the analysis of tests much easier as one can compare experimental results directly to establish the effect of perfusion. Any random variation in any of these parameters during a test makes direct interpretation of the results more difficult (this is discussed further in Section 6.6). In practice achieving repeatability is the most difficult aspect of experimental testing. Initially there was no realistic method of holding the ambient temperature constant over the course of the year but later tests were conducted in a temperature controlled room, significantly reducing this variable. However of greater difficulty was the variation in the temperature of the compressed air supply and in the air flow rate (implying an associated change in the heat transfer coefficient) during a test. The variability in compressed air temperature is associated with the ambient weather conditions whereas the fluctuations in air flow rate (+/- 9%) are linked to variations in the available pressure of the centralized compressed air supply due to the variable demands of other users of the system. This effect was reduced to +/-4% by adding a reservoir to damp the fluctuations in the air flow rate.

To remove the initial probe temperature as a factor in the determination of the initial peak heat flux and temperature drop, compressed air could be blown through the probe to cool the plate to a standard temperature. However, this could not ensure full consistency between test sequences due to the fluctuation in the compressed air temperature. In summary, it was not practical to remove completely the variation in the parameters listed above between test sequences and so it was not possible to directly compare results for the estimation of perfusion. This is discussed further in Section 6.6.1. However, significant achievements were made in reducing variations in test parameters during an individual test.

6.5   EXPERIMENTAL PROCEDURE AND MODEL OPERATION

The underlying principle of the Forced Convection Approach is that a measurement of tissue perfusion can be inferred from the rate of tissue temperature decay during a given localised cooling of the tissue. A rapid tissue temperature decay indicates a low perfusion level as little warm blood is entering to maintain the tissue temperature.

Conversely a less rapid temperature decay indicates a higher perfusion level as a greater level of heat is deposited by the warm blood entering the cooled region. Thus to make an estimation of perfusion a series of temperature measurements are taken during the cooling period. A numerical model incorporating the various initial and boundary conditions used in the experimental tests is run for a range of perfusion values. When the numerical and experimental results match, perfusion is said to be estimated.

Throughout the study an iterative process of testing and modelling was used. A series of tests would be completed, the model run, the results analysed and then some improvement would be made to the model or experimental procedure. Many of these iterations were completed during the project. Most of the discussion in this chapter is based on the final version of the experimental procedure and numerical model (prior to developments outlined in Chapter 7), although important experimental or numerical improvements along the route to the final procedure and model are discussed. First the experimental procedure is explained. Operation of the numerical model is then discussed and a sensitivity analysis is conducted, after which the numerical and experimental results are compared.

6.5.1 Experimental procedure

The standard test procedure is as follows. All relevant test settings and physiological variables (listed below) are inputted into the data acquisition program. A standard air flow rate of 120SLPM is set using the air flow meter and a throttle valve on the air supply line (feed from a reservoir as discussed in Section 6.4.5). Initial skin temperature at the measurement site is recorded. The probe is now ready to be positioned on the arm. The user initiates a 30 second countdown sequence in LabView after which time LabView opens the computer controlled valve in the compressed air supply line to start the air flow at the pre-set level. The first 15s of the countdown are for preparation for placement. During the second 15 seconds the probe is placed on the arm and inflated to the standard pressure of 45mmHg. The arm is then rested on two specially designed stands, which provide support at the wrist and the elbow as shown in Figure 17. This must be completed within 15 seconds or the test is abandoned. After the 30 seconds have elapsed the air flow starts and the test begins.
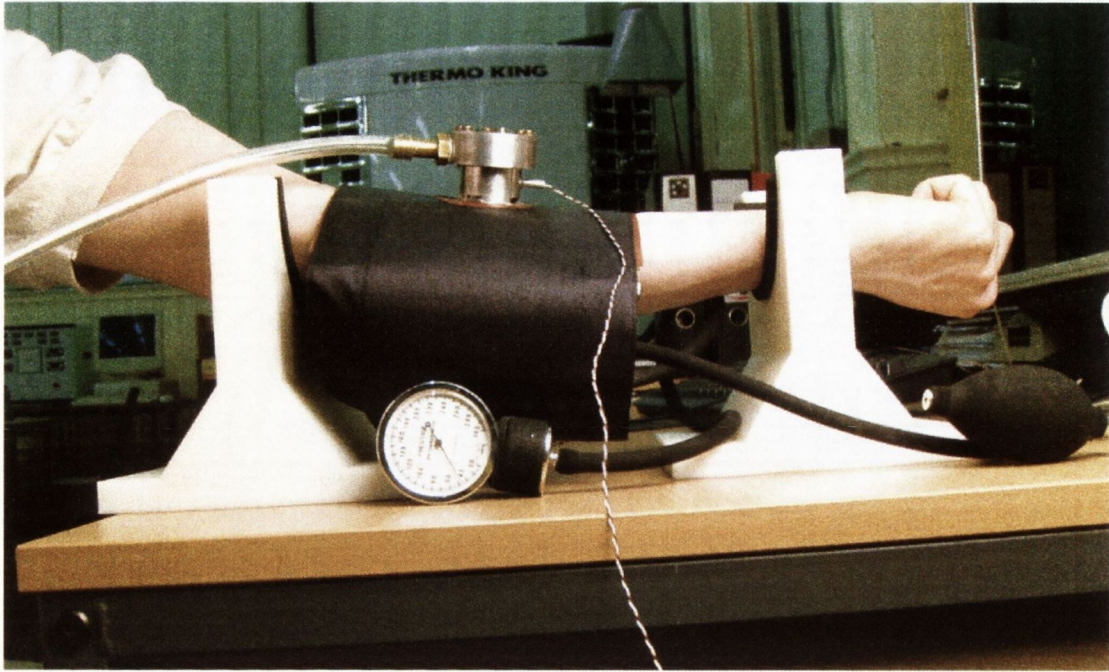
Figure 17 Photo of arm resting on stands in test position

The rest of the arm is covered to avoid cooling by the compressed air. During the test the candidate is asked to move as little as possible to avoid disturbances in the measurements. Cooling of the skin generally lasts 120 seconds and causes approximately a 5°C temperature drop.

Measurements are taken of

o   Heat Flux between skin and copper plate (RdF micro foil sensor)

o   Temperature of heat flux sensor (T type thermocouple embedded in sensor)

o   Flow rate of compressed air (Alicat air flow meter)

o   Impinging air temperature (T type thermocouple)

o   Ambient temperature (T type thermocouple)

Various physiological measurements are also taken

o   Heart rate (using heart rate monitor)

o   Body core temperature (before test)

Other parameters recorded included:

o   Candidate name

o   Sex

o   Factors affecting perfusion: current health, recent exercise level, age etc.

If two tests are to be conducted in one session, fifteen minutes is left between tests to allow the arm to regain its original temperature profile.

6.5.2 Finite Difference Numerical Model

This section will deal with a description of the model, its development, validation, operation and sensitivity to errors in thermal constant values and contact resistance. The numerical model simulates the experimental procedure outlined in the previous Section. After the relevant experimental test conditions have been inputted the model automatically completes multiple runs for a range of physiologically realistic perfusion levels. The time varying temperature profile from the experimental test is compared with the time varying temperature profiles for the various perfusion values at the corresponding test location in the numerical model. The perfusion value is then altered manually to achieve the best fit. At this point the level of perfusion is said to be estimated. Initially an explicit model was employed, as it was easier to implement. However it was found to be slow (as it required small time steps to ensure stability) and was replaced with an implicit version of the code.

Stages of development of numerical model

The model was developed and refined during the course of the study to account for changes in the experimental procedure or to address obvious simplifying assumptions. The stages of development were:

1. A change from square to rectangular mesh to allow the depth and width of the mesh to vary independently as shown in Figure 6-18. This is to account for the fact that the depth of the mesh is equal to the depth of the mid point of the arm while the width of the mesh is set to be wider to give an even surface temperature profile.
2. Inclusion of copper base plate of probe
3. Automatic analysis of experimental data for test being modelled for estimation of initial conditions and incorporation of time-varying boundary conditions such as convective heat transfer coefficient and free stream temperature
4. Inclusion of contact resistance between plate and arm
5. Automatic plotting of numerical and experimental results
6. Control of time steps during run sequence to optimise run times
7. Automatic running for multiple perfusion values

Operation of the model

The model works through the following steps:

1. Reads constant values (e.g. property values for tissue and probe, cooling time, node spacing, contact resistance, tissue dimensions, range of perfusion values etc.)

2. Reads in time varying parameters such as size of time step and experimentally varying parameters such as convective heat transfer coefficient and free stream temperature.

3. Defines the mesh

4. Computes dimensionless parameters

5. Computes a steady state temperature distribution using the surface temperature measurement of the arm prior to cooling from the experimental test

6. Computes the change of temperature distribution (using the transient model) during the cooling part of the test using the steady state solution from 5 as the initial condition. This is repeated multiple times for a range of perfusion values.

7. Plots results of the individual runs for different perfusion levels against the corresponding experimental test

Description of mesh and boundary conditions

The model uses an implicit finite difference formulation of the bio-heat equation. A 2-D mesh representing a longitudinal cross section down along the arm is defined as shown in Figure 6-18.
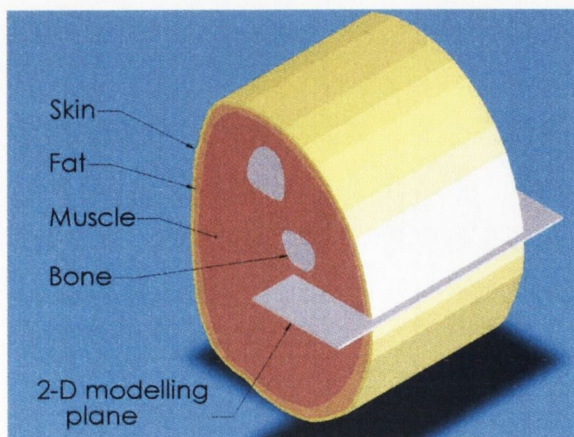
Figure 6-18 Plane of 2-D mesh used in finite difference model

A schematic of the mesh is shown in Figure 6-19. A cooling convective heat flux is applied to part of the top row, which represents the copper base plate of the perfusion probe. (The copper plate is modelled using the lumped capacitance theory as the Biot number is found to be <<0.1.) The next row represents the skin surface. Here the bio-heat equation is applied. Contact resistance between the skin surface and copper plate is accounted for by its inclusion in the finite difference formulation of the equations applied between rows one and two. The sides of the mesh are taken to be adiabatic boundary conditions. The bottom of the mesh is at the centre of the arm and was originally assigned a constant boundary temperature equal to the body's core temperature but this was later changed to an adiabatic boundary condition, as it was impossible to accurately define the constant temperature. The bio-heat equation is assigned to all the internal nodes.
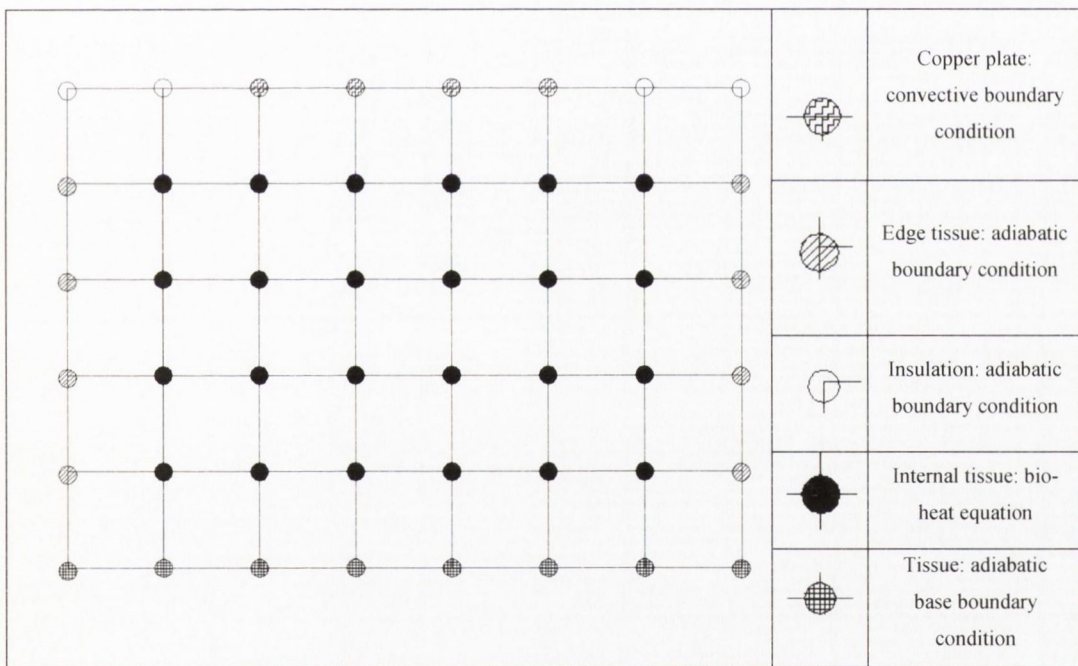
Figure 6-19 Schematic representation of the mesh used to evaluate numerical model. Actual mesh has 120 x 60 nodes which corresponds to a physical dimensions equal to 60mm width x 30mm depth

Model Validation

Before the model was used, its operation was first validated. Various boundary and initial conditions were altered to confirm the model functioned as expected. The model was then run at various node spacings (Figure 6-20) and time steps (Figure 6-21) to investigate the effect these parameters have on convergence and stability of

the results. A mesh size of 2nodes/mm and time step of less than 2s were chosen to give a reasonable compromise between computation time and accuracy. As explained earlier, variation of the time step was possible during run time to give better resolution during large transient changes in temperature such as at the start of a test.
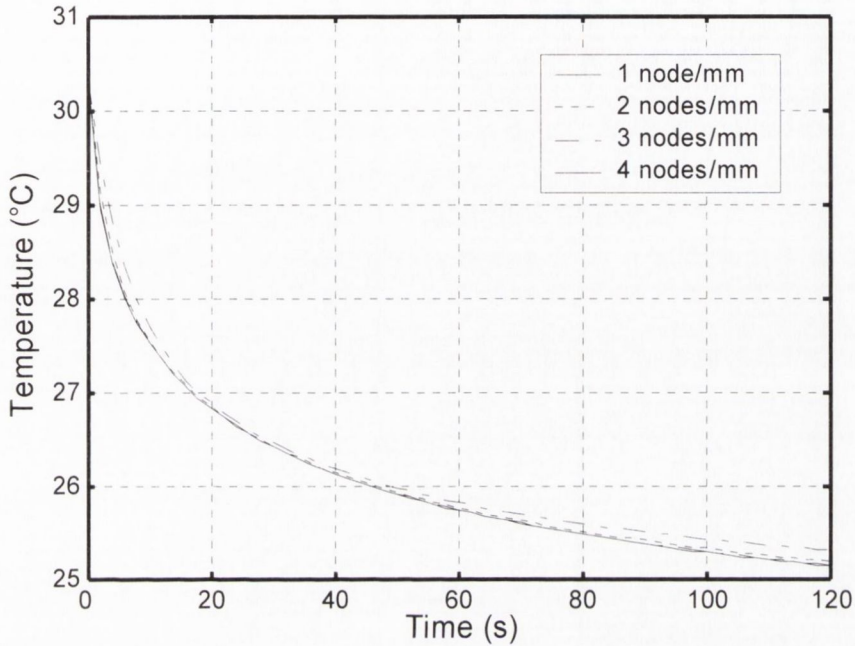
Figure 6-20 Effect of variation of mesh size on numerical surface temperature results
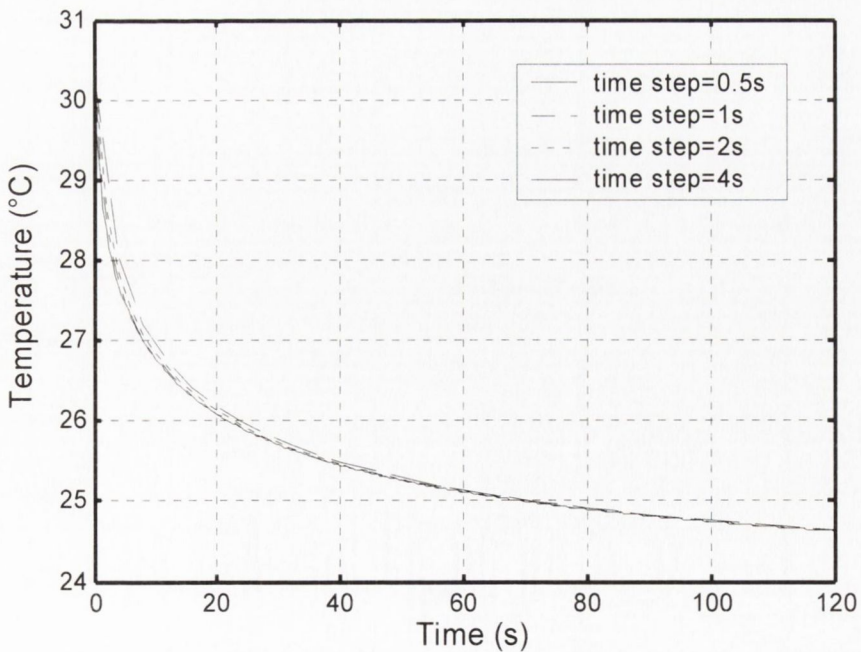
Figure 6-21 Effect of variation of time steps on numerical surface temperature results

6.5.3 Sensitivity Analysis using numerical model

Before comparison with experimental results, a study was undertaken to establish the sensitivity of the numerical results to the variation of constant values such as specific heat capacity, density and thermal conductivity of tissue over the reported range in the literature. These findings were then compared with the temperature variation due to perfusion to judge the likely impact on the estimation of perfusion values.

It is clear that the variation in specific heat capacity over the accepted range in literature from 3700 to 4000J/kg°C, as illustrated in Figure 6-22, has an insignificant effect on the surface temperature. The effect of the variation in the thermal conductivity from 0.4 to 0.5 W/m²°C, as shown in Figure 6-23 is not quite so insignificant however neither should hinder determination of the level of blood perfusion. Further properties such as density exhibited similarly small effects on the results.

A further sensitivity analysis was conducted to quantify the effect of probe contact pressure. The effect of contact resistance on the temperature and heat flux response is shown in Figure 6-24 and Figure 6-25 using the measured experimental values from Section 6.4.
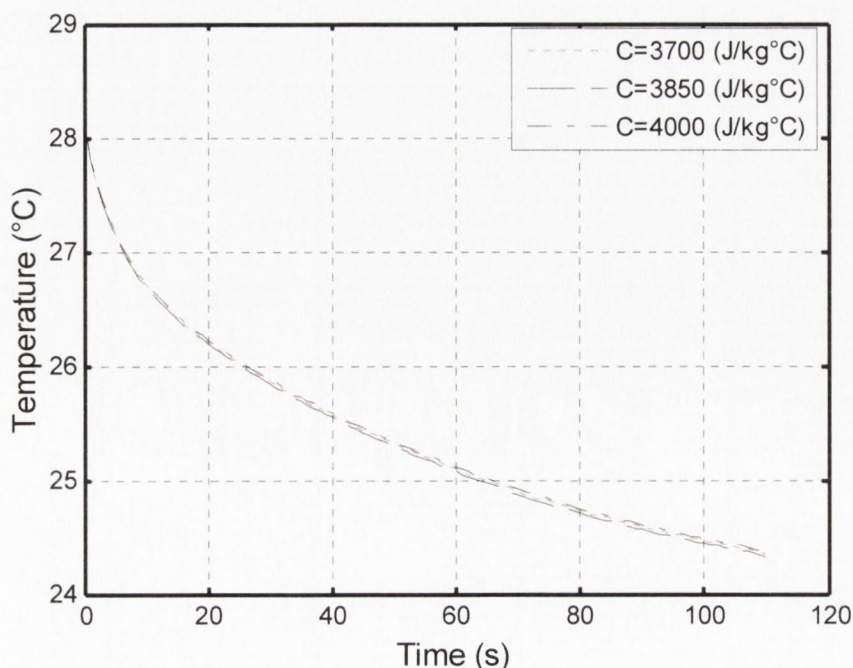
Figure 6-22 Effect of variation of specific heat capacity on numerical surface temperature results

95
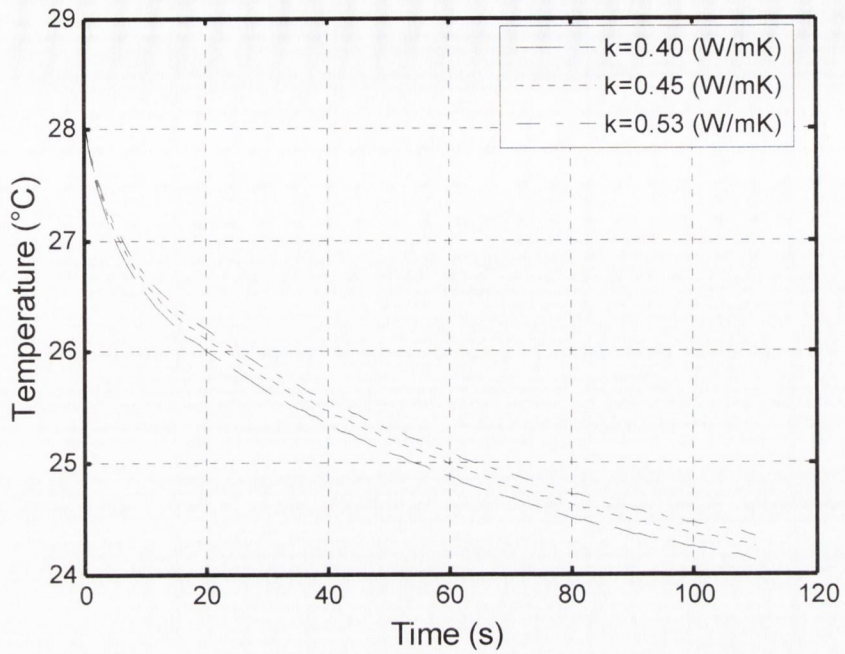
Figure 6-23 Effect of variation of thermal conductivity on numerical surface temperature results
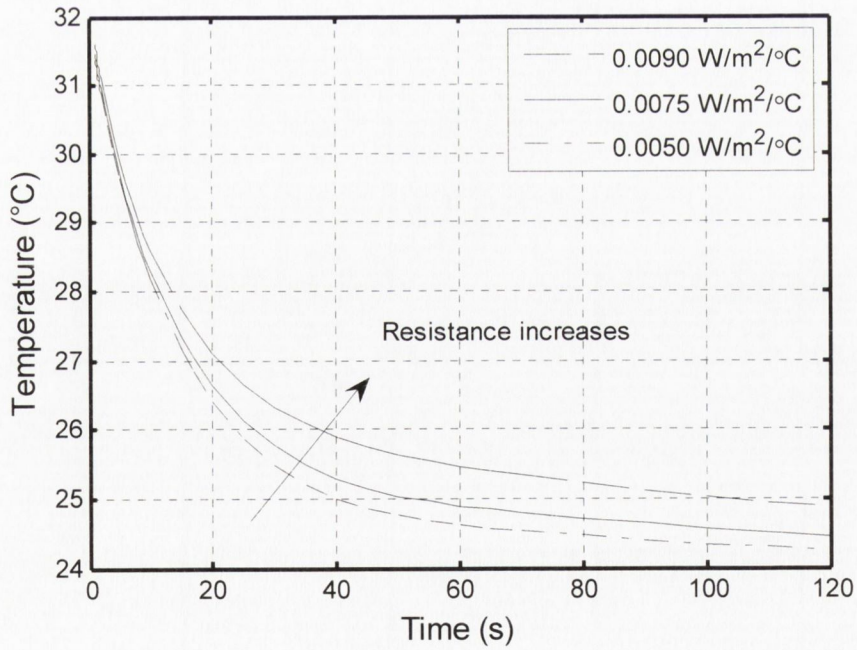
Figure 6-24 Effect of variation of contact resistance on numerical surface temperature results
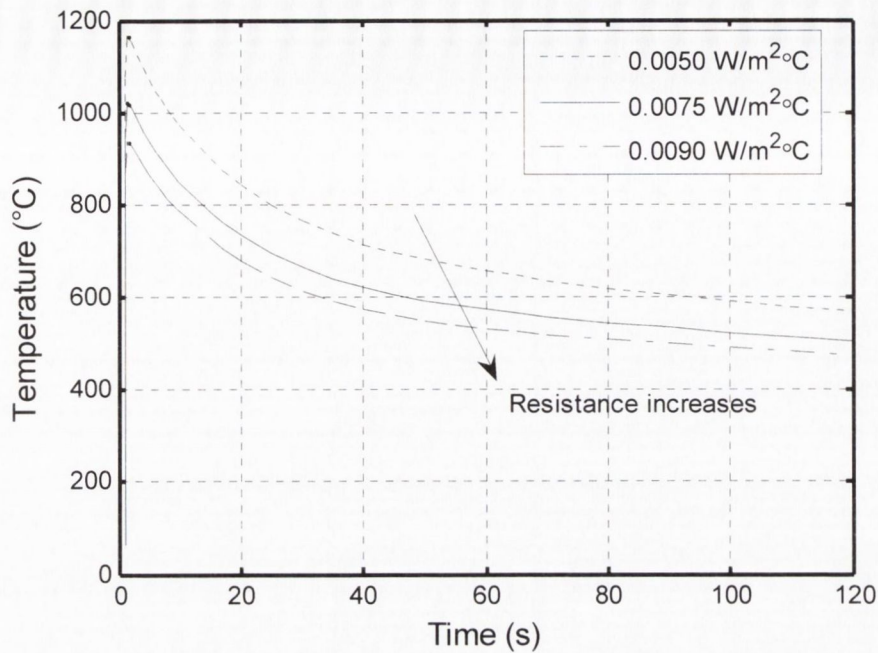
Figure 6-25 Effect of variation of contact resistance on numerical heat flux results

The trends agreed with those predicted by O'Reilly et al. [60], in that contact resistance has an effect on the magnitude of the heat flux particularly at the start of a test while the effect on the temperature response manifests itself with increasing with time.

The effect of the variation of arterial temperature (Figure 6-24) and of perfusion (Figure 6-27) on predicted surface temperature was also examined. As found by Michener et al. [59] and O'Reilly et al. [60] it is clear that the effect of perfusion becomes more pronounced as a test progresses. However, it is evident also that the variation in estimated surface temperature with arterial temperature is quite significant.
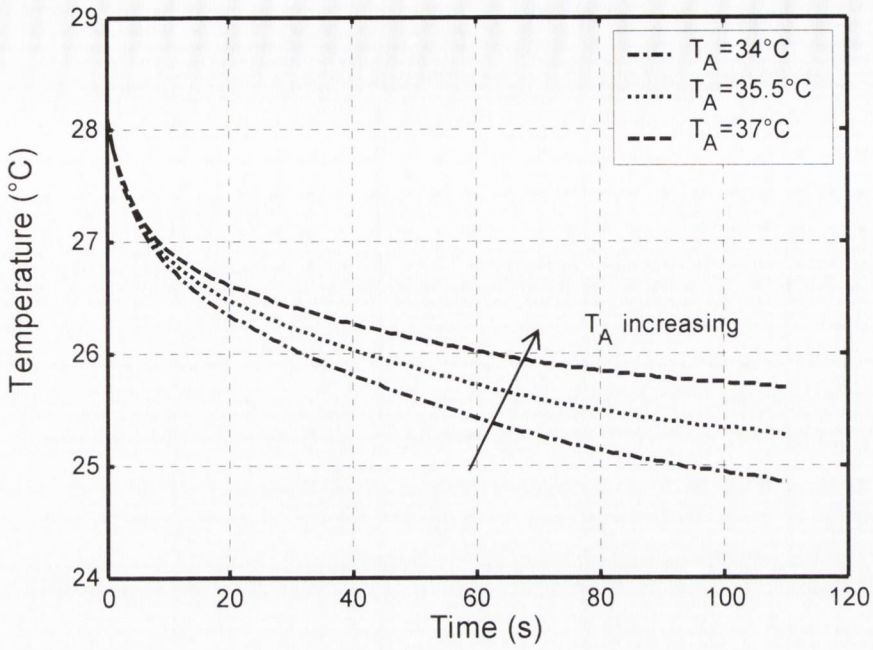
Figure 6-26 Effect of variation of arterial temperature on numerical surface temperature results
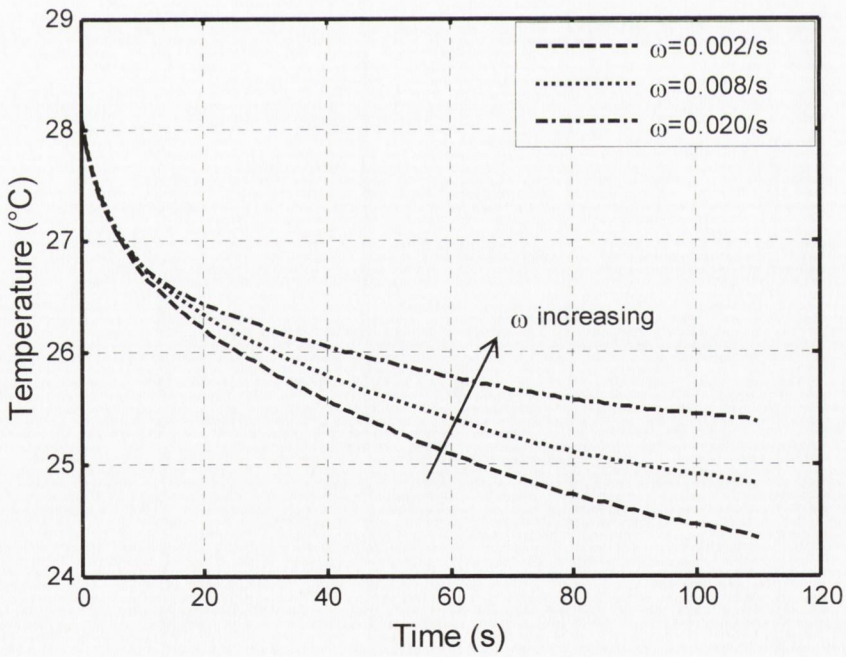
Figure 6-27 Effect of variation of perfusion on numerical surface temperature results

The perfusion term in the bio-heat equation shows that the perfusion and arterial temperature terms are directly related. Thus, if the arterial temperature is over estimated then the level of perfusion will be underestimated. Therefore knowing the actual arterial temperature is crucial for accurate absolute measurements.

The sensitivity analysis has shown that after 120 seconds of cooling, the temperature difference due to variation in perfusion levels is much larger than the temperature difference due to the uncertainty of tissue thermal properties. This finding supports the case that perfusion estimation should be possible using this method. This issue is discussed further in Chapter 7.

6.6 Comparison of Numerical and Experimental Results

Once satisfied that the numerical model was functioning as expected and that the experimental set-up was sufficiently refined it was possible to compare the numerical and experimental results for the purpose of estimating perfusion. This section will describe developments in the numerical model early in the testing process, and the validation of the technique will be explained. Finally other testing methodologies, such as re-heat tests, will be discussed. The process of establishing a perfusion value is as follows: a test is conducted and the boundary and initial conditions from the experiment are then entered into the model. The model is run for a range of perfusion levels until the best fit is achieved between the experimental and numerical results, at which point the perfusion level is said to be established.

The heat flux graphs are not shown as it was decided to use the surface temperature readings as the primary diagnostic index. This is because the temperature maps are the primary output of the numerical model. The heat flux values are then calculated from these maps and so at best can only be as accurate as the temperature values. However the heat flux reading is used to calculate the convective heat transfer coefficient and is therefore still an important experimental parameter.

6.6.1 Inclusion of variations in air flow rate and temperature

As discussed in Section 6.4 there was found to be a variation in the volumetric flow rate and temperature of the compressed air supply during the course of a test even when using a reservoir to damp the fluctuations. Initially averaged values of compressed air temperature and flow rate over the course of a test were used in the model. However this approach resulted in a poor correlation between the experimental and numerical temperature responses. Figure 6-28 and Figure 6-29 show the effect of the maximum variation of the free-stream temperature and

convective heat transfer coefficient respectively. It is clear that the variation of both parameters has a significant effect on the results. This is particularly the case for the free stream temperature, as its fluctuations were proportionally larger than the fluctuation in the air flow rate. To overcome this problem the actual variation of free-stream temperature and air flow rate with time were included in the model such that these values changed as the model progressed through its calculation time interval. The results in Figure 6-28, showing the effect of the variation of free stream temperature include the variation of convective heat transfer coefficient with time, while alternatively Figure 6-29 incorporates free stream temperature as a function of time in order to clearly show the effect of each parameter. As shown in Figure 6-28 and Figure 6-29, this led to a dramatic improvement in the correlation between the experimental and numerical results, meaning that the variability of air flow rate and air temperature did not affect the accuracy of the model.

It had been hoped that it would be possible to directly relate the rate of temperature decay to the level of perfusion by developing a relationship between a curve fitted to the experimental results and the perfusion level. That is to say if there were no variation in the parameters listed above and testing could be conducted at constant ambient conditions, then the only unknown parameter would be the level of perfusion. If this were the case it should be theoretically possible to directly relate the level of perfusion to the rate of decay of the temperature curve. A table of decay rates for various perfusion rates and ambient conditions could then be calculated from the model. This would dramatically simplify analysis of the experimental tests. However this approach requires the boundary conditions to remain constant during and between tests. As this was not the case this approach could not be used. Instead as discussed, the random variation of flow rate and compressed air temperature for a given test are included for each run of the model.
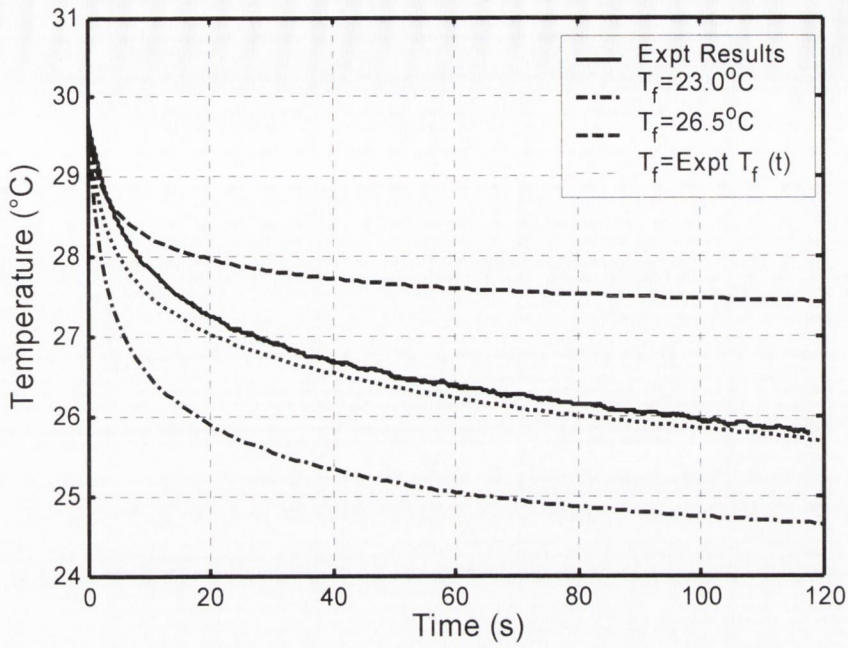
Figure 6-28 Effect on numerical results of variation of free stream temperature during testing
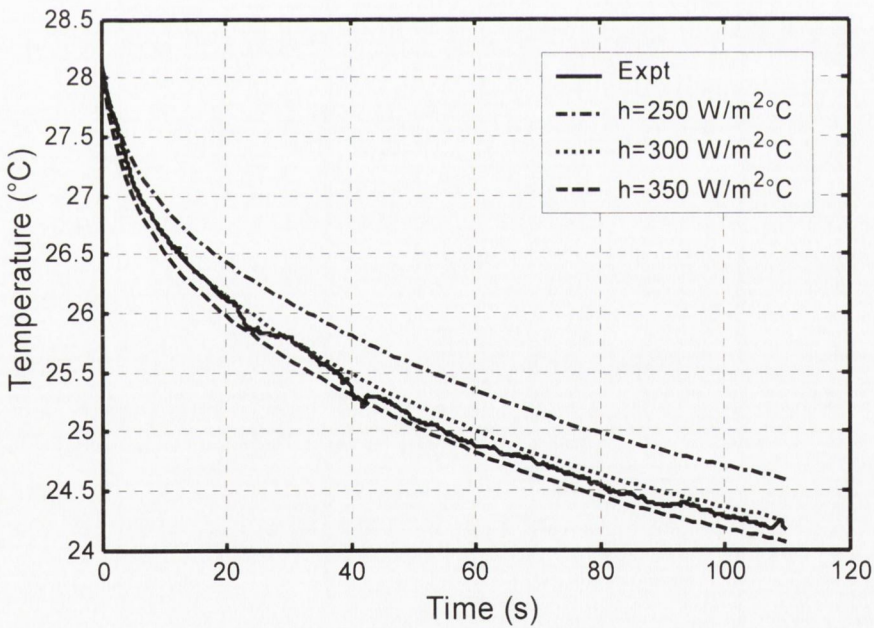
Figure 6-29 Effect on numerical results of variation of convective heat transfer coefficient during testing

6.6.2 Validation of technique

In the absence of a definitive method to experimentally verify the perfusion measurements, the first option was to examine whether the approach yielded the

expected trends. Thus the plan was to try and detect an induced variation in the level of perfusion through testing at different atmospheric temperatures. This meant that testing had to take place in a temperature-controlled environment. To realise this, tests were conducted in a small room, which was easy to maintain at a specific temperature. The first test is taken at ambient room temperature; the room is then heated for the second test. A candidate remains at rest during this time. Skin temperature is monitored until a new steady state condition is reached.
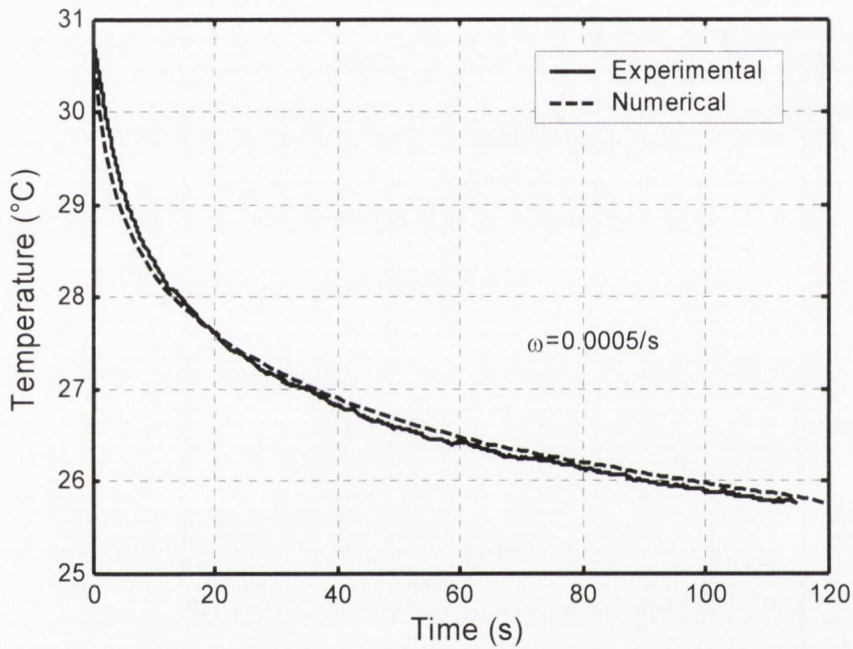
Figure 6-30 Comparison of numerical and experimental surface temperature results for perfusion testing conducted on a human candidate at T_{atm}=20.7°C

As can be seen from Figure 6-30 and Figure 6-31 the correlation between the experimental and numerical results is very good. As expected, it is found that the perfusion value predicted from the model is greater for the tests at a warmer room temperature, with a predicted value of 0.0013/s as opposed to 0.0005/s. These values lie within the range typically reported in the literature.
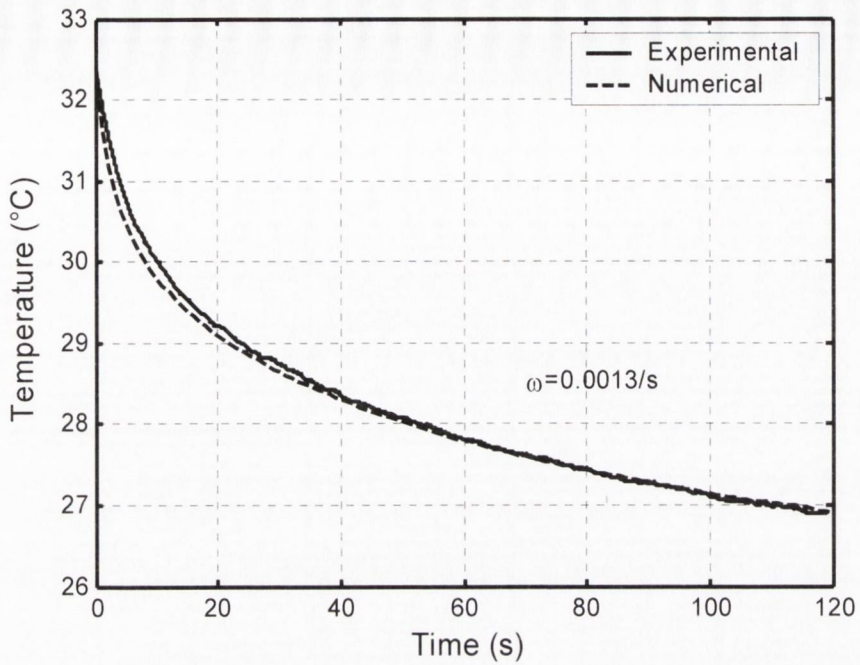
Figure 6-31 Comparison of numerical and experimental surface temperature results for perfusion testing conducted on a human candidate at $T_{atm}=25.0°C$

6.6.3 Re-heat tests

Measurements of heat flux and temperature after the completion of the cooling phase were made and are shown in Figure 6-32 and Figure 6-33 respectively. The aim was to establish how accurately the model would function under these different test conditions. The results showed that on cessation of cooling the heat flux rapidly dropped to a constant value of $300W/m^2$; the temperature recovery was initially very rapid but slowed with time.

The model poorly predicted the reheating part of the test as it didn't include heat conduction into the main part of the probe from the copper plate. This conduction was insignificant during the cooling part of the test.
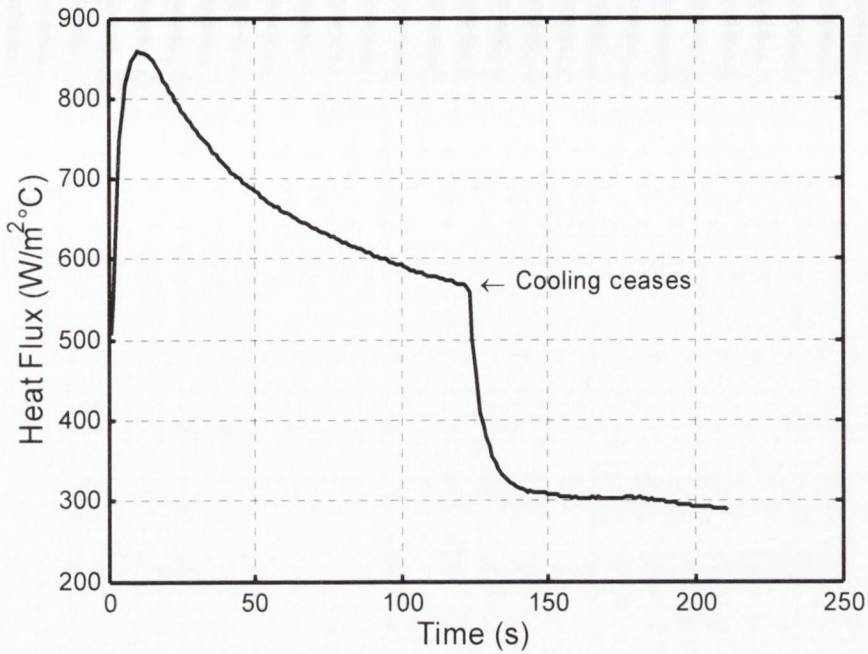
Figure 6-32 Heat Flux readings during reheat test from heat flux sensor embedded in the copper base plate
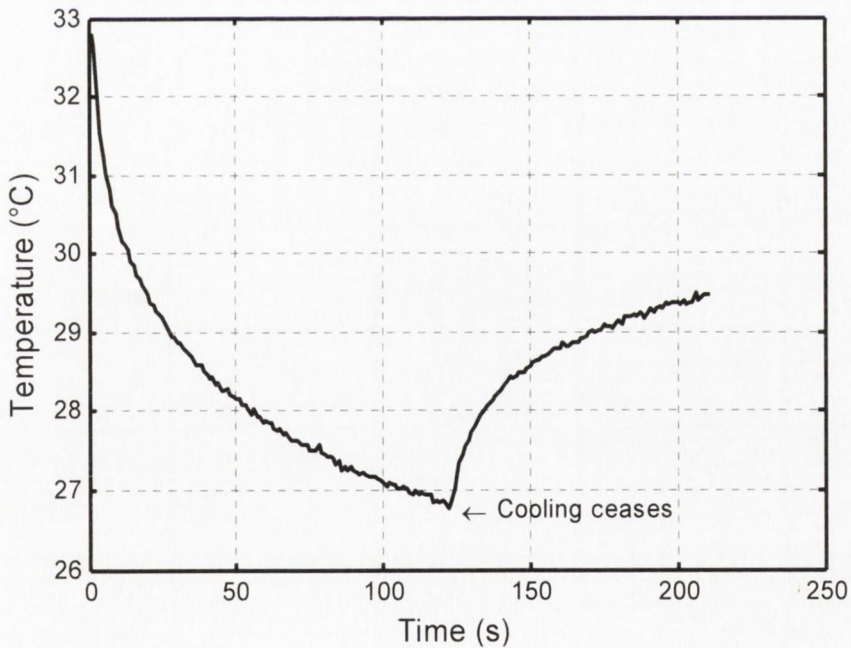
Figure 6-33 Temperature readings during reheat test from temperature sensor embedded in the copper base plate

6.7 SUMMARY

The work described in this chapter built on that carried out by previous researchers in this area by incorporating a number of improvements in probe design, modelling and

experimental techniques. A sensitivity analysis concluded that the temperature curves were more sensitive to changes in global perfusion then they were to errors in thermal properties. Although this indicates that the forced convection approach has potential for the measurement of perfusion levels in the forearm, a number of difficulties remain which need to be addressed. Thus it was decided to critically appraise the technique and to question some of the assumptions and simplifications made in its development.

One difficulty with the forced convection approach lies in the cooling of the arm during placement which was not accounted for. Another issue to be addressed is the effect of different perfusion levels between different tissues types. However the principal problem is that to correctly model the transient test an accurate initial condition is required, which itself requires the level of perfusion to be known. The search for solutions to these problems caused this study to diverge from previous investigations in this area. These issues are addressed in the following chapter.

7 REFINEMENTS IN FORCED CONVECTION APPROACH

This chapter outlines a number of refinements in the forced convection technique along with advances in the estimation method of perfusion levels. A number of experimental and numerical assumptions made in the previous chapter are questioned, which results in changes to the numerical and experimental procedures. Tests are conducted using these new procedures, following which an optimisation analysis is run in order to increase the sensitivity of the method. Finally the form of the temperature response curves is explained.

7.1 TREATMENT OF INITIAL TEMPERATURE PROFILE

This section deals with inconsistencies in the modelling of the initial temperature profile associated with the inadvertent cooling of the skin that takes place when the probe is placed on the arm prior to the forced convection part of the test. Figure 7-1 and Figure 7-2 show heat flux and temperature readings for a test carried using the procedure described in Section 6.5.1. As outlined the first fifteen seconds are used to prepare for placement. Fifteen seconds into the test the probe is placed on the arm. Before placement the plate and probe are cooler than the arm and so when they are placed on the arm, heat is conducted into them. This is shown in Figure 7-1 by the dramatic peak in the heat flux reading as recorded by the heat flux sensor embedded in the copper base plate. This heat flow into the plate results in an increase in plate temperature as shown in Figure 7-2. Over the next 15 seconds the heat flux decreases as the temperature difference between the plate and the arm decreases. Cooling is initiated thirty seconds into the test. This causes the plate temperature to rapidly drop which in turn causes the heat flux to again rise as the temperature difference between the plate and arm increases. The characteristics for the rest of the test are as described previously in Section 4.1.1.

From Figure 7-1 it is clear a large amount of thermal energy is removed from the arm during this period. Most studies, including this one, take the initial skin temperature in the model, to be equal to that of the plate when cooling begins so that the temperature responses match at the start of the test. In reality, this does not give a truly accurate representation of the initial temperature profile of the arm. To remove

this inaccuracy in the procedure a number of approaches were attempted, as outlined below.
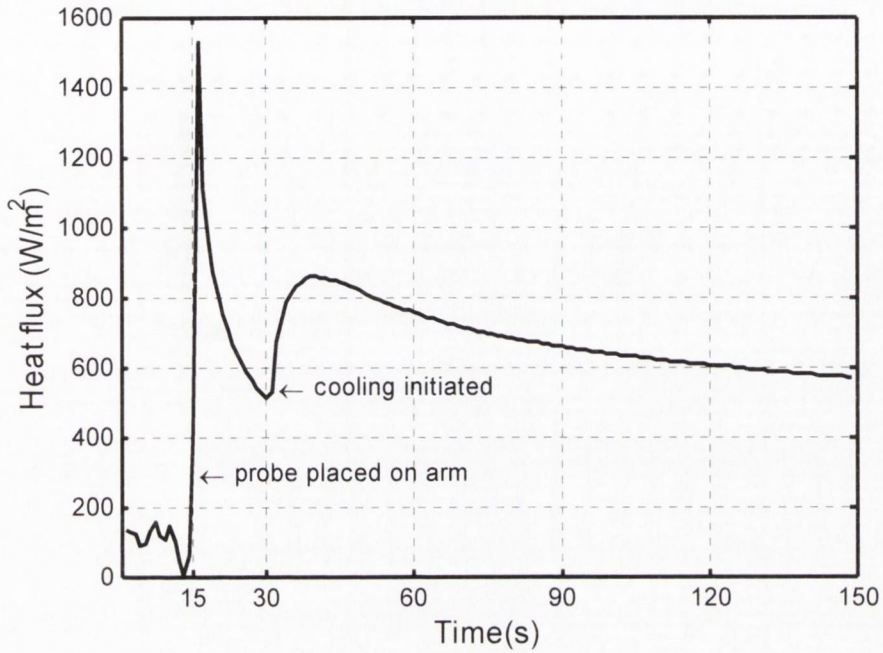
Figure 7-1 Heat flux measurements from heat flux sensor on base plate of probe during placement (15-30s) and during test (30-150s)
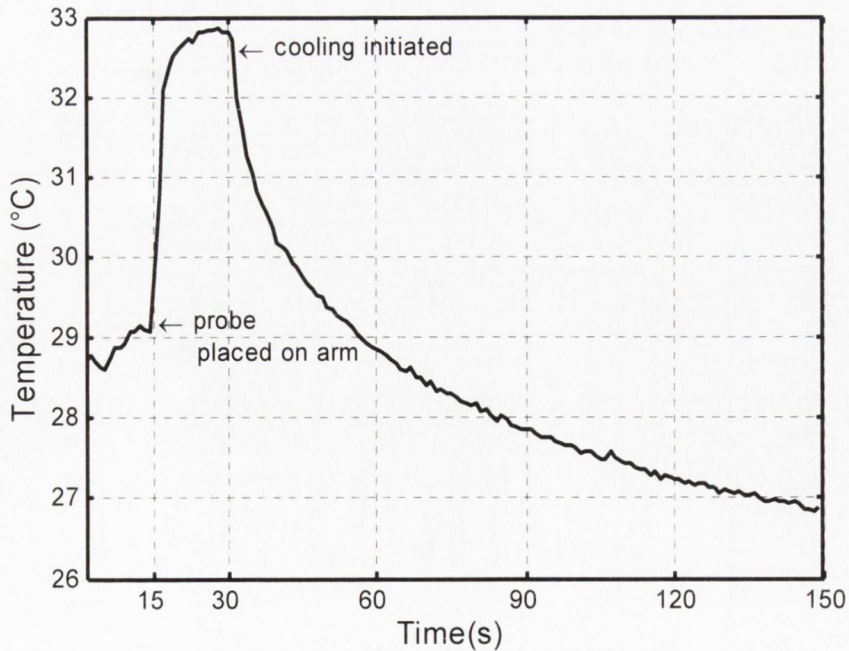
Figure 7-2 Temperature measurements from heat flux sensor on base plate of probe during placement (15-30s) and during test (30-150s)

107

The first attempt to mitigate this effect was to pre-heat the probe to a temperature equal to that of the skin by using a hot plate. However, this proved difficult to achieve in practice as once heated the probe cooled rapidly before it could be placed on the arm and so it was difficult to ensure equilibrium. This approach also caused an increase in the temperature of the cooling air flow for a period of seconds at the start of the forced convection part of the test, as heat stored in the probe was transferred to the air. This cooling of the plate and probe also tended to mask the cooling of the skin in the initial part of the forced convection test (15-30s). Thus it was decided not to proceed with heating the plate. Scott et al. [63] addressed this issue by placing the probe on one arm until it was in thermal equilibrium, at which point the probe was moved to the other arm for testing. However Scott et al. [63] merely held the probe on the arm whereas the use of the pressure cuff in the present study made such a transfer more difficult to effect. Nevertheless this procedure was implemented although, as with heating on the hot plate, there is a temperature drop during the transfer process.

Another solution was to model, using the transient code developed, the cooling that occurred during the placement period. The results from this would then be used as the initial condition for the forced convection part of the model. However as the level of contact resistance varies significantly during the placement period, it is difficult to accurately model the process. This is because contact resistance is a function of strapping pressure which increases sporadically as the cuff is inflated from 0mmHg when the probe is first placed on the arm to the final pressure of 45mmHg.

A further option to avoid preliminary heat transfer between the arm and the probe is to place a slim piece of insulating material between the cuff and the arm during the placement period; which can then be quickly removed once cooling starts. Results from such a test are shown in Figure 7-3.
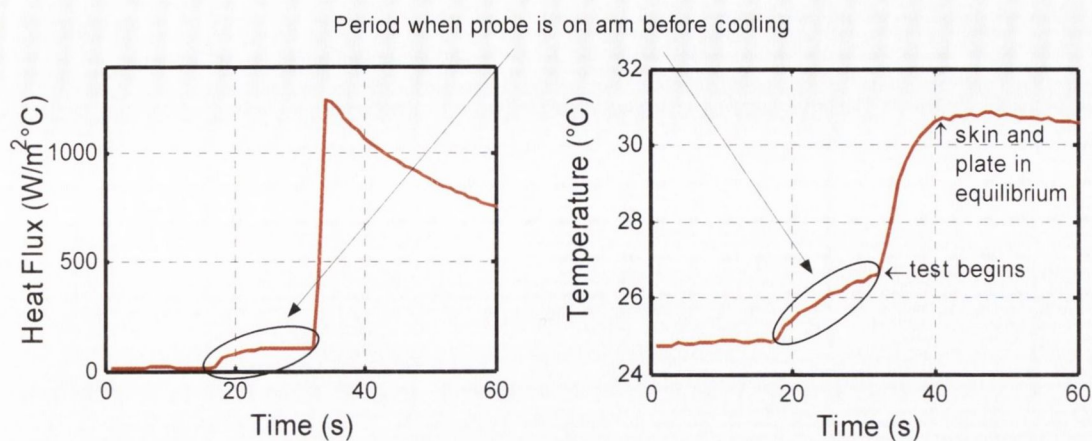
Figure 7-3 Effect on heat flux and temperature response during placement period with insulation between plate and skin

As can be seen, there is still some increase in the rate of heat transfer and plate temperature during the placement period, due to a limit on the thickness of the insulating material which must fit under the blood pressure cuff; although this level of cooling could be approximated as insignificant. As the insulating material is removed and cooling begins, the plate temperature must first increase to be in equilibrium with the skin temperature. After 40s both the skin and plate temperatures decrease together.

There are thus two possible options for minimising cooling of the tissue and hence disruption to the initial temperature profile during the placement period. The first is to pre-heat the probe on one arm before transferring it to the test arm and the second is to add insulation between the probe and the arm. However, before choosing one of these approaches it was decided to investigate the possibility of testing with the probe but without the copper base plate, which would simplify both the experimental and numerical procedures.

The plate performs two functions as described in section 6.2, the first is to hold the sensor in contact with the skin and the second is to provide an even level of cooling. However, due to the large number of impinging jets an even level of cooling is achieved without the presence of the copper plate. A method is then required to hold the sensor to the skin. Following testing, it was established that double sided adhesive tape worked very well in this regard. Removing the copper plate simplified the

experimental test by removing the need for the pressure cuff whose function had been to minimise contact resistance; it also simplified the model as there was no longer a requirement to model the contact resistance between the plate and the skin. This leads to a decrease in the level of uncertainty of the method. The final benefit is that the temperature of the skin is measured directly rather than inferred from the temperature of the copper plate when in contact with the skin. It may seem logical to question the reasoning for ever employing a base plate. It is felt that its use is a legacy from the first study in this area by Michener et al. [59], who used a water cooled probe which obviously required some interfacing material to contain the water within the probe. The use of a base plate then became standard practice in future studies which employed air cooling. The decision to test without a base plate alters the test procedure and leads to new results; this will be addressed in future sections.

7.2   VALIDITY OF MODELLING ASSUMPTIONS

After refining the experimental approach a number of the assumptions made in the development of the original finite difference as used in Chapter 6 were investigated. The main issues are:

1. whether a simple rectangular mesh running longitudinally along the arm can accurately reflect the geometry
2. the accuracy of modelling the problem in two rather than three dimensions

7.2.1 Longitudinal vs. transverse modelling planes

Due to the difficulty of defining curvature with a finite difference model, the original mesh was on a plane running longitudinally along the arm as shown in Figure 7-4. For this approach to work, two assumptions are necessary. The first is that there is no heat transfer normal to the plane and the second is that the base of the mesh is at the warmest point of the arm, such that the adiabatic boundary condition is accurately realised. The depth of the mesh was taken as half the perpendicular thickness of the arm at the measurement site. To test the accuracy of these assumptions it is necessary to construct a model on a transverse plane as shown in Figure 7-5.
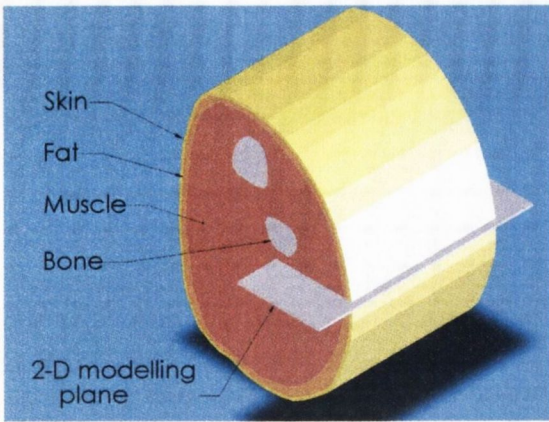
Figure 7-4 Mesh on longitudinal plane
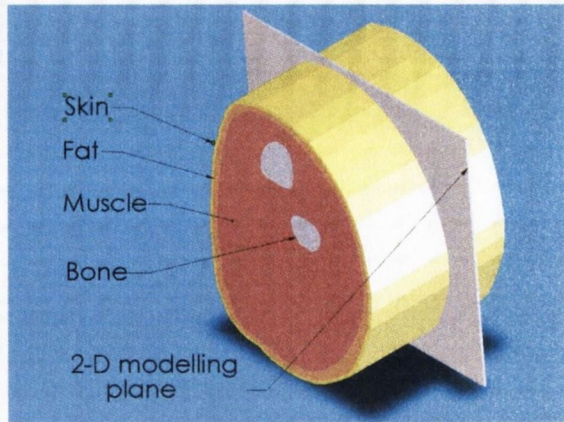
Figure 7-5 Mesh on transverse plane

An accurate transverse cross section requires realistic images of the human forearm. These were obtained from the Visible Human [83], two examples of which are shown in Figure 7-6 and Figure 7-7. The Visible Human was developed at the Centre for Human Simulation (CHS), which is located at the University of Colorado. It uses human specimens and sophisticated three-dimensional imaging techniques to generate high resolution images of human anatomy. For reasons outlined in Chapter 5, it was decided that rather than writing a bespoke finite difference mesher with the capability of handling curved surfaces, an existing commercially available finite element package would be employed with this capability; namely FemLab. The geometries obtained from the visible human were traced in AutoCAD and then imported into FemLab as DXF files for analysis. A full description of the analysis procedure is given in Section 7.4.2, for now only the results are presented.

Figure 7-6 Section 1720 from the visible human [83] with tracing
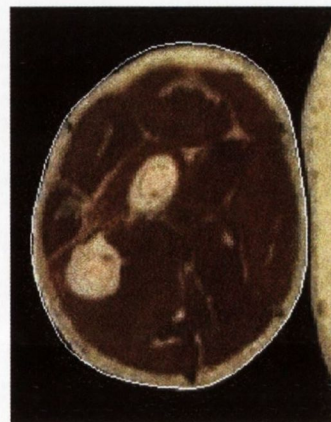
Figure 7-7 Section 1650 from the visible human [83] with tracing

111

To establish if the heat transfer normal to the longitudinal plane is significant, Figure 7-8 and Figure 7-9 show arrow plots and streamlines for the heat flux results under free convection conditions for cross section 1720 and 1650 (as shown in Figure 7-6 and Figure 7-7). For both cross sections it is clear that the choice of the measurement plane is limited to the principal axis of the limb where the assumption of no heat flow normal to the longitudinal plane is met. For axi-symmetrical cross sections such as these the depth of the mesh is well approximated by half the perpendicular thickness of the arm, i.e. the adiabatic boundary condition is realised at the base of the model.

Principle axis marked by bold lines
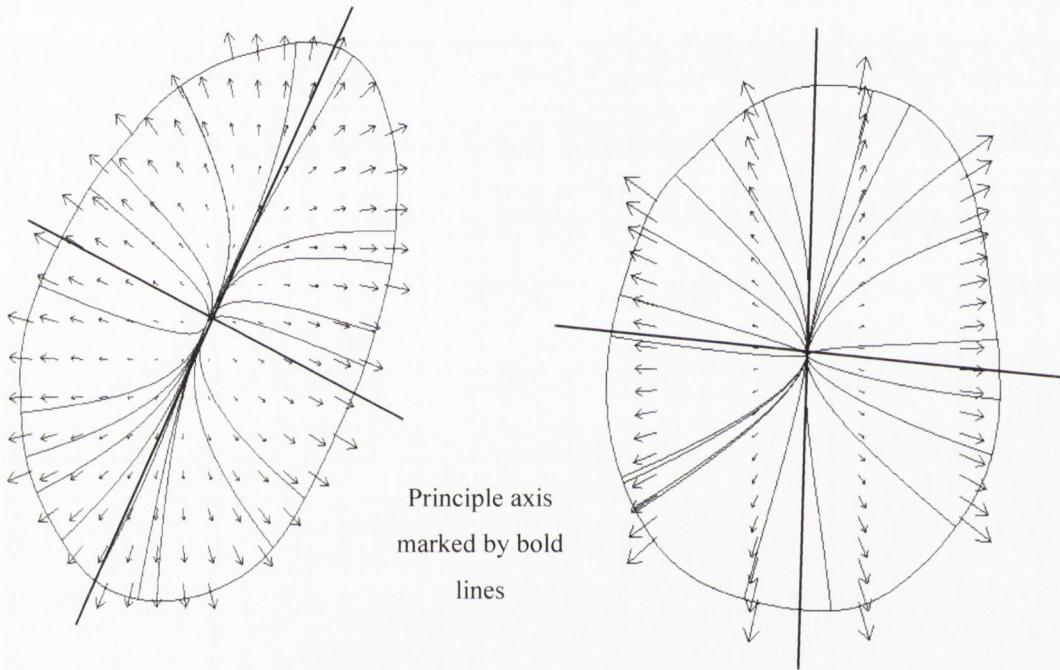
Figure 7-8 Streamline and arrow plots of heat flux results from FemLab, for cross section 1720, taken from the visible human [83]

Figure 7-9 Streamline and arrow plots of heat flux results from FemLab, for cross section 1650, taken from the visible human [83]

In conclusion, the longitudinal plane is easier to model as it requires only a simple rectangular mesh but there is a restriction on the choice of measurement location on the circumference of the arm, in order to satisfy the assumption of no heat transfer normal to the plane. An error in positioning of the centre of the mesh is unlikely to be critical as the temperature gradients in the centre of the arm are small and so the adiabatic boundary condition is well approximated. It was decided to proceed using the transverse cross sections modelled in FemLab, as this approach provides more useful information, namely the circumferential variation in surface temperature data.

7.2.2 Two vs. three dimensional modelling

The forced convection approach represents a three-dimensional (3-D) heat transfer problem, although to date any heat transfer normal to the modelling plane has been assumed to be negligible, in order to allow it be treated as a 2-D problem. The previous section showed this assumption to be accurate under limited conditions, i.e. when modelling using longitudinal cross sections on the principal axis of the arm under free convection conditions. For transverse cross sections under free convection conditions it was expected that this assumption would also hold true as the temperature gradients along the arm are small compared to those normal to it. However it is necessary to evaluate this assumption under forced convection conditions when more significant temperature gradients are established along the arm. To do this, surface temperature readings from a 3-D model are compared with those from a standard 2-D model formulated with the same material properties, boundary conditions and initial conditions. Figure 7-10 shows an initial temperature profile prior to application of cooling.

Figure 7-11 shows the tissue temperature distribution after cooling is applied by the probe. It is clear that the cooling area is well defined and symmetrical. Surface temperature distributions are recorded along the line x-x and displayed in Figure 7-12.
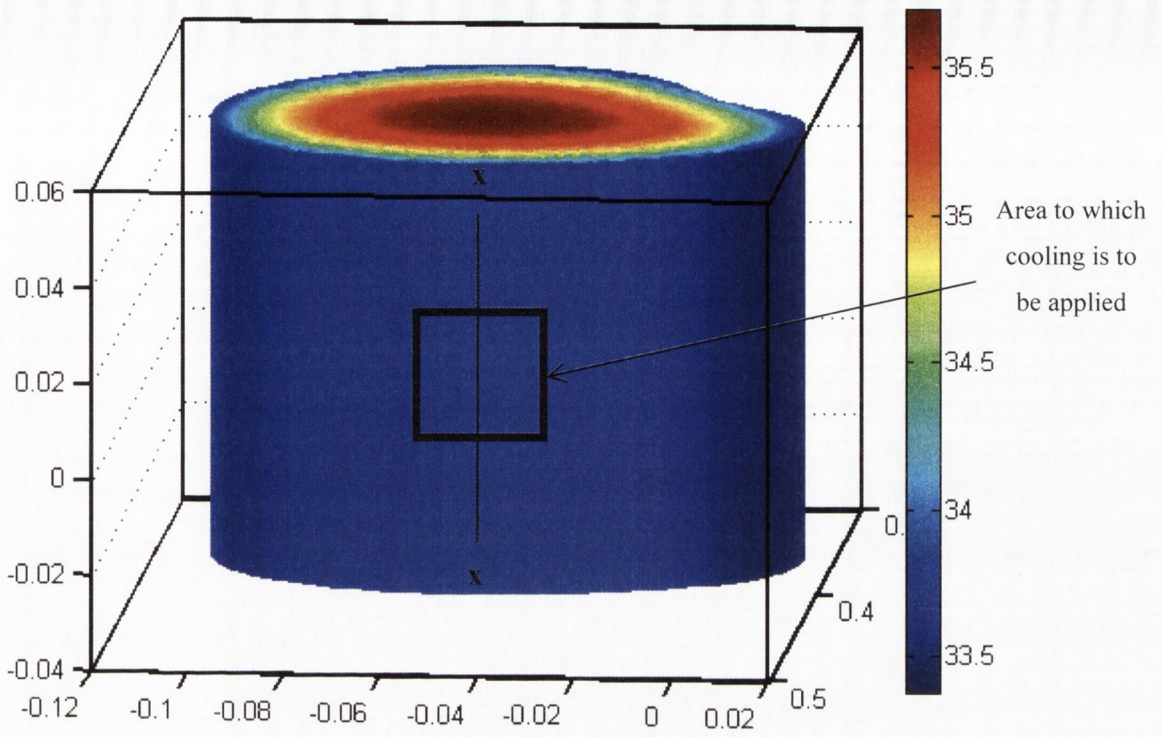
Figure 7-10 3-D model from FemLab showing initial tissue temperature distribution
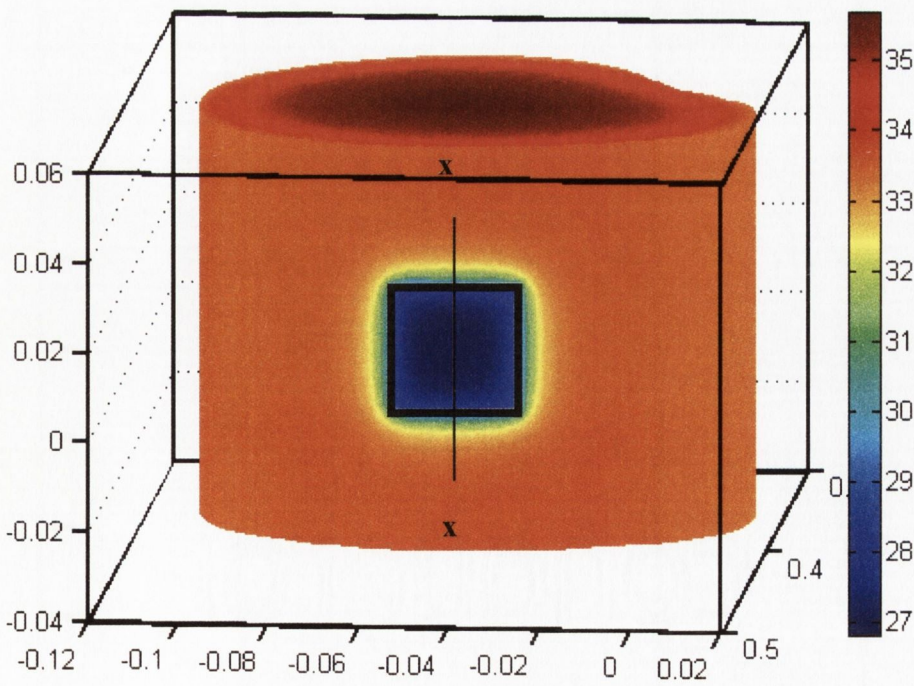
Figure 7-11 3-D model from FemLab showing tissue temperature distribution after cooling

114

From Figure 7-12 it is clear that at times less than 200s, that the temperature profile is very U shaped, with steep thermal gradients at the edge of the cooling region bounding a central plateau. This implies very gentle temperature gradients within the cooling area and so negligible levels of longitudinal heat transfer. As is to be expected, the 2-D and 3-D temperature profiles therefore match well within the area of the probe. Between 200-500s, the temperature profiles become more rounded. Above 500s the level of heat transfer into the area from the longitudinal direction is significant enough to cause a divergence in the temperatures of the two and three dimensional models. The 3-D model cools less rapidly as it has an extra heat source, i.e. it receives a heat input from the remainder of the arm. From the results it is clear that the error at the central measurement location associated with the 2-D assumption is minimal but increases with cooling time.
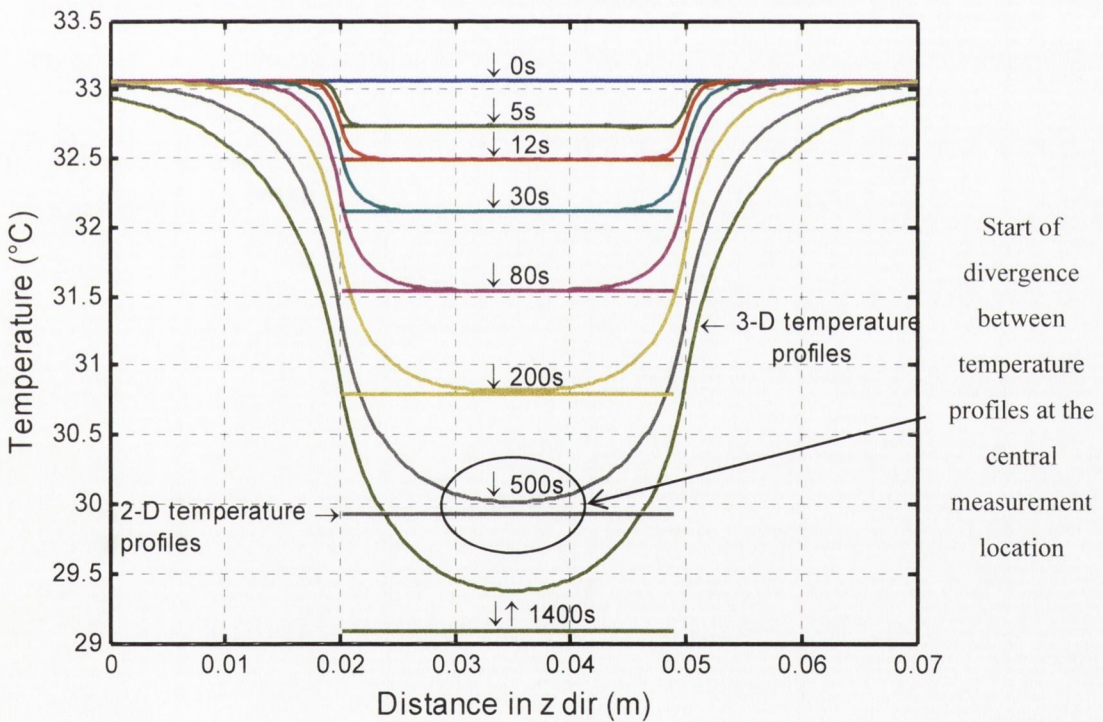
Figure 7-12 2-D vs. 3-D temperature profile for times [0, 5, 12, 30, 80, 200, 500, 1400s]

Table 7-1 and Table 7-2 show the cooling times above which the temperature difference between the 2-D and 3-D models at the central measurement location increases above 0.1°C for a range of convective heat transfer coefficients and levels of perfusion at ambient temperatures of 17°C and 25°C. In this context a temperature difference of 0.1°C is taken to represent a break down of the 2-D assumption. For a

115

given set of perfusion levels and convective heat transfer coefficients it was found that the maximum cooling times are longer at higher ambient temperatures. This is because less heat is stored in the arm at lower ambient temperature and so it takes less time for the heat transfer along the arm to become significant.

h ω	30W/m²°C	75W/m²°C	135W/m²°C	200W/m²°C
0.0001/s	600	500	650	700
0.001/s	650	650	600	750

Table 7-1 Maximum cooling times (in seconds) before which 2-D assumption breaks down for various perfusion and convective heat transfer levels at ambient temperature of 17°C

h ω	30W/m²°C	75W/m²°C	135W/m²°C	200W/m²°C
0.0001/s	800	700	800	1200
0.001/s	800	600	850	1200

Table 7-2 Maximum cooling times before which 2-D assumption breaks down for various perfusion and convective heat transfer levels at ambient temperature of 25°C

It is not practical to define a complete table of maximum cooling times for 2-D modelling as the problem is so multi-factorial. Instead maximum cooling times should be established prior to testing for the given cross section and convective heat transfer coefficient, expected perfusion levels and ambient conditions. Another point to note is the importance of taking temperature measurements at the centre of the cooling area, particularly when testing at longer times when the temperature profile becomes more rounded. In summary, 2-D modelling provides accurate data for surface temperature distributions provided that the period under consideration is appropriate and provided that care is taken in taking the temperature measurements for comparison.

7.3 ADVANCES IN ESTIMATION OF PERFUSION

The new modelling technique using transverse cross-sections and FemLab facilitate advances in the method of estimation of blood perfusion levels using the forced

convection approach. This section explains the theoretical basis for these improvements. First some issues relating to the use of cross sections from the visible human [83] are briefly discussed.

7.3.1 Applicability of images from the visible human

As the images from the human project clearly show the distribution of the various tissues, it is a simple matter to include these and their corresponding thermal properties in the model. Initially the images from the visible human [83] were scaled down to the size of the test subject. However from inspection of the images it became clear that the geometry and tissue distribution were different to the test subject's, whose arm was much leaner. A study was conducted to evaluate the importance of these factors.

Cross sectional geometry

The external shape of the cross section (circular or oval) affects the internal and surface temperature profile. Figure 7-13 shows a temperature map of a cross section from a human leg. Homogeneity is assumed and so the various tissues are not represented, in order to clearly show the effect of the external geometry. Table 7-3 shows the corresponding maximum range of temperature variation around the circumference for different perfusion levels.
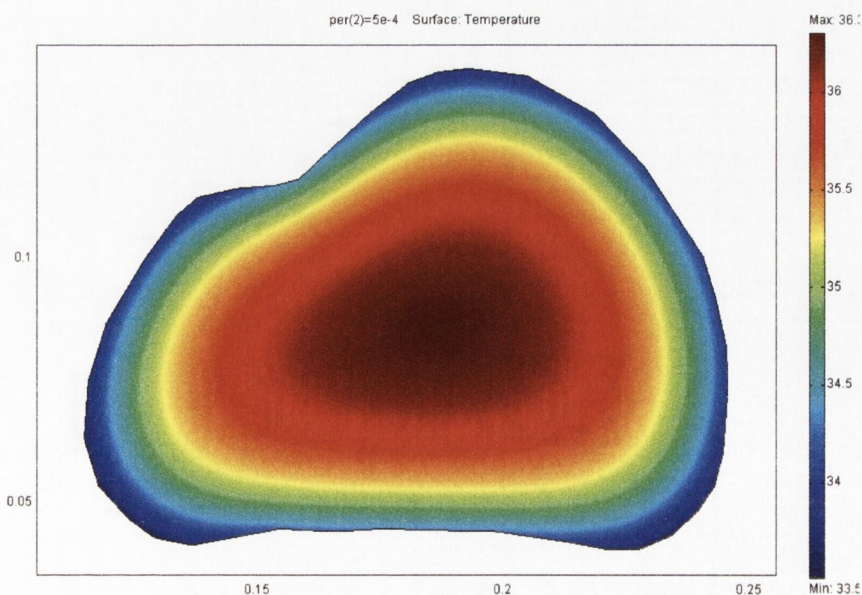
Figure 7-13 Temperature distribution through irregular cross section

117

Perfusion (1/s)	0	0.0005	0.001	0.0015	0.002
Max ΔT (°C)	0.3	0.65	0.4	0.35	0.3

Table 7-3 Maximum range of circumferential temperature values for different perfusion levels without tissue differentiation

This geometric temperature distribution is determined by the surface area to volume ratio for a given angular segment, and by the distance from the hottest point. It will tend to zero as the cross section becomes more circular.

Variation in underlying tissue distributions

A variation in the thickness of a layer of fat tissue will affect the cross sectional temperature profile. To illustrate this, a simplified circular three tissue model is presented to isolate the effect on the cross sectional temperature of a variation in fat thickness; this is shown in Figure 7-14. Constant perfusion is assumed throughout.
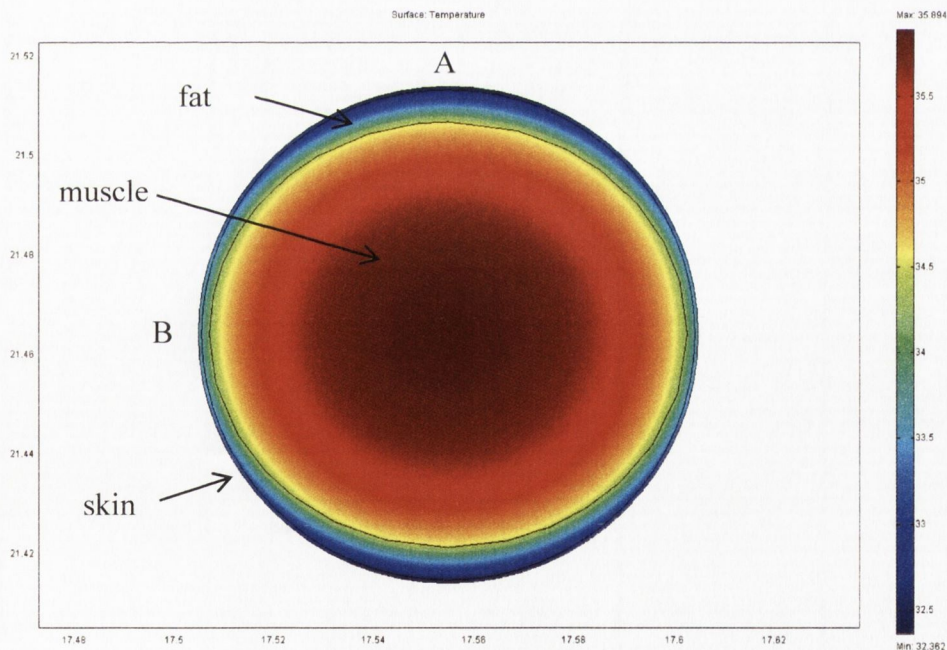
Figure 7-14 Distribution of various tissues and measurement locations

Variation in the fat thickness (between positions A and B) leads to a temperature difference, as shown in Table 7-4 for a range of perfusion values. The surface temperature for the fatty region is shown to be lower.

118

Perfusion (1/s)	0.0005	0.001	0.0015	0.002	0.0025	0.003
A (°C)	27.4	28.9	29.8	30.4	30.7	31.0
B (°C)	28.0	29.8	30.7	31.3	31.7	32.0
ΔT (°C)	0.6	0.8	0.9	0.9	1.0	1.0

Table 7-4 Variation in temperature between point A and B

The lower temperature at the fatty region is explained by the insulating effect of the fatty tissue, which decreases the level of heat conducted to the skin, as shown in Table 7-5.

Perfusion(1/s)	0.0005	0.001	0.0015	0.002	0.0025	0.003
A	46.8	47.3	46.2	44.8	43.3	41.8
B	57.6	60.1	60.3	60	59.4	58.7
ΔHF	10.8	12.8	14.2	15.2	16.1	16.8

Table 7-5 Heat conducted to the skin at point A and B

As the both the external geometric profile and the internal tissue distribution were found to have a significant effect on the surface temperature, it was decided that use of profiles from the Human Experiment were not appropriate. Instead it was considered necessary to acquire MRI images of the test subject's arm, to give a realistic and accurate representation of both external geometry and internal tissue layers.

7.3.2 Description of Possible Perfusion Values (PPV) curve

Using the FemLab model and the acquired MRI scans, described in Section 7.4, this study now had available to it a more accurate representation of the tissue distribution and cross sectional shape of a test subject's arm than any prior study conducted in this area. Once this model had been set-up it seemed inadequate to assign the entire volume a singular perfusion value, as done in previous studies, as the factors driving the levels of muscle and skin blood flow differ dramatically. Therefore the skin and muscle perfusion were assigned independent values. (As noted by Wilson and Spence [57] the thermal contribution of perfusion to the fatty tissue is considered negligible.) This led to the critical realisation that, for a specific case where the limb geometry and tissue distributions are defined, a given value of skin temperature under steady state

119

free convection conditions, can only be produced by certain combinations of skin and muscle perfusion. Such steady state free convection conditions would pertain at the beginning of a forced convection test. For example, a specific skin temperature could be due to a very high muscle perfusion and a very low skin perfusion or to a low muscle perfusion and a high skin perfusion value. These possible skin and muscle perfusion combinations can be described by what shall be defined as a Possible Perfusion Values (PPV) curve. A theoretical example of such a curve is shown in Figure 7-15.
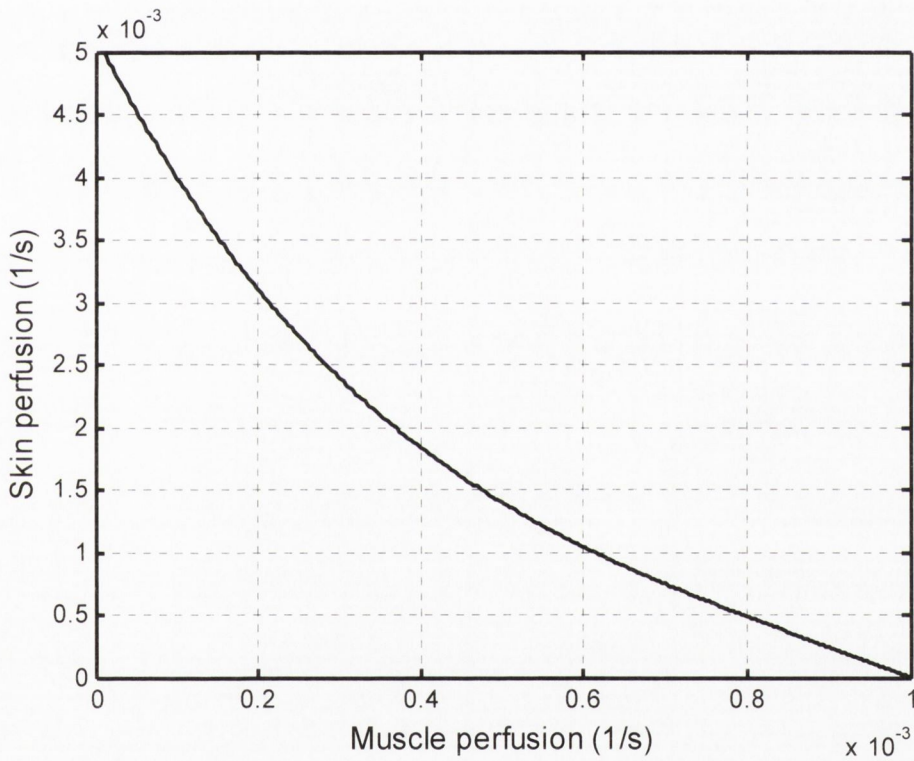
Figure 7-15 Possible Perfusion Values Curve: showing the possible combinations of skin and muscle perfusion occurring in a specific human limb for given ambient conditions and skin surface temperature

The use of this curve, in conjunction with the forced convection approach, now offers the opportunity to make real progress in the determination of perfusion from forced convection testing. Thus, previous studies using the forced convection approach have been ambiguous in how they define the initial temperature distribution. This approach which links possible surface temperatures to tissue perfusion levels is much more rigorous and physiologically realistic. However from a surface temperature reading it is impossible to deduce which particular combination of perfusion values from the

PPV curve is actually occurring. The expectation was that when an area was subject to a forced convection test and the model run for a range of perfusion values identified from the PPV curve, only one resulting temperature response would match, as shown in Figure 7-16.
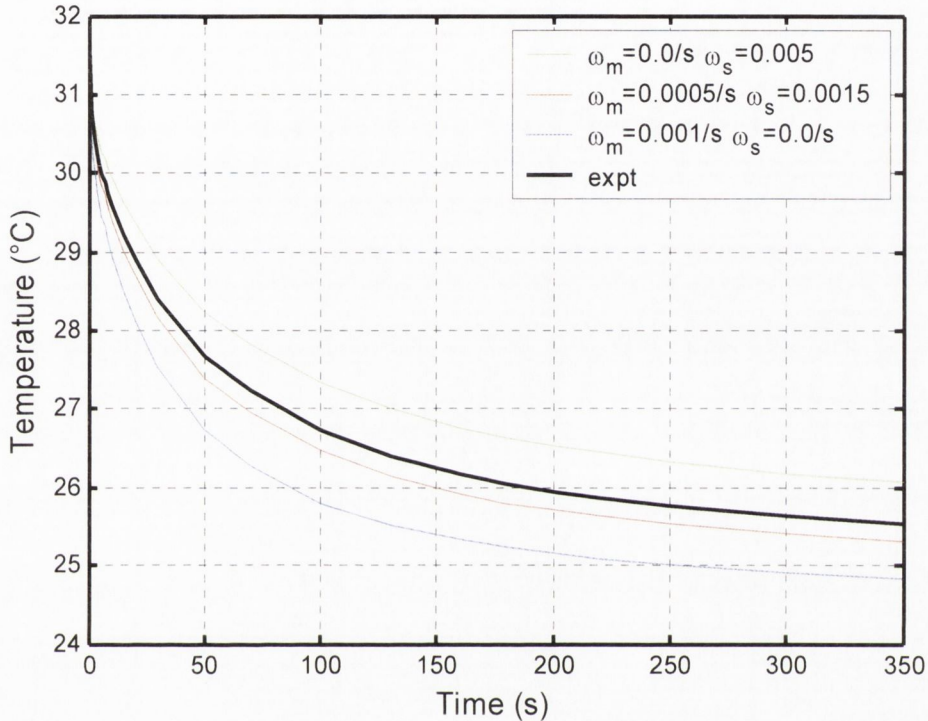
Figure 7-16 Theoretical experimental and numerical comparison of temperature results from a forced convection test for various perfusion combinations of skin and muscle perfusion from the PPV curve shown in Figure 7-15

For the theoretical case shown in Figure 7-16, the results would suggest that the skin and muscle perfusion values can be estimated as 0.0015/s and 0.0005/s respectively as this particular combination is most consistent with the measured temperature distribution with time. This is the theoretical basis for the advancement in the perfusion estimation procedure using the forced convection test.

7.4 IMPLEMENTATION OF REFINED APPROACH

The theory behind the proposed perfusion estimation method has been outlined in the previous section. This section describes the new experimental and numerical test procedures required to implement the proposed developments. An important consideration is that at this point testing switched from the forearm to the lower leg.

This was for three reasons. Firstly, while MRI scans were taken of both the forearm and lower leg, the images of the leg were found to be of higher quality. The second reason was that it was found that the value of convective heat transfer coefficient varied circumferentially around the arm. To measure this variation a heat flux sensor was placed on the lateral surface of the arm. The horizontally supported arm was then rotated in increments of 90°. It is not physically possible to achieve a rotation of 360° so symmetry was assumed. Readings of heat flux and surface temperature were taken at 0°, 90°, 180°. This procedure was repeated a number of times. In each case it was found that there was a maximum value of heat transfer coefficient at the lower surface and a minimum value at the top surface; this is shown in Table 7-6. This is broadly consistent with standard heat transfer theory as outlined by Kreith and Bohn [84] for a heated isothermal horizontal cylinder under natural convection.

Bottom	Side	Top
100%	90%	70%

Table 7-6 % variation of h around the circumference compared to bottom value

While it is possible to incorporate this variation into the computer model it is rather cumbersome. The leg can be approximated as a vertical cylinder and so does not experience this variation. Finally with the leg, it is easier to provoke changes in the muscle blood flow through exercise.

7.4.1 Experimental testing

The experimental test contains two parts, a free convection test to derive the PPV curve and a forced convection test to establish the position on the curve and hence the perfusion values. Both tests are conducted in one sitting, with the free convection test being carried out first. At this point in the study the thermocouples were dispensed with in favour of the thermistors, which have greater accuracy and better stability, as discussed in Section 6.3.

The test procedure is as follows. For accuracy it is important that the experimental test position can be matched precisely to the numerical test position. To achieve this, a traced cross section (with the measurement location marked) is printed out and the

inside of the cross section is cut out allowing the marked measurement location on the sheet to be transferred to the leg, as shown in Figure 7-17. The vertical distance is measured from the ankle bone and corresponds to the distance up the leg at which the MRI scan was taken. A measurement site on the lateral side of the leg was chosen as it is the easiest position at which to physically perform a test, when the test subject is themselves conducting the test. During the cooling part of the test a tufnol sheet is used to isolate the cooling area. To aid placement its shape is now also traced onto the leg.
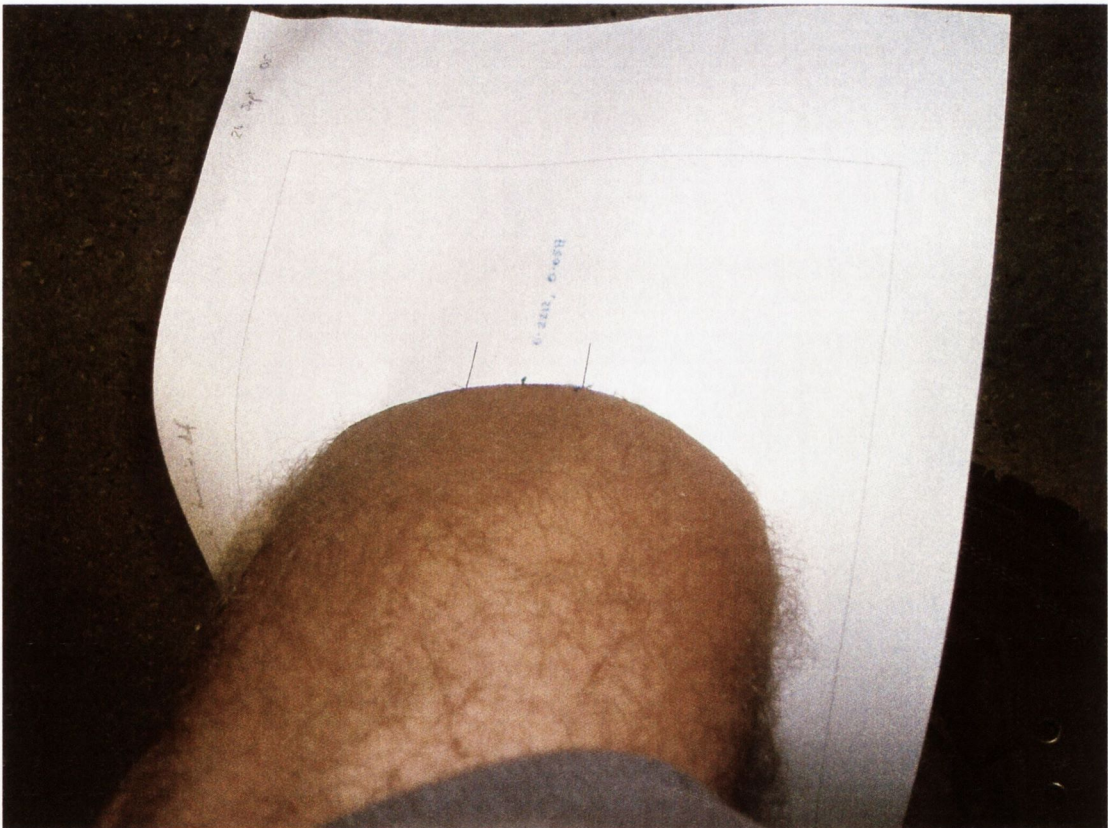
Figure 7-17 Photo showing the measurement location being marked on the leg

Before a test begins, the candidate sits at rest for a period of fifteen minutes with the leg uncovered to allow it to equilibrate with the ambient environment in order to give a true steady state temperature measurement. After this time, the heat flux sensor and thermistor are stuck to the leg using double sided tape. The thermistor is placed in the central location with the heat flux sensor displaced slightly to the side. The test sequence may now begin.

The first part of the test is to take steady state free convection measurements of temperature and heat flux for the determination of the convective heat transfer coefficient. Once again LabView is used to record the various measurements, namely, heat flux, skin temperature, ambient temperature and free stream temperature. The program begins recording and continues recording until the transient test is completed. The free convection part of the test continues until it is confirmed that a steady state condition has been reached. Once this has been established the forced convection part of the test may begin.

The tufnol sheet is placed over the traced area. Before the test the cooling air stream is on and preset to give the desired convective heat transfer coefficient. The probe is then taken and held against the leg. There is no need for the cuff as the contact pressure is now no longer a factor without the plate. It is important that the probe is positioned correctly and held firmly in position. The test continues for the allotted time period after which time the probe is removed and measurement of temperatures ceases. Typical experimental results for the free and forced convection parts of the test are shown in Figure 7-18.

As can be seen, this testing procedure is simpler than the original as there is no complicated placement procedure and the experimenter can be confident that cooling begins with an undisrupted initial temperature profile. The next step in the procedure is to compare the results with the numerical simulation.
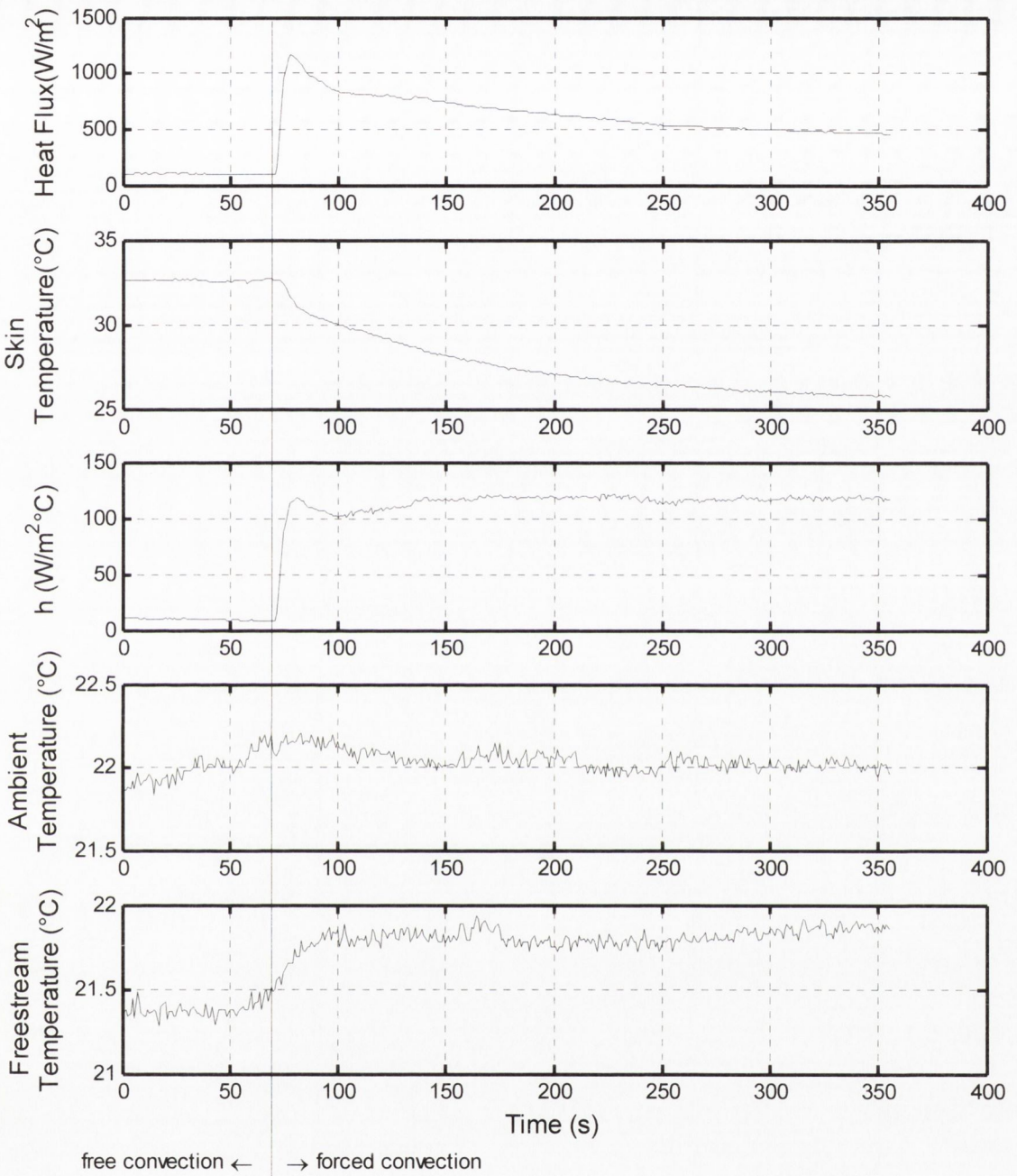
Figure 7-18 Typical free and forced experimental results

7.4.2 Numerical simulation

The full procedure for developing the numerical model will be outlined here although not all of it needs to be repeated for each test. First the relevant cross section corresponding to the test location is chosen from the set of MRI scans. Three examples of MRI scans of the test subject's leg are shown in Figure 7-19. The external shape and tissue distribution from the chosen MRI scan must be traced in AutoCAD for use in the model. However as apparent in Figure 7-19 (a) the profile of the leg is flattened as the test subject is lying down when the MRI scans are taken, but testing is conducted with the candidate standing. As the profiles between standing and sitting are dramatically different, the external profile needs to be altered to that of the leg for its standing position. This is done iteratively by changing the shape in AutoCAD and comparing a cut out version with the leg (in a similar manner to that shown in Figure 7-17). The shape is then again corrected in AutoCAD and the process continues until there is a good match. The profile of the front of the leg remains unchanged which allows the location of the bones to be fixed. The fat distribution is measured at fixed distances around the circumference. Once the external shape is correct the internal tissue distributions are added using the measurements taken. A check is done to ensure the area of the original and final cross sections are the same and that the tissue thicknesses are correct around the circumference. Surprisingly perhaps this process is quite simple and only requires 3 or 4 iterations before there is a good fit. It was found that cross sections taken further down the leg, such as shown in Figure 7-19 (c) do not need correction. The altered profile from Figure 7-19 (a) is shown in Figure 7-20.

(a)   (b)   (c)
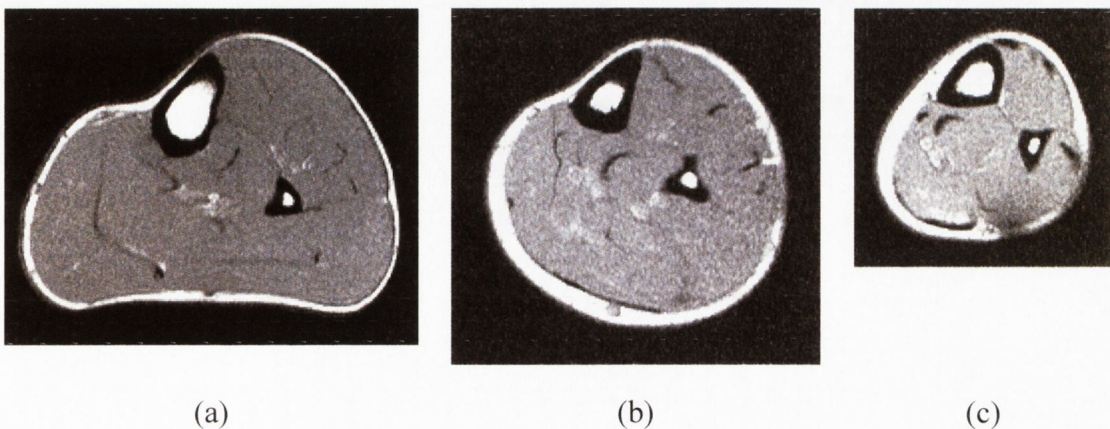
Figure 7-19 Examples of MRI scans taken of test subject's lower leg
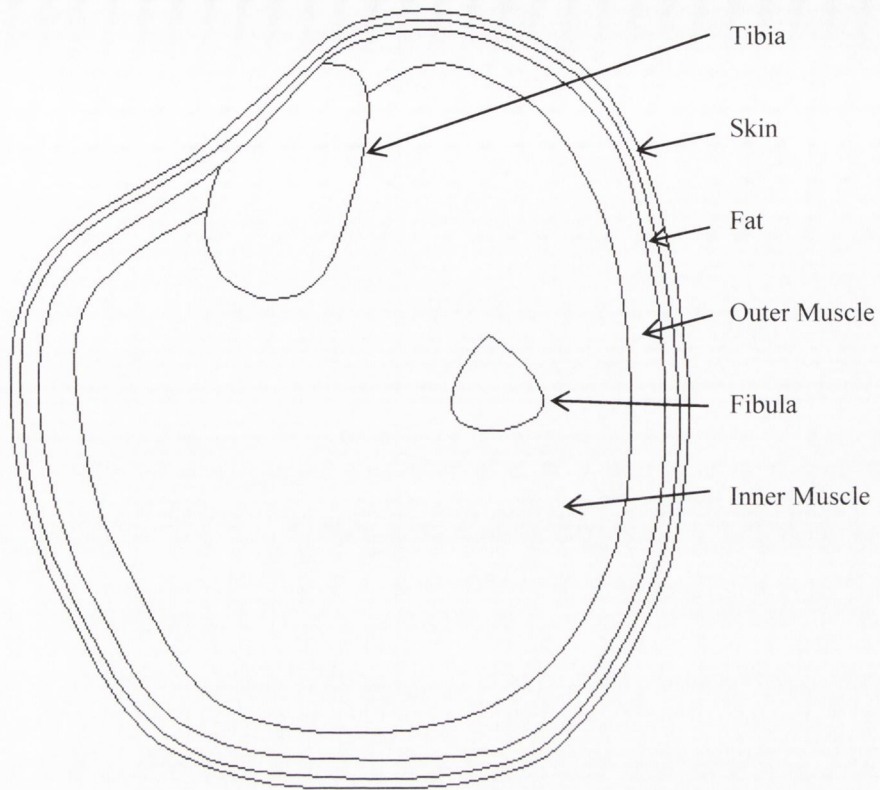
Figure 7-20 Traced cross section of MRI scan from test subject

The muscle domain is divided into inner and outer regions to allow application of Brink and Werner's [36] correction factor for the heat contribution from the muscle perfusion. The completed cross section is now ready to be imported into FemLab for analysis. The numerical analysis is divided into free and forced convection parts for clarity.

Modelling of free convection part of test

The object of this part of the test is to derive the PPV curve. The steps in the solution process are as follows:

1. The bio-heat application mode is selected in FemLab
2. The relevant cross section is imported into FemLab
3. The material properties are applied using values from Appendix A 1. The experimentally measured boundary conditions are applied; namely ambient temperature and convective heat transfer coefficient

4. The domain is now meshed with greater mesh density proximal to the cooling area as shown in Figure 7-21

5. The steady state non-linear solver is selected

6. A convergence test is carried out for various element sizes to verify the mesh. This is shown in Figure 7-22.
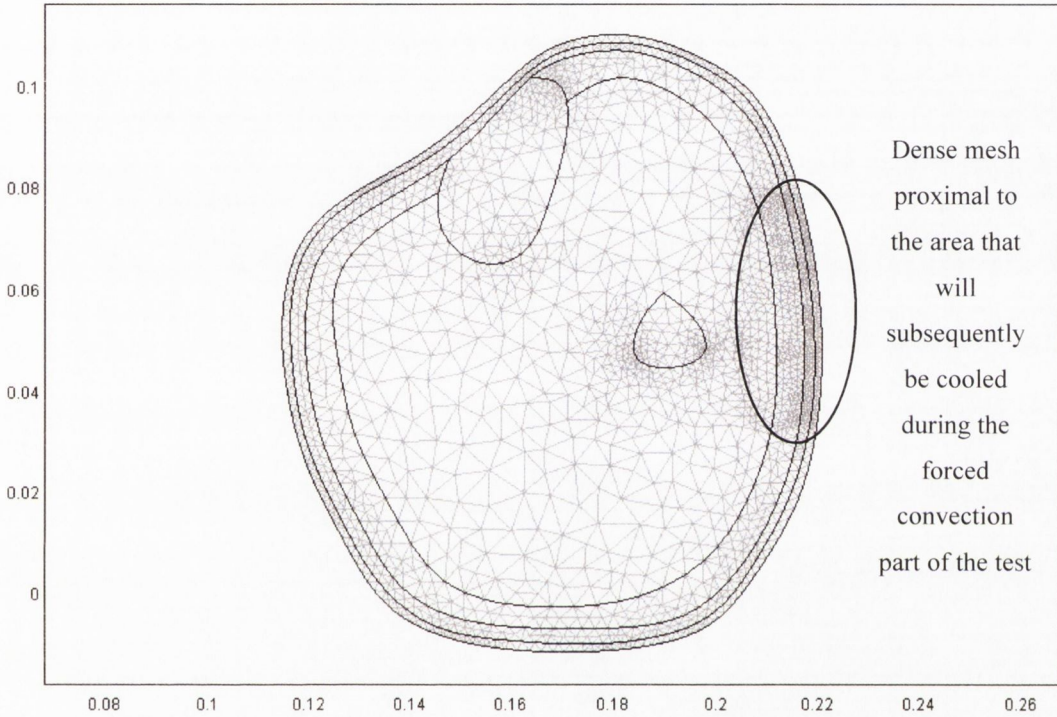
Figure 7-21 Screen capture from FemLab showing typical mesh
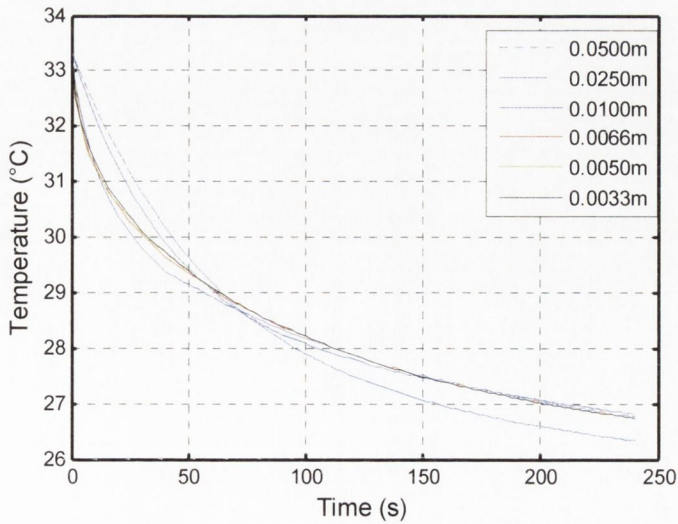
Figure 7-22 Convergence test from FemLab for various element sizes

The model is now ready to be solved. In order to derive the PPV curve it is highly beneficial to take advantage of the MatLab interface. The aim is to find the specific values of skin and muscle perfusion, that give the same steady state temperature as measured under free convection conditions in the experimental tests. This requires running the model for a large range of possible skin and muscle perfusion combinations. This is achieved by running the steady state model inside two loops, one to iterate the value of muscle perfusion and one to iterate the value of skin perfusion. This code is implemented in MatLab. For a given value of muscle perfusion, the value of skin perfusion which correlates to the experimental temperature value is found by interpolating between the two perfusion values which gave the closest temperature readings. This procedure continues until the maximum value of muscle perfusion has been reached (which can take up to 60 separate runs.) The PPV curve for test data from Figure 7-18 is shown in Figure 7-23. Next the forced convection part of the test is conducted in order to isolate the specific combination of perfusion values occurring from the PPV curve.
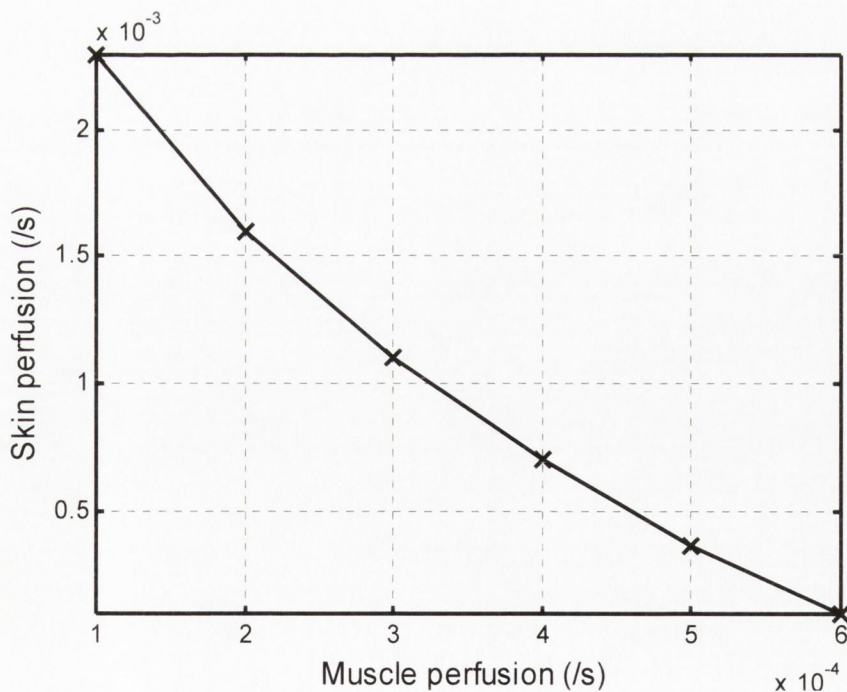
Figure 7-23 PPV curve for test data shown in Figure 7-18

Forced convection test

A range of values are chosen from the PPV curve. The values of convective heat transfer coefficient and free stream temperature measured during the forced convection test are applied to the boundary of the cooling area. The areas proximal to the cooling area are assigned an intermediate value of convective heat transfer coefficient to account for an increased level of cooling that occurs when air exiting the probe blows over these regions. All other boundary conditions are left unchanged. If any significant variations in these parameters are noted during the test they are included as time varying properties in the model. Use is again made of the MatLab interface to run the model for the various combinations of perfusion levels. The perfusion levels are inputted and the model uses these perfusion values to once again run the steady state model so that the initial temperature profile is correct. This result is then used as the initial condition for the transient model which is then run for the allotted time. Finally the results are then automatically compared with those from the experimental test, an example of which is shown in Figure 7-24.
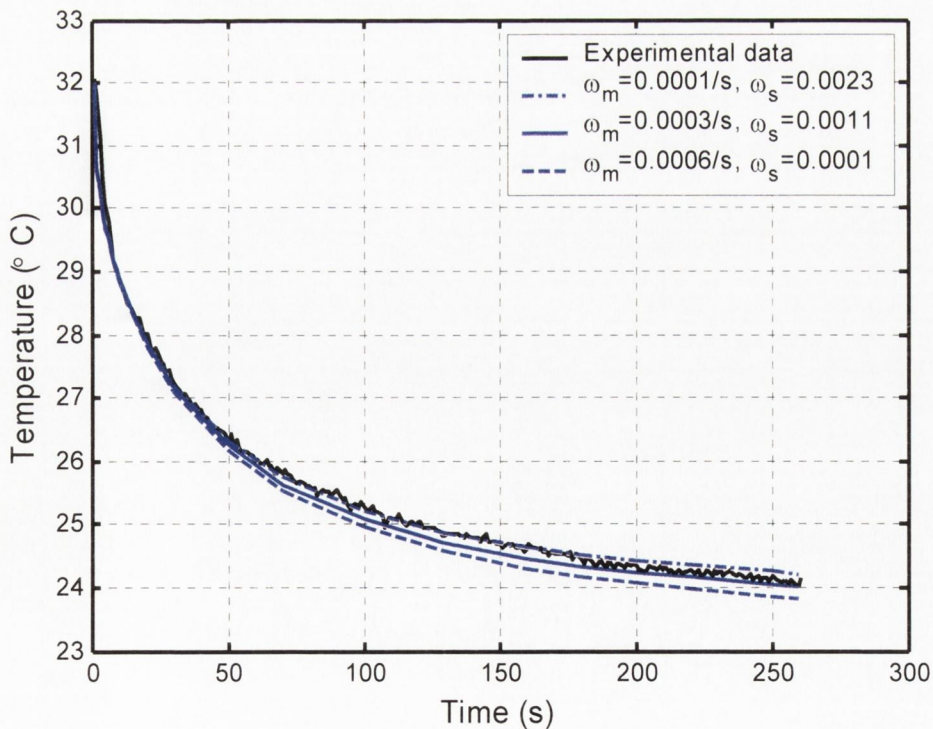
Figure 7-24 Comparison between experimental and numerical results for forced convection part of test

130

In general the correlation between the experimental and numerical results was reasonable, although some tests were shown to exhibit poor correlation. This could be due to a number of factors such as movement of the probe during testing, mis-positioning of the sensors or an inaccurate measurement of the free convection heat transfer coefficient. However, returning to Figure 7-24 it is obvious that the main problem with the results is that there is only a small difference in temperature (0.4°C) over the entire range of perfusion combinations, which implies that the results are very insensitive to perfusion values. Considering that the experimental error associated with the thermistors alone is +/- 0.1°C, this temperature range is clearly not large enough to allow accurate determination of perfusion. The next section deals with optimising the test parameters.

7.5   OPTIMISATION OF TEST SENSITIVITY

After this initial phase of testing had been completed, it was clear that changes in the perfusion combinations did not generate significant temperature differences. At a minimum it was considered that there should be at least a 1.0°C difference (between the extreme values on the PPV curve), such that the effect of the uncertainty of the method would be reduced to an acceptable level. In order to increase the temperature difference between the curves and hence the sensitivity of the method an optimisation analysis was conducted on the cooling time and heat transfer coefficient.

The procedure for this optimisation analysis is as follows. A free convection experimental test is completed, for which a PPV curve is derived. The transient numerical model is then run for the extreme values from the PPV curve for a range of forced convective heat transfer coefficients at long cooling times, in order to establish the maximum achievable temperature difference. The results of this are shown in Figure 7-25.
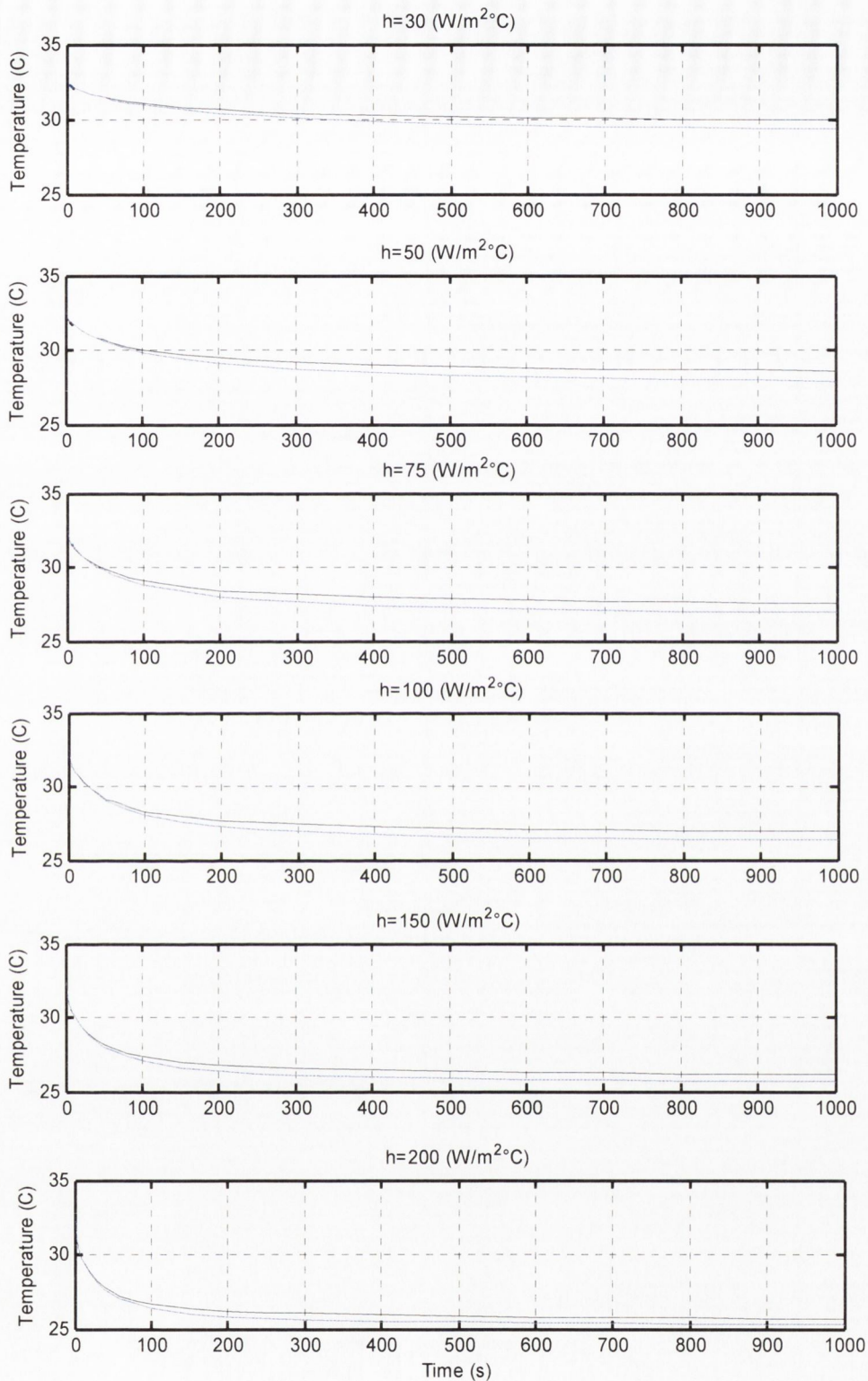
Figure 7-25 Temperature responses for extreme values on PPV curve for various h values. Top line corresponds to (ω_s=0.0034/s, ω_m=0.0001/s) and bottom line corresponds to (ω_s=0.0001/s, ω_m=0.0006/s)

The maximum temperature difference between the curves achieved in each test is recorded along with the time at which it occurred. The maximum temperature

difference from each test is then plotted against the convective heat transfer coefficient for the test as shown in Figure 7-26.
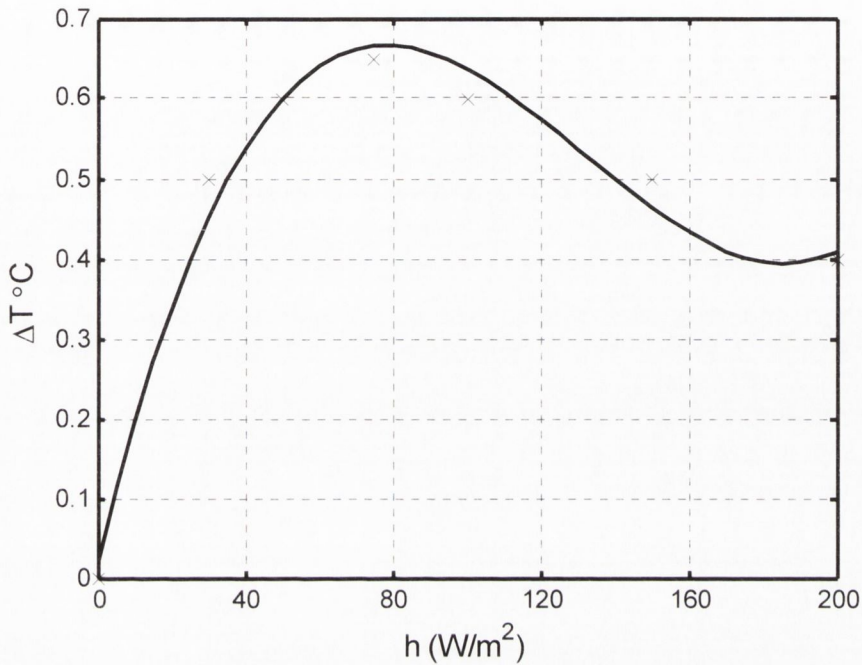
Figure 7-26 Maximum temperature difference for various values of convective heat transfer coefficient from Figure 7-25

For this particular case the optimum value of convective heat transfer coefficient is at 75 $W/m^2°C$ and the maximum temperature difference occurs at 500s into the test. The reason for this particular convection coefficient being the optimum value has to do with the ratio of heat conducted from muscle tissue to the rate at which heat is generated from the skin perfusion source term. As the skin temperature decreases the temperature difference between the skin tissue and the arterial temperature increases and so the heat generated by perfusion increases. However as the skin temperature drop is not very large at low values of convective heat transfer coefficient there is no dramatic increase in perfusion heat generation and so the temperature difference for varying perfusion levels remains small. As the value of convective heat transfer coefficient increases the tissue temperature drops and so the perfusion term becomes greater thus increasing the temperature difference between the curves with high and low skin perfusion. However as the cooling increases further the heat generated by

133

the perfusion becomes small compared with the overall loss of thermal energy and so there is no major effect and the temperature difference once again decreases.

7.6   EXPLANATION FOR LACK OF SENSITIVITY

To explain the lack of sensitivity of the method it is useful to examine how the heat flowing from the limb divides among it various sources. It was found that most of the heat flowing from the skin surface comes from the heat energy extracted from the tissue associated with its temperature drop. The heat conduction into the cooling area and heat generated by perfusion are both relatively small and so have a minor effect on the temperature profiles. The reason for the curves with higher skin perfusion values having a less rapid fall in temperature can also be explained with this analysis. As the tissue temperature drops the rate of perfusion heat generation increases as it is proportional to the temperature difference between the arterial and tissue temperature. The curves with a higher skin perfusion value maintain a higher temperature value as the skin perfusion generation term increases more rapidly than the conduction term.

7.7   SUMMARY

The work in this Chapter describes a range of developments in the FCA. These include improvements in the experimental procedure, investigation of the modelling assumptions and development of the PPV methodology. The PPV methodology accounts for the division between skin and muscle perfusion while also allowing the model to generate accurate initial temperature profiles. However, when this technique was implemented it was found to be not capable of discriminating between various combinations of perfusion values from the PPV curve under the test conditions described. This issue is discussed further in Section 9.2. With this result in mind another method was attempted to estimate skin and muscle perfusion using thermal measurements at the skin surface as outlined in the following chapter.

8 STEADY STATE PERFUSION MEASUREMENTS

As the sensitivity of the Forced Convection Technique was shown to be poor it was decided to attempt inferring perfusion by using surface temperature measurements under free convection conditions. Initially the simple case of the finger was examined before a technique was developed for the rest of the limb. Results of these tests will be presented, which demonstrate the overall effectiveness of this method.

8.1 FINGER PERFUSION MEASUREMENTS

The finger is a simpler problem than either the forearm or the leg in terms of geometry and in that perfusion can be assumed to be isolated to the skin tissue as the perfusion to the bone and fatty tissue is negligible. There are two further advantages of testing on the finger; the first is that an accurate estimation of arterial temperature is possible by insulating a neighbouring finger, thus eliminating any heat loss such that the finger attains the temperature of arterial blood. Secondly, it is possible to validate the test results, using finger plethysmography as described in Section 4.2.2. To date, many researchers have concluded that their results are accurate provided that they lie within the range stated by literature. However, clearly the ability to verify the results against an accepted method is highly beneficial. Advice was sought from Bell [61] in this area.

Experimental and numerical techniques

As described in section 6.5.3 for accurate absolute perfusion measurements it is important to know the arterial temperature. For limb measurements it is assumed that arterial temperature is close to the body core temperature, however as the fingers are so far from the core it is reasonable to expect that significant cooling of the blood will occur. This is measured by insulating one finger and waiting for the temperature to come to equilibrium. One can assume that this is the arterial temperature as there is little heat generation due to metabolism in the finger.

The heat flux sensor is taped mid way along the medial surface of the finger. The strain gauge for the plethysmograph is placed on the end of the finger while the pressure cuff is positioned around the wrist. The perfusion level was altered in a

135

number of ways, namely by changing the ambient temperature, by use of a pressure cuff and by placing the un-instrumented hand in either a warm or cold water bath to provoke a sensory reaction.

After experimental testing, a three dimensional model was constructed in which the finger is approximated as a rectangular volume. The temperature at the root of the finger is measured at the start of the experimental test from which a steady state temperature distribution is calculated for the nodes on the first cross section. This is then set as a constant temperature boundary condition. A natural convection boundary condition is assigned to the nodes on the remaining surfaces. The measured arterial temperature is then inputted. The solution process is straightforward as there is only one perfusion varying term, namely skin perfusion. The model loops through a range of skin perfusion values for each of which it outputs a surface temperature measurement at the measurement location. The program then interpolates between these values to establish the level of skin perfusion. Initial testing showed good correlation between the experimental and numerical measurements, as shown in Table 8-1 providing a positive indicator for a more comprehensive investigation based on the steady state approach.

	Test 1 (after being in warm room)	Test 2 (after being cooled)
Plethysmograph	60-65 (ml/100ml/min)	19-21 (ml/100ml/min)
From model	59 (ml/100ml/min)	23 (ml/100ml/min)

Table 8-1 Results from initial testing on finger using plethysmograph

8.2 THEORETICAL METHOD FOR MEASURING SKIN PERFUSION UNDER STEADY STATE CONDITIONS

As explained in Chapter 7, when a PPV curve is derived from a surface temperature reading, it is impossible to infer which particular combination of skin and muscle perfusion is actually occurring, without carrying out a forced convection test. However, the forced convection approach showed poor sensitivity in isolating the particular combination of perfusion values, which therefore led to an investigation of

other methods. It was theorised that if a second surface temperature measurement were to be taken at a different circumferential location with a different level of underlying fatty tissue, that this might give a PPV curve with a different slope to the first. The intersection of these two PPV curves would then give the relative values of skin and muscle perfusion. This concept is illustrated in Figure 8-1.
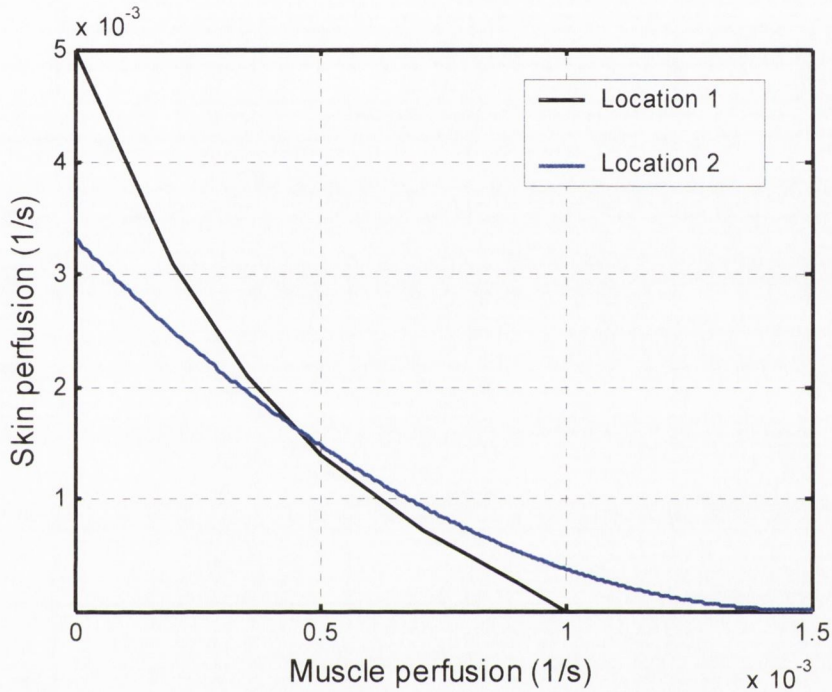
Figure 8-1 Theoretical intersection of two PPV curves

This technique requires no significant further development in the experimental or numerical procedures as the existing modelling techniques and experimental set-up can be utilised. In fact it is a simpler case as no transient modelling is required.

8.3   TEST PROCEDURE

The aim of the test is to generate at least two PPV curves by measuring temperature simultaneously at two different circumferential locations. However, generally three or four measurement locations are used to confirm the result, such that the multiple curves intersect at the same point. The method of generating the individual perfusion curves is identical to the method used in Chapter 7. The experimental and numerical procedure is once again briefly listed here:

1. Various measurement locations are chosen, preferably with differing thickness of underlying fat tissue.

2. These locations are then marked on the leg

3. The uncovered leg is allowed to equilibrate with environment for 15 minutes

4. The thermistors are taped to the leg at the measurement locations

5. Measurements are taken until steady state conditions have been confirmed

6. Test locations on the leg, boundary conditions and surface temperature measurements are inputted into numerical model

7. The model is run

8. Model outputs PPV curve for each test location

A range of tests were carried out at different cross sections and measurement locations on the leg as marked in Figure 8-2, Figure 8-4, Figure 8-6 and Figure 8-8. The corresponding perfusion curves are shown in Figure 8-3, Figure 8-5, Figure 8-7 and Figure 8-9 respectively.

Test 1
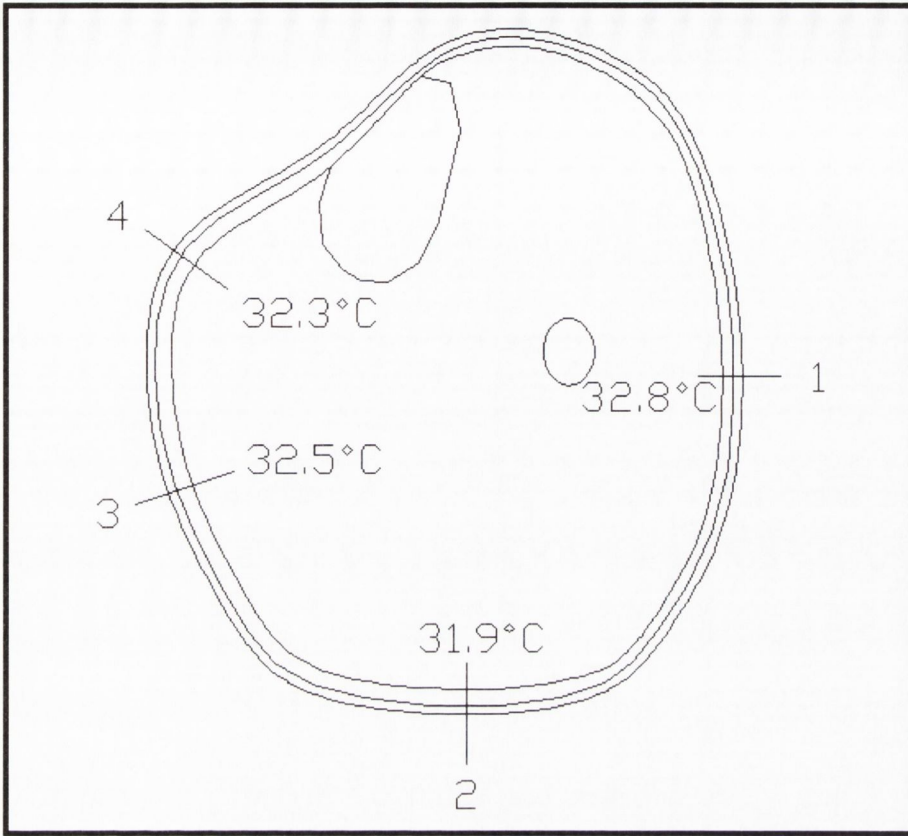
Figure 8-2 MRI 15 showing sensor locations and corresponding temperatures for Test 1 (T_{amb}=24.0°C)
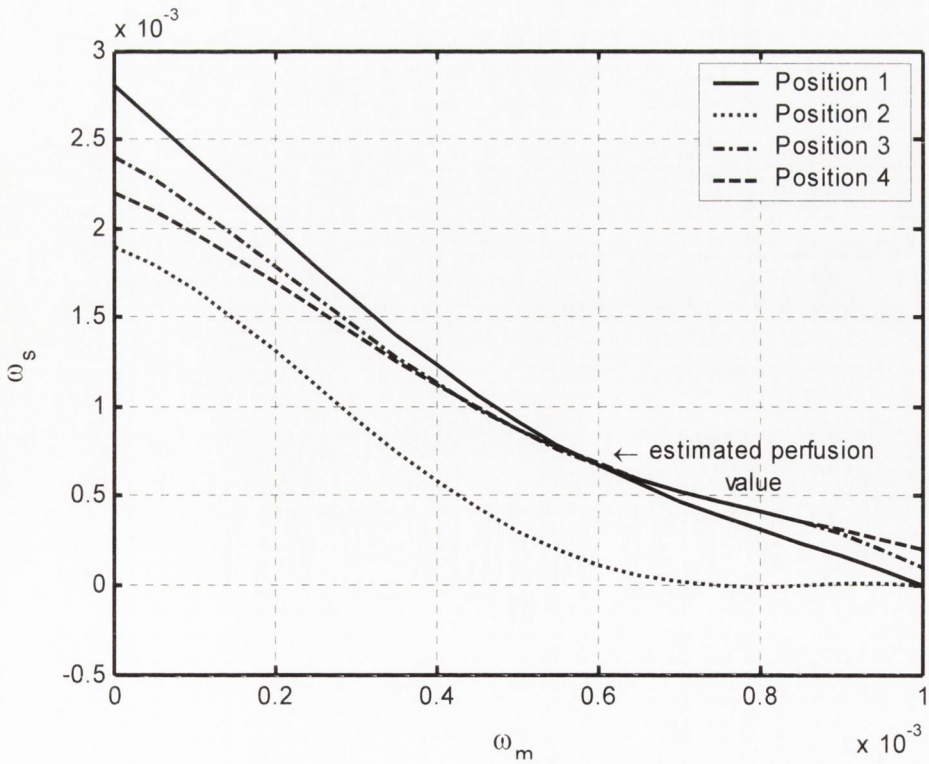
Figure 8-3 PPV curves for Test 1

139
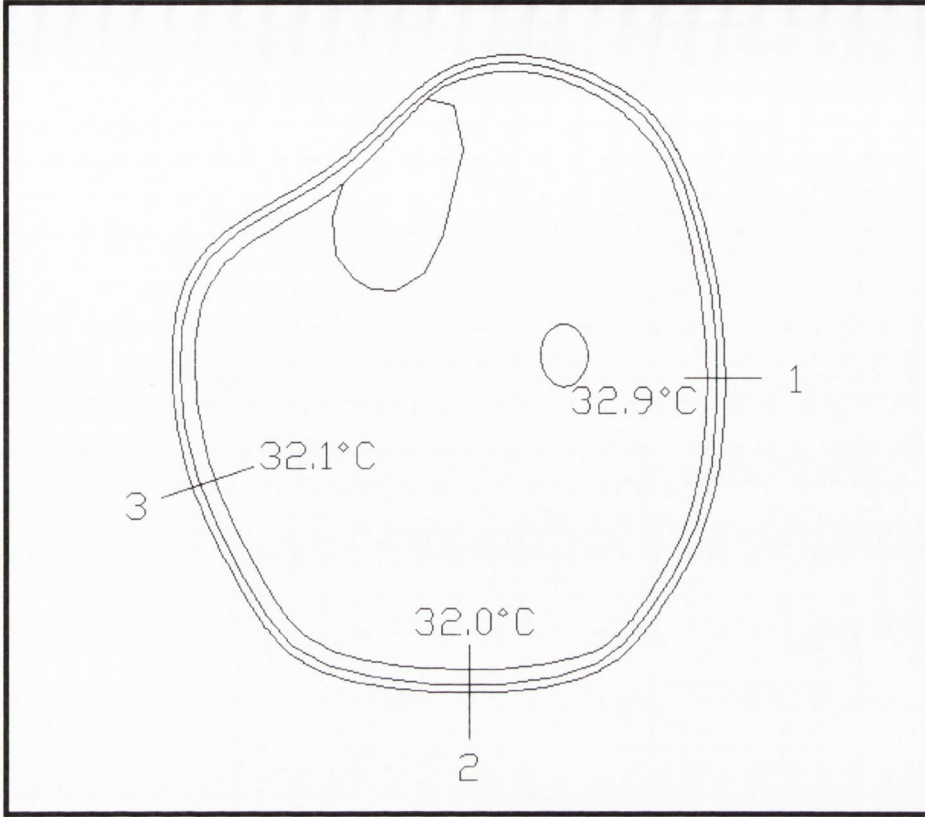
Test 2

Figure 8-4 MRI 15 showing sensor locations and corresponding temperatures for Test 2 (T_{amb}=23.5°C)
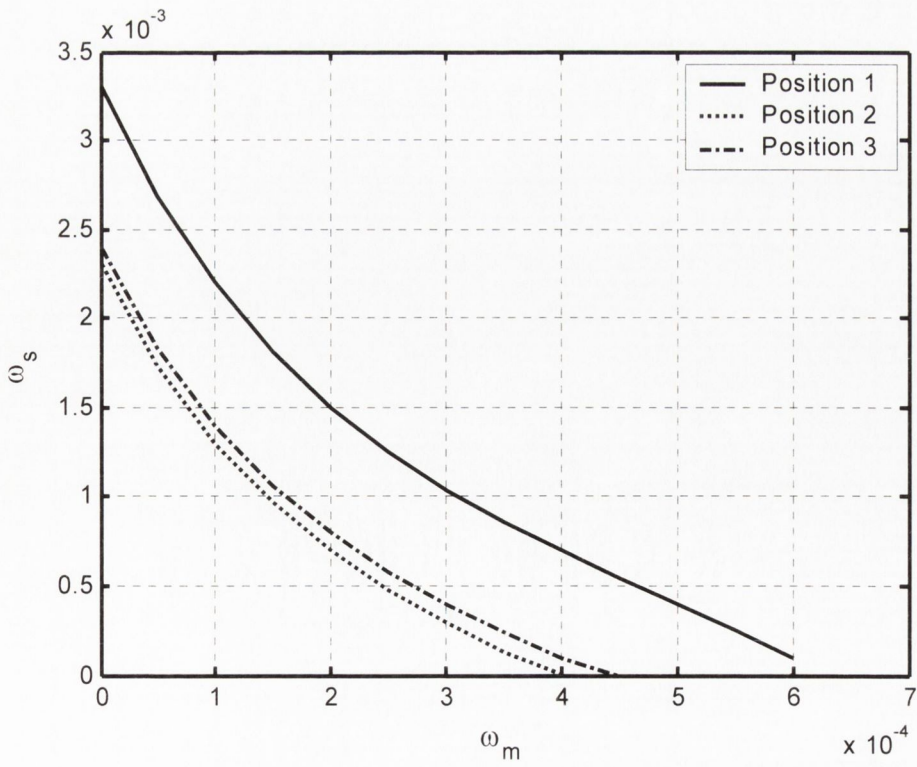
Figure 8-5 PPV curves for Test 2

Test 3
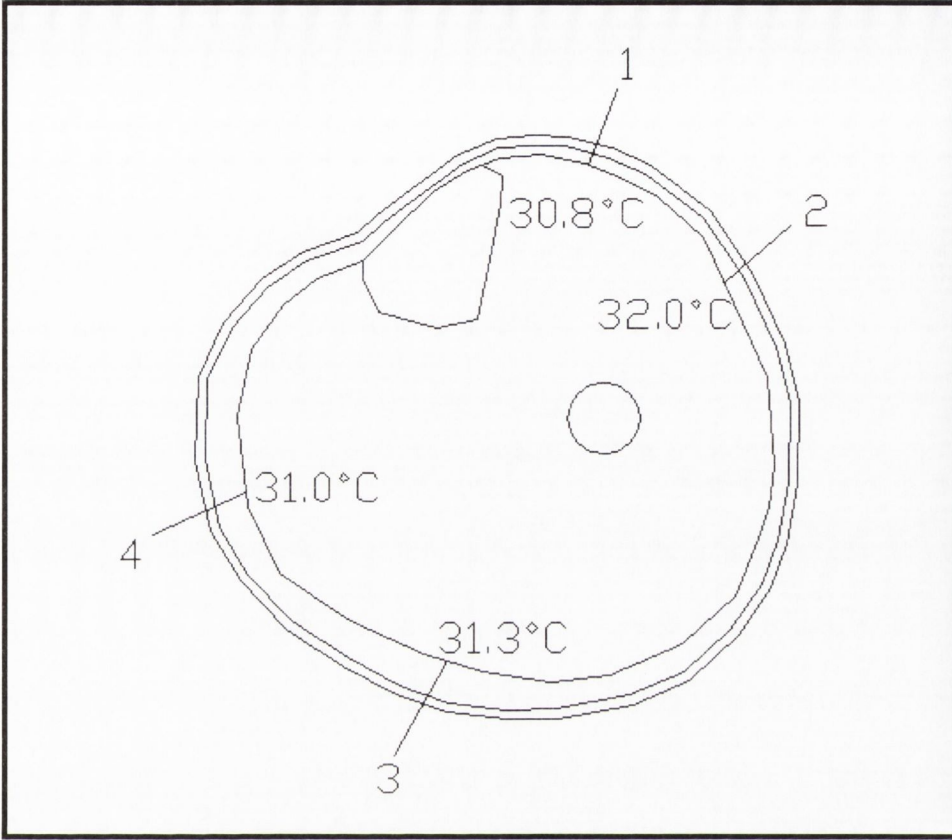
Figure 8-6 MRI 22 showing sensor locations and corresponding temperatures for Test 3 (T_{amb}=24.0°C)
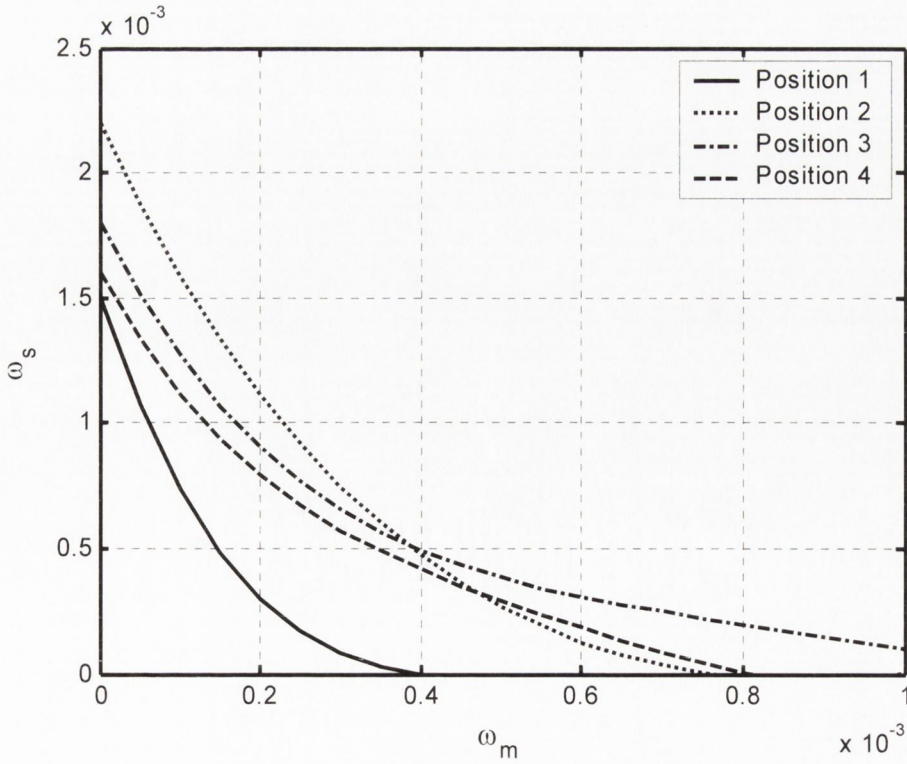
Figure 8-7 PPV curves for Test 3

Test 4
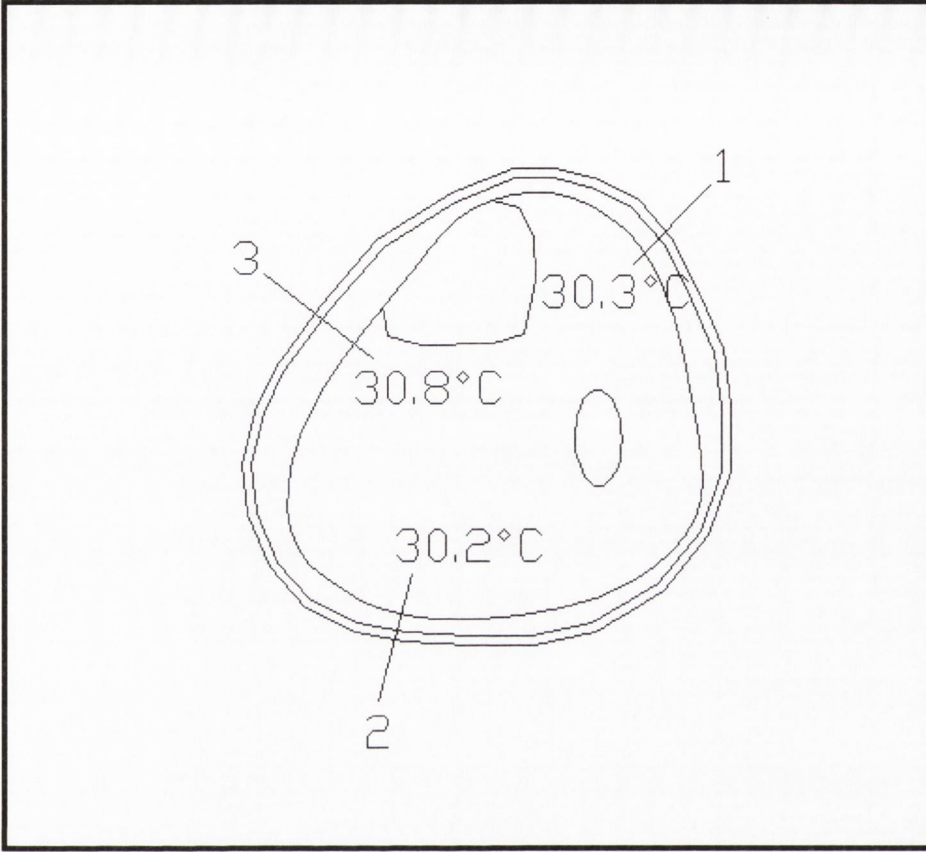
Figure 8-8 MRI 16 showing sensor locations and corresponding temperatures for Test 4 (T_{amb}=23.1°C)
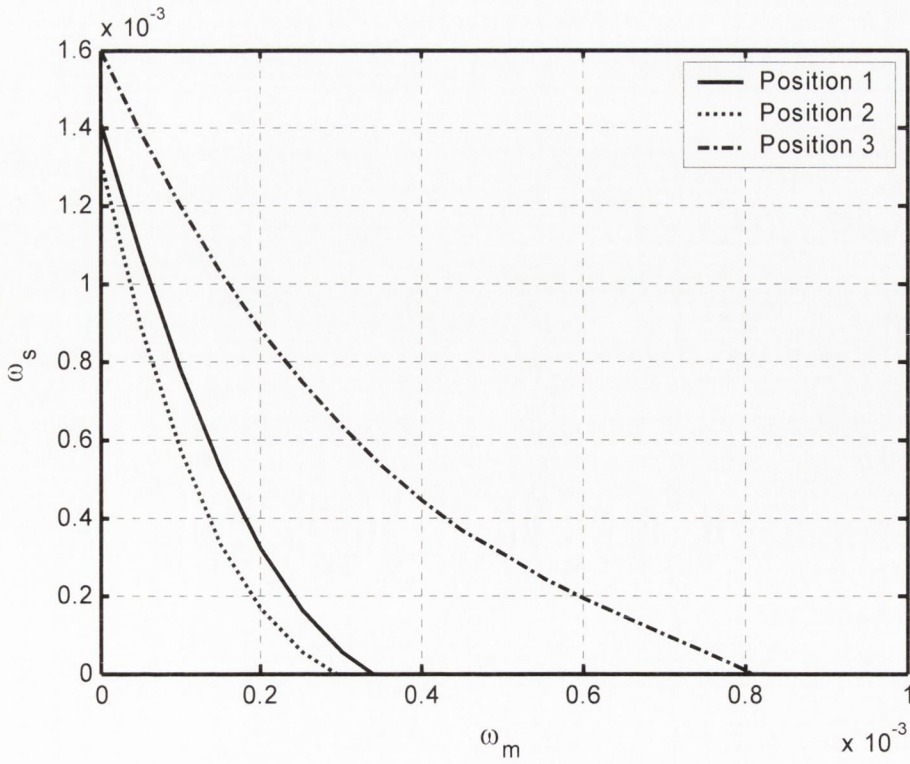
Figure 8-9 PPV curves for Test 4

Analysis of results

A brief overview of the results reveals that Tests 1 and 3 have some curves that intersect and some that do not, while Tests 2 and 4 have curves that are roughly parallel with no intersections. A closer examination of each test yields further information.

Test 1 exhibits the best set of results with three of the four PPV curves intersecting at roughly the same point (ω_m=0.00056/s, ω_s=0.00073/s). However, the PPV curve for position two does not intersect with any of the other curves. This position has the lowest temperature reading, which the model accounts for by assigning it a lower PPV curve.

In Test 2, the PPV curves do not intersect and so give no information on a possible specific perfusion value. However the curves are clustered reasonably closely together which shows that there is a reasonable agreement about the possible perfusion values. This is discussed further in Section 8.4.

Test 3 is taken at a cross section lower down the leg. Unlike MRI 15 this cross section exhibits a significant variation in the thickness of the fat layer between positions one and two and positions three and four. This variation in fat tissue thickness can be correlated to the slope of the PPV curves. At positions three and four the fatty layer is thicker and so presents a greater resistance to conductive heat transfer than the leaner regions. Therefore as the skin perfusion decreases and more heat must be supplied by the muscle perfusion to maintain the skin temperature, the muscle perfusion must increase more rapidly than for a leaner region. This means PPV curves at fatty regions have gentler slopes than curves at leaner regions.

Test 4 also show the effect of a variation in fat tissue thickness as the PPV curve from the fattier region at position three has a more gentle slope. Therefore, for the curves to intersect in this case the value of skin perfusion for position three at a zero muscle perfusion value would have to be lower than for the other two positions, but as it is not the lines cannot intersect.

The four tests show that the results do not all intersect at a common point as hoped. This lack of correlation could be caused by a number of factors:

1. Misrepresentation of geometry. This is assumed not to be significant as the MRI scans of the test subject were of good quality

2. Experimental error. The experimental technique was felt to be robust enough to ensure accurate results. There is an uncertainty associated with the measurement of temperature and convective heat transfer coefficient. A sensitivity analysis was carried out to gauge the magnitude of this error for which the findings are reported in section 8.4.

3. A final cause for the lack of correlation could be that one of the fundamental assumptions is incorrect. This is discussed in Chapter 9.

8.4 SENSITIVITY ANALYSIS

Figure 8-10 shows the change in the PPV curve for an error in temperature reading of +/-0.1°C, which corresponds to the precision uncertainty of the thermistors. A small error in temperature is shown to lead to a relatively larger error in the PPV curve, particularly at higher muscle perfusion values. However, the magnitude of the error cannot account for the major discrepancy between some of the PPV curves.
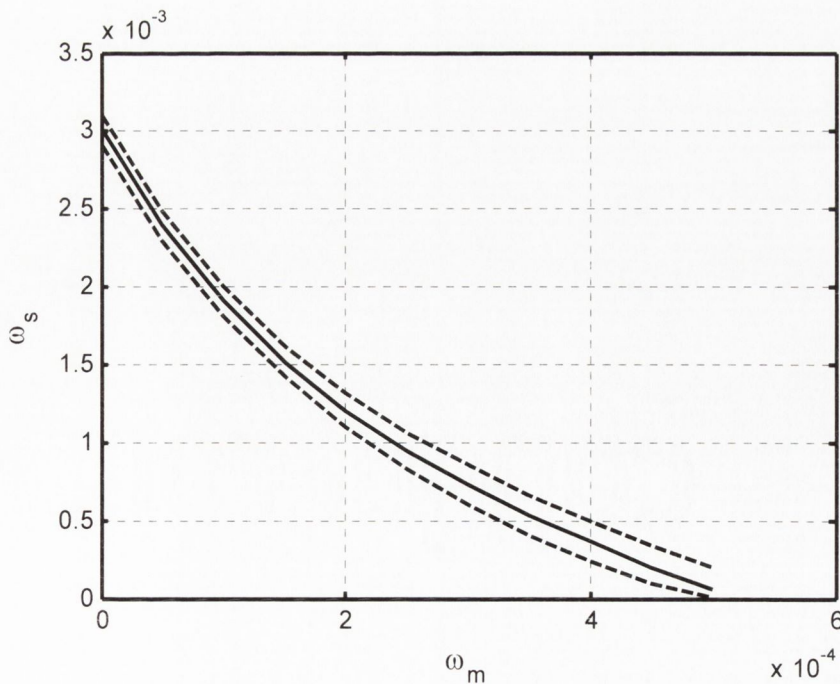
Figure 8-10 Effect of an error of +/- 0.1°C from temperature reading on the PPV curve

8.5   SUMMARY

The work in this chapter describes the development of a new perfusion measurement technique using only steady state measurements based on the PPV concept. It seeks to allow measurement of perfusion by taking advantage of different PPV responses at different circumferential locations around the limb. In order to conclude that the technique works, the curves would have to intersect consistently relatively closely together. This is clearly not the case. The fundamental issue arising out of this is that if the geometry, experimental technique and experimental uncertainty are judged not to be capable of causing the divergence in the results, then one of the more fundamental assumptions of the analysis must be incorrect. This possibility will be discussed in Chapter 9.

9 DISCUSSION

This chapter will discuss the findings reported in previous chapters on both the forced convection approach and the newly developed steady state measurement approach. It will also suggest a method of improving the sensitivity of the forced convection approach through the application of a constant cooling load rather than a constant convective heat transfer coefficient. The relationship between global and specific perfusion values is discussed, the derived perfusion levels are examined to determine whether they lie within expected ranges and finally the results from the various validation tests are considered.

9.1 PRELIMINARY INVESTIGATION OF FORCED CONVECTION APPROACH

Initially, this research focused on replicating and subsequently improving on that of previous researchers in the forced convection area. Thus, this investigation incorporates a number of refinements, such as reduction of contact resistance from previous studies, inclusion of time varying properties in the model and careful estimation of parameters such as free stream temperature. These refinements provide a systematic and robust test procedure. When calibrated the thermocouples and thermistors, in particular, exhibited a low level of uncertainty although there is a higher uncertainty associated with the heat flux sensor. This leads to an uncertainty in the calculation of the convective heat transfer coefficient; however this uncertainty does not pose problems for the forced convection testing. The most important result from the initial testing of the forced convection approach reported in Chapter 6 was that the approach was shown to be capable of detecting shifts in blood perfusion induced by a variation in ambient temperature. Even though there were found subsequently to be a number of issues with the method at this early stage of its development, the finding is still valid as the errors affect only the absolute accuracy of the measurements rather than the relative comparison. The first issue identified is associated with the initial cooling of the skin on placement of the probe, which will be similar for each test and so should not cause any major error in terms of relative changes. At this time there was no separation between skin and muscle perfusion and so both tests used a global perfusion measurement, which again should be acceptable

for examination of relative values. The preparatory work carried out in Chapter 6 laid the foundation for the progress made in both modelling and experimentation as described in Chapters 7 and 8.

9.2 NEW DEVELOPMENTS IN FORCED CONVECTION APPROACH

Chapter 7 marks the divergence between this and previous studies in this area. This divergence, and ultimately the critical development of the Possible Perfusion Values (PPV) curve, came about through the questioning of a number of the experimental procedures and numerical assumptions used in Chapter 6, namely the disruption the plate causes to the initial temperature profile of the skin and the accuracy of such a simplified physiologically un-realistic model. These developments culminated in the implementation of one of the most comprehensive and physiologically realistic numerical models developed in this area. The key to its accuracy is the incorporation of actual MRI scans of the test subject's arm, which allows more accurate representation of the distribution of the various tissues than previously possible. The developments made with this new modelling procedure required a more rigorous approach for dealing with the differing perfusion levels in the skin and muscle tissues; hence the development of the concept of Possible Perfusion Values (PPV) curves. A PPV curve describes all the possible allowable combinations of skin and muscle perfusion at a certain location on the skin, that can generate a specific skin temperature under a given set of ambient conditions as measured at a steady state. This led to a new procedure for perfusion estimation using the forced convection approach, whereby the actual relative values of perfusion occurring in the tissue are estimated from whichever combination of values from the PPV curve gives the best fit to the experimental temperature on cooling of the skin. When applied in experimental testing, however, it demonstrated a lack of sensitivity. An optimisation procedure then led to the main finding of this chapter, which is that while such an approach is theoretically possible, in practice it is not possible to generate a temperature difference which is large enough to overcome the experimental error, even under optimum test conditions.

9.3 Future developments using a constant cooling approach

However, while the forced convection test may not be feasible using a constant value of convective heat transfer coefficient, a numerical investigation showed that a test conducted with a constant cooling load would have almost double the sensitivity. This is because as a constant convective heat transfer coefficient test progresses, the temperature of the tissue decreases and so the level of cooling decreases. A test carried out at constant cooling more clearly shows the added heat generated by increased perfusion than one where cooling decreases with time. However, to implement this approach is more technically challenging. To achieve it with a compressed air cooling system one would have to vary the flow rate, presumably using a computer controlled system. A further challenge is that it would be difficult to ensure that the cooling is constant over the entire cooling area. However initial indications are that this technique could provide great enough sensitivity to allow estimation of perfusion using the procedure outlined for the forced convection approach.

9.4 Steady State perfusion estimation

Chapter 8 outlined a new perfusion estimation technique based on steady state measurements alone. This came from an initial steady state study on finger perfusion that was shown to compare well with results from a finger plethysmograph. It worked on the principle that two perfusion curves from two different circumferential locations on the limb having different slopes should intersect and that intersection point should describe the relative values of skin and muscle perfusion. A difference in the slope of a PPV curve can be due to differences in the thicknesses of the underlying fatty tissue layer, or in the surface profile at the measurement location. This approach has the advantage of greatly simplifying the experimental set-up and numerical model. Results from a number of tests showed both intersecting but also non-intersecting curves. If the resulting curves from the PPV graph are parallel and close together they can be said to have the same perfusion response and so cannot be used to infer perfusion values. Any small difference in displacement can be explained by the combined experimental uncertainties of the method. However the results from the testing also showed that some of the curves were displaced significantly from the

other curves. It is more difficult to infer that this is due to experimental error because the calculated uncertainty is too small to explain this divergence. A possible reason for the curves not intersecting may be that the perfusion level around the limb is not constant; this would imply that the technique is providing accurate PPV curves but that it is not capable of inferring which particular combination of skin and muscle perfusions is occurring, as it is based on the assumption that perfusion is constant around the arm.

To test this hypothesis, a laser Doppler probe was used to verify the uniformity of perfusion around the circumference of the arm in the skin tissue. As explained in Chapter 4, laser doppler devices are not capable of measuring absolute levels of skin perfusion. However, using a Post Occlusive Reactive Hyperaemia test on two different circumferential locations at the same height on the leg will show the change in perfusion from a base level on release of the occlusion. If the blood perfusion level is constant one would expect the post-hyperaemic responses to be similar at different locations. Two separate tests were carried out with the sensor attached to two locations; one on the posterior medial and one on the posterior lateral surface of the left leg. The results for both the superficial and deep skin tissues show the hyperaemic response to be greater for the Posterior medial tests. Esan [85] concludes that 'the laser Doppler demonstrates that from the hyperaemic response in both the superficial and deep skin layers, that the skin perfusion is not completely constant around the limb at the same level.' Therefore it seems reasonable to conclude that the main reason the curves in the steady state temperature method do not always intersect is due to a circumferential variation in the perfusion levels. This effect is less significant for the forced convection approach, which is confined to one measurement location.

9.5 AVERAGE LIMB PERFUSION VALUES

It is also interesting to note how average limb perfusion varies with respect to the PPV curve. This is calculated by multiplying the areas of the various tissues (for a 2-D case), with their respective perfusion rates. The sum of these values is then divided by the total area of the limb to give an average limb perfusion value. For instance, when the value of muscle perfusion is zero, the PPV curve shows that the level of skin

perfusion will be high. However, as shown in Figure 9-1, the average limb perfusion level is still low as only a small volume of tissue is perfused, albeit at a high level.

It may be theoretically possible to use a measurement of average limb perfusion from a plethysmograph, to estimate the skin and muscle perfusion values from the PPV curve. For instance, if the average limb perfusion value from the plethysmograph was 0.0003/s then from Figure 9-1 the values of muscle and skin perfusion would be 0.0002/s and 0.0022/s respectively. Further to this, as the slope of the average limb perfusion curve is quite low, it is possible to roughly estimate the range of perfusion values. For example, if the extreme values from the left and right of the PPV curve are deemed to be physiologically unrealistic, the average limb perfusion value can be said to be between 0.0002/s - 0.0006/s. This could be a useful measurement in the diagnosis and treatment of circulatory disorders.
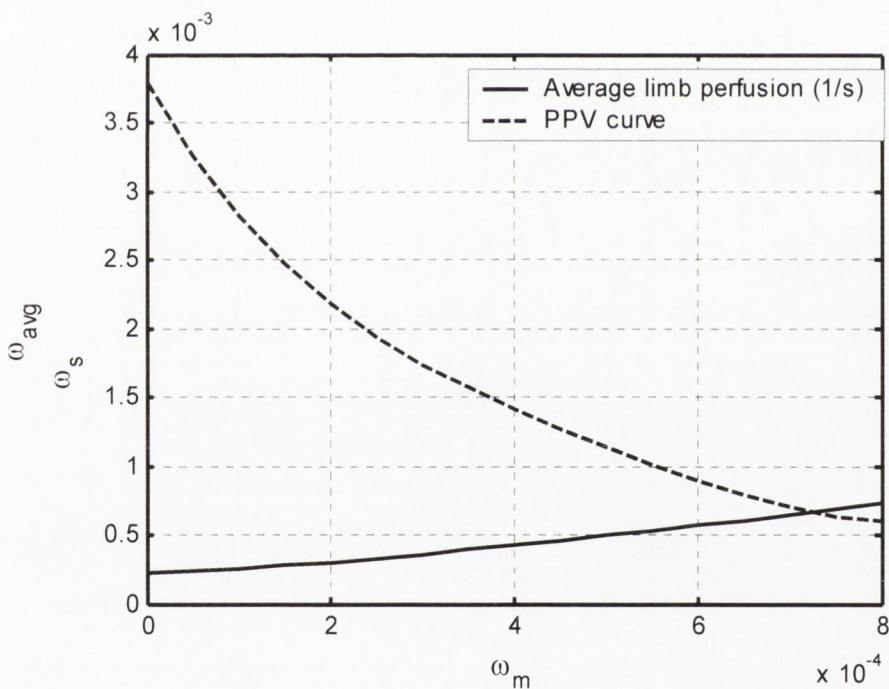
Figure 9-1 Comparison between Average Limb Perfusion (ALP) curve and PPV curve

9.6 GENERAL COMMENTS

It is important to assess whether the perfusion values reported in this study are physiologically realistic. It has been found that the blood perfusion values lie within the range reported in the literature, albeit at the lower end of that range. This is to be

expected, as testing was generally conducted with the candidate at rest in a relatively thermo-neutral environment. In general the skin perfusion values are higher than the muscle perfusion values, which is again a function of the test conditions. To establish if the PPV curves respond as expected to different test conditions a series of tests were carried out with the test subject exercising by doing calf raises at approximately 2/s. A separate series of tests were conducted with the candidate at rest under varying ambient temperatures. Figure 9-2 shows the dramatic increase in muscle perfusion values on the PPV curve when exercising under normal ambient conditions. Stoner et al. [86] note that the total blood flow through the calf increases by a factor of three with exercise, but is not accompanied by any significant increase in calf skin perfusion. This is consistent with results shown in Figure 9-2. Figure 9-3 shows the shift in the PPV curves which corresponds to a drop in perfusion as the ambient temperature drops for a series of tests conducted in a temperature controlled room.
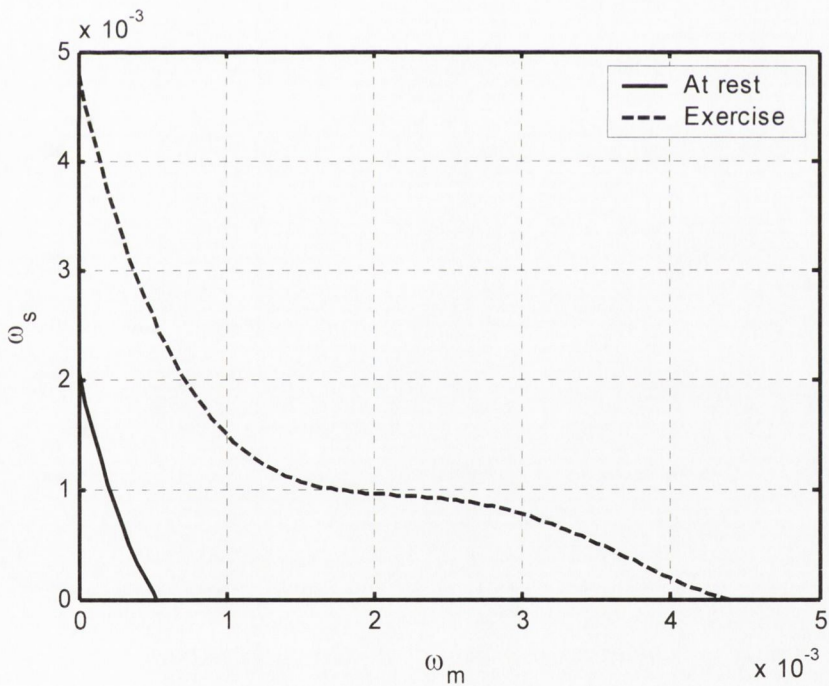
Figure 9-2 Comparison of effect of exercise and rest on PPV under constant ambient conditions
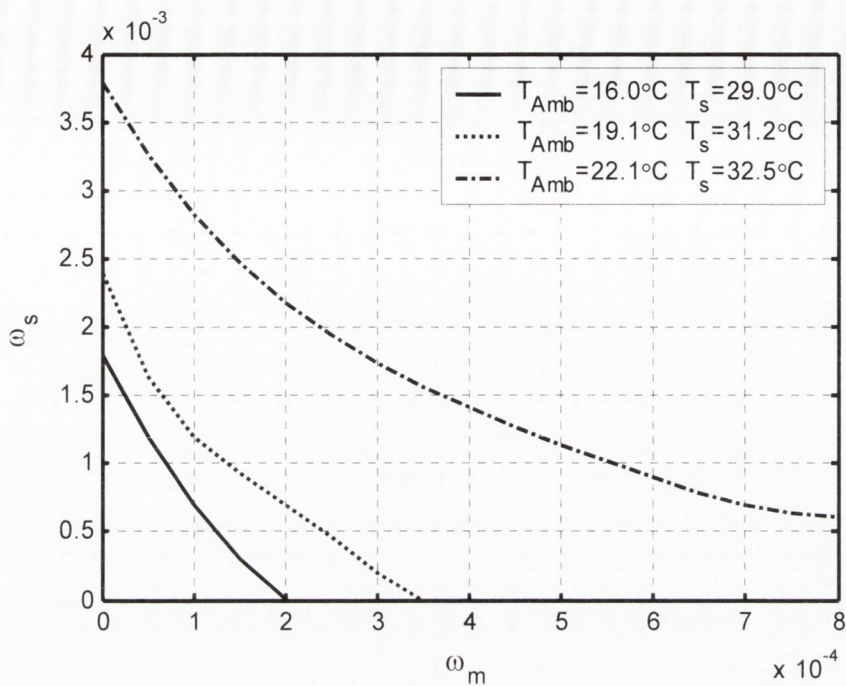
Figure 9-3 PPV curves for various ambient conditions

These results, together with the successful finger perfusion comparison with the plethysmograph, the validation tests carried out in Chapter 6 and the agreement between the forced convection numerical and experimental results reported in Chapter 7 confirm the validity of the numerical model and test methodology outlined here.

The following chapter will draw conclusions from this research.

10 CONCLUSIONS

This study set out to use existing bio-heat transfer theory to investigate the feasibility of measuring blood perfusion in the extremities using non-invasive thermal methods at the skin surface. Development of such a system would be of great benefit to medical practitioners for use with a wide range of medical conditions as at present there is no cheap and accurate method of measuring blood perfusion. There are currently a number of researchers investigating various thermal techniques requiring either heating or cooling of a particular skin region. A literature review of the existing techniques identified the Forced Convection Approach as the most promising. Work began using the current state of the art as a basis from which significant developments were made.

A number of conclusions can be drawn from the research carried out:

- Initial work on the original Forced Convection Approach was encouraging, but it identified a number of practical difficulties with the experimental procedure and oversimplifications in the numerical model, particularly in how the initial temperature profile was generated.

- A more comprehensive study of the experimental set-up concluded that testing should no longer be conducted using a copper plate and instead the sensors should simply be taped to the skin. It was also found that it is not possible to directly relate perfusion to the decay rate of the experimental temperature readings due to variability in test parameters such as air flow rate.

- A comprehensive study on the numerical assumptions was conducted. This was carried out using both 2-D and 3-D models implemented in FemLab. The models were constructed using actual MRI scans of the test subject's limbs. It showed that the 2-D modelling assumption is generally applicable as the assumption breaks down at times much longer than the standard test runs. Using MRI scans of the test subject's limb, a study on the importance of accurate representation of the geometry and tissue distribution of the limb concluded that it is possible to model on the longitudinal cross section of the limb. Fat thickness can be assessed from external measurements. This has the advantage of not requiring MRI scans of the test location for each test subject

and avoids also the difficulty associated with circumferentially varying perfusion.

- The development of the concept of the Possible Perfusion Values curve during this study is novel and is the only method available that can generate accurate initial temperature distributions. This technique was shown to be theoretically capable of allowing measurement of both skin and muscle perfusion from a single surface measurement when used in conjunction with a forced convection test.

- Tests conducted on a healthy subject using this refined version of the forced convection approach showed poor sensitivity. An optimisation study revealed that, using a constant cooling air flow rate it is not possible to generate a large enough temperature difference to allow accurate estimation of perfusion for this particular candidate under standard ambient conditions.

- However, numerical simulations indicate that this test procedure should be much more sensitive at lower blood perfusion rates as experienced in many of the medical conditions listed in the Introduction. It is also expected that a constant heat flux cooling regime should increase the sensitivity of the technique further.

- A novel method of perfusion measurement based on steady state temperature readings around the limb circumference was proposed but, unfortunately, research identified that skin perfusion varies around the circumference of the limb, so that the proposed method cannot work in its current simple form. However, the possibility is there to develop a method that induces a different PPV response at an alternate longitudinal measurement location on the limb.

- The most significant contribution of this study is the realisation that the PPV methodology is applicable to other thermal techniques (as described in Section 4.1). In fact for any thermal method it is the only way to ensure an accurate initial temperature distribution and to infer the relative values of skin and muscle perfusion.

- This study proposes that future thermal studies use the PPV technique while modelling on the longitudinal cross section of the arm. The study has therefore developed a framework methodology for measuring perfusion that is applicable to any thermal technique.

The problem of measuring perfusion using thermal methods is extremely complex, as with any biomedical problem. In over fifty years since the publication of Pennes' bio-heat equation, a range of developments in bio-heat transfer theory and in particular the advent of numerical techniques have allowed for much improved modelling. This progress has given rise to a number of new measurement techniques. However, to date no research group using any one of a wide range of differing methods has been able to develop a practical perfusion measuring device. Application of the PPV methodology will help greatly in assessing the feasibility of thermal techniques. These findings have contributed to an improved understanding of the relationship between skin surface thermal measurements and tissue perfusion, which may eventually lead to the development of a practical tool for measuring blood perfusion.

10.1 FUTURE WORK

There were two main difficulties in this study. The first was that it is impossible to control the physiological variability to such an extent that absolute repeatability could be ensured from test to test and day to day. The second obstacle was the unavailability of a technique against which to quantitatively validate the measurement. Therefore to learn more about the fundamental underlying heat transfer problem and its ability to accurately measure perfusion levels in a repeatable manner it is logical to simplify the problem by first testing on a mock-up of the limb. A number of studies such as that by Eriksson et al. [87], have utilised such a model. A simple comparison can be made between the derived and the actual controlled flow rate into the arm in order to clarify the feasibility of the method in isolation without also trying to account for any physiological variation. If results from this were positive then testing could return to the human limbs.

In this regard, further work should involve the following:

1. Implementation and testing of a system using a constant rate of cooling to verify the greater sensitivity of this proposed method.
2. Assessment of the usefulness of an average limb perfusion measurement as an indicator of the severity of circulatory disorders such as Peripheral Vascular Disease (PVD).

3. Use of the laser doppler probe to conduct a comprehensive assessment of the variation of skin blood perfusion at various measurement locations on the limbs. If two or three measurement locations can be found that have similar perfusion levels then the PPV measurement technique should work more consistently. Also this could be used to verify the assumption that localised cooling of a region of skin does not alter the level of perfusion.

REFERENCES

[1]   Li H. J., Zhang X. X., Yi Y. F., *Measurement of blood perfusion using the temperature response to constant surface flux heating*, International Journal of Thermophysics, Vol. 23, No.6, pp1631-1644, Nov. 2002.

[2]   Arkin H., Xu L.X., Holmes K.R., *Recent developments in modelling heat transfer in blood perfused tissues*, IEEE Transactions on Biomedical Engineering, Vol. 41, No. 2, 1994.

[3]   Henriques F.C., Moritz A.R., *Studies of thermal injury, I. The Conduction of heat to and through skin and the temperatures attained therein. A theoretical and experimental investigation*, American Journal of Pathology, Vol. 23, pp431-549, 1947.

[4]   Diller K.R., Hayes I.J., *A finite element model of burn injury in blood-perfused skin*, ASME Journal of Biomechanical Engineering, Vol. 105, pp300-307, 1983.

[5]   Dai W., Yu H., Nassar R., *A fourth-order compact finite-difference scheme for solving a 1-D Pennes' bio-heat transfer equation in a triple layered skin structure*, Numerical Heat Transfer, Part B, Vol. 46, pp447-461, 2004.

[6]   Cooper T. E., Trezek G.J., *Analytical prediction of the temperature field emanating from a cryogenic surgical probe*, Cryobiology, Vol. 7, pp79-93, 1970.

[7]   Budman H., Shitzer A., Del Giudice S., *Investigation of temperature field around embedded cryoprobes*, ASME Journal of Biomechanical Engineering, Vol. 108, pp42-48, 1986.

[8]   Olsen R. W., Hayes L. J., Wissler E. H., Nikaidoh H., Eberhart R.C., *Influence of extra-cerebral temperature distribution during induction of deep hypothermia with subsequent circulatory arrest*, ASME 1984 Advances in Bioengineering, pp29, 1984.

[9]   Eberhart R.C., Shitzer A., Hernandei E.J., *Thermal Dilution Methods. Estimation of Tissue Blood Flow and Metabolism*, Annals of the New York Academy of Sciences, Vol. 335, pp107-132, 1980.

[10]   Martini F.H., *Fundamentals of anatomy and physiology*, Prentice Hall, 2001, pp149.

[11]   Berne R. M., Levy M. N., *Principles of Physiology*, Mosby, 2000.

[12] Arts M.G.J., *A mathematical model of the dynamics of the left ventricle and the coronary circulation*, Ph.D. Thesis. R.U. Limburg, Maastrich, 1978.

[13] Wilmore J.H., Costill D.L., *Physiology of sport and exercise*, Champaign Leeds, pp549, 1994.

[14] Herrman E.C., Knapp C.F., Donofrio J.C., Salcido R., *Skin perfusion responses to surface pressure-induced ischemia: Implication for the developing pressure ulcer*, Journal of Rehabilitation Research and Development, Vol. 36, No. 2, pp109-120, 1999.

[15] Pitman R. M., Lamb J.F., Ingram C.G., Johnston I.A., *Essentials of physiology*, Blackwell Scientific Publications, 1991.

[16] Doone B., *Private communication*, Dept. of Physiology Trinity College Dublin, 2003.

[17] Luckwell R.G., *Private communication*, Dept. of Physiology Trinity College Dublin, 2003.

[18] Humphries J. J., *Computational heat transfer modelling in the human leg*, Final year dissertation, Department of Mech. and Man. Engineering, Trinity College Dublin, 2005.

[19] Pennes, H. H., *Analysis of Tissue and Arterial Blood Temperatures in the Resting Human Forearm*, Journal of Applied Physiology, Vol. 1, No. 2, pp93-122, 1948.

[20] Sejrsen P., Dan. Med. Bull. 18 Supple. 3 1-38.

[21] Holman J.P., *Heat Transfer*, McGraw Hill, 9th Ed., 2002.

[22] Barcroft H., Edholm O.G.E, *Temperature and blood flow in the human forearm*, Journal Physiology, pp104-366, 1946.

[23] Wissler E.H., *Pennes' 1948 paper revisited*, American Physiology Society, Vol.85, pp35-41, 1998.

[24] Chen, M. M., Holmes, K. K., *Microvascular contributions to tissue heat transfer*, Ann. N.Y. Acad. Sci., Vol. 335, pp137–150, 1980.

[25] Wulff W., *The energy conservation equation for living tissue*, IEEE Trans. Biomed. Eng., BME-21, pp494-495, 1974.

[26] Klinger H.G., *Heat Transfer in Perfused Biological Tissue – I: General Theory*, Bull. Math. Biol., Vol. 36, No. 4, pp403-415, 1974.

[27] Bazett H.C., McGlone B., Temperature *Gradients in the Tissue in Man*, Am. J. Physiol., Vol. 82 pp415-425, 1927.

[28] Mitchell, J.W. and Myers, G.E., *An analytical model of the countercurrent heat exchange phenomena*, Biophys. Journal, Vol. 8, pp897-911, 1968.

[29] Keller, K.H. and Seiler, L., *An analysis of peripheral heat transfer in man*, J. Appl. Physiol., Vol. 30, No.5 pp779-786, 1971.

[30] Xu L.X., *The Evaluation of heat transfer equation in the pig renal cortex*, PhD dissertation University of Illinois of Urbana-Champaign, 1991.

[31] Xu L.X., Chen M.M., Holmes K.R., Arkin H., *The evaluation of the Pennes, the Chen-Holmes, the Weinbaum-Jiji Bio-heat transfer models in the pig kidney cortex*, ASME WAM, HDT-Vol. 189, pp15-21, 1991.

[32] Wren J., *On Medical Thermal Treatment*, Linkoping Studies in Science and Technology Dissertation No.763, 2002.

[33] Roemer R.B., Dutton A.W., *A generic tissue convective energy balance equation: Part 1 – theory and derivation*, Journal of Biomechanical Engineering, Vol. 120, pp395-404, 1998.

[34] Weinbaum S., and Jiji, L. M., *A new simplified bio-heat equation for the effect of blood flow on local average tissue temperature*, ASME J. Biomech. Eng., Vol. 107, pp131–139, 1985.

[35] Weinbaum S., Xu, L. X., Zhu, L., Ekpene, A., *A new fundamental bio-heat equation for muscle tissue: Part I - Blood Perfusion Term*, ASME J. Biomech. Eng., Vol. 119, pp278–288, 1997.

[36] Brinck H., Werner J., *Efficiency function: improvement of classical bio-heat approach*, Journal of Applied Physiology, Vol. 77, Issue 4, pp1617-1622, 1994.

[37] Brinck H., Werner J., *Estimation of the thermal effect of blood flow in a branching countercurrent network using a three-dimensional vascular model,"* ASME J. Biomech. Eng., Vol. 116, pp324–330, 1994.

[38] Baish J.W., *Formulation of a statistical model of heat transfer in perfused tissue*, Journal of Biomechanical Engineering, Vol. 116, pp521-527, 1994.

[39] Van Leeuwen G.M.J., Kotte A.N.T.J., Raaymakers B.W., Lagendijk J.J.W., *Temperature simulations in tissue with a realistic computer generated vessel network*, Phys. Med. Biol. Vol.45, pp1035-1049, 2000.

[40] Gottlieb M.E., *"Modelling blood vessels: A deterministic method with fractal structure based on physiological rules"*, Proceedings of the Twelfth international conference of the IEEE EMBS, Vol. 12, pp1386-1387, 1990.

[41] Zhu L., Xu L.X., Qinghong H., Weinbaum S., *A new fundamental bio-heat equation for muscle tissue – Part II: Temperature of SAV vessels,* Journal of Biomechanical Engineering, Vol. 124, pp121-132, 2002.

[42] Myrhage, R., Eriksson E., *Arrangement of the vascular bed in different types of skeletal muscles,* Progress in Applied Microcirculation, Vol. 5, pp1–14, 1983.

[43] He Q., Zhu L., Weinbaum S., *Effect of blood flow on thermal equilibration and venous rewarming,* Annals of Biomedical Engineering, Vol.31, pp659-666, 2003.

[44] Stolwijk J.K., Hardy J.D., *Temperature regulation in man – A theoretical study,* Pflugers Archive ges. Physiol., Vol. 291, pp129-162, 1966.

[45] Ferreira M.S., Yanagihara J.I., *Development of the passive system of a human thermal model,* ASME Bioengineering conference, BED-Vol. 50, pp 757-758, 2001.

[46] Huizenga C., Hui Z., Arens E., *A model of human physiology and comfort for assessing complex thermal environments,* Building and Environment, Vol. 36, pp691-699, 2001.

[47] Hegarty R., *Mathematical modelling of the human thermoregulatory system under the influence of general anaesthesia,* Dissertation for M. Eng. Sc., Department of Mechanical Engineering, NUIG, 2004.

[48] Van Leeuwen G.M.J., Janssen F.E.M., Van Marken-Lichtenbelt W.D., Mol B.A.J., Steenhoven A.A, *Modeling patient temperature for improved thermal management during surgery,* Proceedings of the ASME ZSIS International Thermal Science Seminar II, 2004.

[49] Deng Z. S., Liu J., *Blood perfusion-based model for characterizing the temperature fluctuation in living tissues,* Physica A 300, pp521-530, 2001.

[50] Craciunescu O. I., Clegg S. T., *Pulsatile blood flow effects on temperature distribution and heat transfer in rigid vessels,* Journal of Biomechanical Engineering, Vol. 123, pp500-505, 2001.

[51] Barbour R.L., Blattman S., Panetta T., *Dynamic optical tomography: A new approach for investigating tissue-vascular coupling in large tissue structures,* Optical Society of America, 1999.

[52] Cui Z.F., Barbenel J.C., *The influence of model parameter values on the prediction of surface temperature: I. Resting and surface insulation,* Phys. Med. Biol., Vol. 35, No. 12, pp1638-1697, 1990.

[53]   Rai K.N., Rai S.K., *Effect of metabolic heat generation and blood perfusion on the heat transfer in the tissues with a blood vessel*, Heat and Mass Transfer, Vol. 35, pp75-79, 1999.

[54]   Stolwijk J.A., Hardy J.D., *Partition calorimetric studies of responses of man to thermal transients*, Journal of Applied Physiology, pp967-977, 1966.

[55]   Fiala D., *Dynamic simulation of human heat transfer and thermal comfort, Thesis*, De Montfort University, Leicester.

[56]   Draper J.W., Boag J.W., *Skin temperature distributions over veins and tumours*, Phys. Med. Biol., Vol. 16, No. 4, pp 645-654, 1971.

[57]   Wilson S.B., Spence V.A., *A tissue heat transfer model for relating dynamic skin temperature changes to physiological parameters*, Phys. Med. Biol., Vol. 33, No. 8, pp895-912, 1988.

[58]   Nelson D. A., *Invited editorial on "Pennes 1948 paper revisited"*, Journal of Applied Physiology, Vol. 85, Issue 1, 1998.

[59]   Michener M., Hager J.M., Tarrell, J.P., Veit H., Diller T.E., *Non-invasive blood perfusion measurement with a heat flux microsensor*, Advances in Heat and Mass Transfer in Biotechnology, HTD-Vol. 189/BED-Vol. 18, ASME, pp. 1 – 8, 1991.

[60]   O'Reilly T.B., Diller T.E., T.B., Gonzales T.L., *Development of a non-invasive blood perfusion probe*, Advances in Heat and Mass Transfer in Biotechnology, HTD-Vol. 337/BED-Vol. 34, ASME, pp67-73, 1996.

[61]   Bell C., *Private communication*, Dept. of Physiology Trinity College Dublin, 2003.

[62]   Scott E.P., Robinson P., Diller T.E., *Estimation of blood perfusion using a minimally invasive blood perfusion probe*, Advances in Heat and Mass Transfer in Biotechnology, HTD-Vol. 355/BED-Vol. 37, pp205-212, 1997.

[63]   Scott E.P., Robinson P.S., Diller T.E., *Development of methodologies for the estimation of blood perfusion using a minimally invasive thermal probe*, Meas. Sci. Technol., Vol. 9, pp888-897, 1988.

[64]   Newman W.H., Summit S.C., Balasubramaniam T.A., *In-vitro and in-vivo measurements of low-level tissue blood flow*, Collected papers in heat and mass transfer-1988, ASME-HTD 104, pp51, 1988.

[65]   Balasubramaniam T.A., Bowman H.F., *Thermal conductivity and thermal diffusity of biomaterials: a simultaneous measurement technique*, Journal Biomechanical Engineering, Vol. 99, pp148, 1977.

[66]   Newman W.H., Bowman H.F., Orgill D.P., Klar E., *A Methodology for in vivo measurement of blood flow in small tissue volumes*, Advances in Heat and Mass Transfer in Biotechnology, HTD-Vol.322/BED-Vol. 32, pp99-105, 1995.

[67]   Liu J., Xu L. X., *Boundary information based diagnostics on the thermal states of biological bodies*, International Journal of Heat and Mass Transfer, Vol. 43, pp2827-2839, 2000.

[68]   Rådegran, G., *Limb and skeletal muscle blood flow measurements at rest and during exercise in human subjects*, Proceedings of the Nutrition Society, Vol. 58, pp887-898, 1999.

[69]   Sadaba J.R., Munsch C.M., Parkin A., Burniston M., Maughen J., Conroy J.L., *Harvesting the radial artery for myocardial revascularization significantly reduces tissue perfusion of the hand but does not affect function*, Society of Cardiothoracic Surgeons of Great Britain and Ireland, 1999.

[70]   Holman J.P., *Heat transfer*, McGraw, 2002.

[71]   Incropera F.P., Dewitt D.P., *Introduction to heat transfer*, Wiley 2002.

[72]   Rao S.S., *The finite element method in engineering*, Butterworth Heinemann, 3rd Edition, 1999.

[73]   Deuflhard P., *A modified Newton method for the solution of ill-conditioned systems of nonlinear equations with application to multiple shooting*, Numer. Math. Vol. 22, pp289-315, 1974.

[74]   Vard J.P., *Thermal surface measurements and the developments of methodologies for the estimation of blood perfusion*, BAI Final Year Dissertation, Trinity College Dublin, 2000.

[75]   O'Donovan T.S., *Blood perfusion study*, BAI Final Year Dissertation, Trinity College Dublin, 2000.

[76]   Ashforth-Frost S., Jambunathan K., *Effect of nozzle geometry and semi-confinement on the potential core of a turbulent axisymmetric free jet*, International Communications in Heat and Mass Transfer, Vol. 23 pp. 155-162, 1996.

[77]   *Policy on reporting uncertainties in experimental measurements and results*, ASME Journal of Heat Transfer Policy.

[78] Coleman H.W., Steele W.G., *Experimentation and uncertainty analysis for engineers,* John Wiley & Sons, 2nd Ed., 1999.

[79] Bendat J.S. Piersol A.G., *Random data: Analysis and measurement procedures,* Wiley-Interscience, 3rd Ed., 2000.

[80] Shadlesky P.S., *Stagnation point heat transfer for jet impingement to a plane surface,* AIAA Journal Vol. 21, pp1214-1215, 1983.

[81] Liu T., Sullivan J.P, *Heat transfer and flow structures in an excited circular impinging jet,* International Journal of Heat and Mass Transfer, Vol. 39 pp3695-3706, 1996.

[82] O'Donovan T.S., *Fluctuating heat transfer to an impinging air jet,* Dissertation for PhD, Department of Mech. and Manu. Eng., Trinity College Dublin, 2005.

[83] 'The Visible human' http://www.uchsc.edu/sm/chs/browse/browse_m.html

[84] Kreith F., Bohn M.S., *Principles of Heat Transfer,* 5th Ed., Boston PWS Pub, 1997.

[85] Dr. Esan B., *Private communication,* Art Assist Laboratory, University Hospital Galway, 2005.

[86] Stoner H.B., Barker P., Riding G.S.G., Hazlehurst D.E., Taylor L., Marcuson R.W., *Relationships between skin temperature and perfusion in the arm and leg,* Clinical Physiology, Vol. 11, pp27-40, 1990.

[87] Eriksson R., Persson H.W., Dymling O., Lindstrom K., *A microcirculation phantom for performance testing of blood perfusion measurement equipment,* European Journal of Ultrasound, Vol. 2, pp65-75, 1995.

[88] Fiala D., Lomas K. J., Stohrer M., *A computer model of human thermoregulation for a wide range of environmental conditions: the passive system,* Journal Applied Physiology, Vol. 87, No. 5, pp1957-1972, 1999.

A 1. VARIOUS THERMAL PROPERTIES OF TISSUE

	k (W/m.K)	ρ (kg/m^3)	c (J/kg.K)	q_m (W/m^3)
Bone	0.75 (0.5-2.21)	1,357 (1357-1418)	1,700 (1,700-2094)	0
Muscle	0.42 (0.38-0.54)	1,085 (1010-1085)	3,768 (3,600-3,800)	684 (684-800)
Fat	0.16 (0.16-0.2)	850 (850-940)	2,300 (2,200-2,400)	58 (5-58)
Skin	0.47	1,085 (1,085-1,200)	3,680 (3,680-3,800)	368
Blood		1,069	3,650	

Table A-1 Thermal constant values for various tissue types from Fiala et al. [88] and maximum range of values from literature review

The vast majority of papers reviewed for the study choose to use constant values for the thermal conductivity of the different tissues. This of course is not an accurate representation. The above table shows the values used and the maximum range reported in the literature. All values are assumed to be isotropic.

OMEGA ENGINEERING LIMITED
ONE OMEGA DRIVE
RIVER BEND TECHNOLOGY CENTRE
NORTHBANK
IRLAM
MANCHESTER
M44 5BD
UNITED KINGDOM

Tel: +44 (0)161 777 6611
Fax: +44 (0)161 777 6622

FREEPHONE SALES 0800 488 488 (UK ONLY)

Website:

ISO 9002 REGISTERED COMPANY

NEWPORT®
OMEGA®
omega.co.uk

V.A.T. REG No. GB 620 0439 89   COMPANY REG No. 2564017

Certificate of Calibration

Certificate Number:	M04481		Issue Date:	14-04-2003

Customer.:	University of Dublin			
Description.:	RTD Probe		S. O. No.:	09971
Type No.:	PR-11-2-100-M30-200-1/10DIN		Serial No.:	4

The above instrument has been calibrated. All measurements made were referenced to standards of the laboratory whose values are traceable to UK National Standards. Copies of tests performed are on file at Omega Engineering Limited, Irlam, Manchester and are available upon request.

STD Temperature °C	Recorded Probe Temperature °C	Uncertainty of Measurement °C
0.00	0.05	0.15
49.95	50.10	0.18
99.90	100.05	0.20
200.20	200.20	0.27
300.20	300.1	0.37

Test Conditions	Humidity	35 %
	Temperature	22 °C

Instruments Used:	OE01, OE204, OE52

Calibrated By:	S. C. Roach

Signed: _____

Quality Manager

Ref: RTD.doc

The expanded uncertainties are based on the standard combined uncertainty multiplied by a coverage factor of K=2 providing a confidence probability of 95%

RdF Corporation
23 Elm Avenue
Hudson, New Hampshire 03051-0490
Tele: (603) 882-5195   1-800-445-8367
Fax: (603) 882-6925
E-mail: sensor@rdfcorp.com

ISO 9001 CERTIFIED

Q-116-01 REV A
Q-116-03 REV A
Q-116-13 REV A

MICRO-FOIL™ HEAT FLUX SENSOR

CALIBRATION

RdF PART NO. _____ 27036-3 _____

SERIAL NO. _____ 02052639 _____

HEAT FLUX SENSOR:

Output at 70°F: _____ 1.27 _____ µV/BTU/ ft^2 hr

Polarity: (For heat flow into the surface)
                 White - Positive (+)
                 Red - Negative (–)

Temperature Multiplication Factor: See Attached Graph

*Thermal Resistance: _____ .012 _____ °F/BTU/ ft^2 hr (Typ)   0.009123 °/

*Heat Capacity: _____ .05 _____ BTU/ ft^2 hr/°F (Typ)

Response Time: _____ .400 _____ sec (62% response to step function) (Typ)

THERMOCOUPLE:

ANSI TYPE	MATERIAL	POLARITY	COLOR
T	Copper	Pos. (+)	Blue
	Constantan	Neg. (–)	Red

Output per ANSI MC96.1-1975 and NBS Monograph 125

*Thermal resistance is the temperature difference between the front surface and rear mounting surface of the sensor per unit of heat flow through the sensor. Heat capacity is the amount of heat required to raise the mean temperature of the sensor 1°F. Typical values of these two properties are given primarily to indicate sensor capabilities and are required for heat flow calculations only in very rare instances.

BY: E. Tardy

DATE: 5-10-02

RdF Corporation
Specialists in Temperature Measurement

MICRO-FOIL HEAT FLUX SENSOR
OUTPUT MULTIPLICATION FACTOR VS RECEIVING SURFACE TEMPERATURE (70^{0}F)

RdF
ISO 9001 CERTIFIED
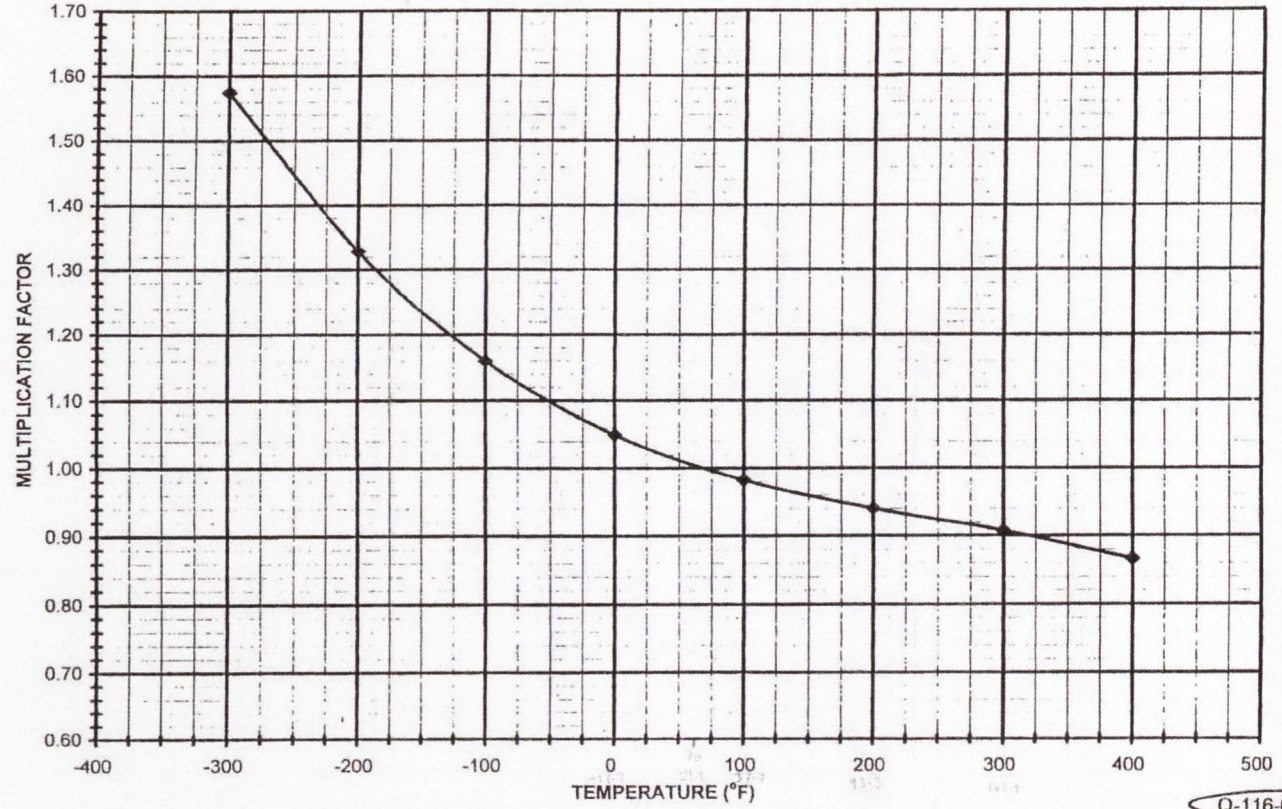
RdF Corporation
23 Elm Avenue
Hudson, NH 03051-0490
1-800-445-8367
INTERNET: sensor@rdfcorp.com

Q-116-03 REV A
Q-116-04 REV A
Q-116-08 REV A
Q-116-11 REV A
Q-116-12 REV A

167

Alicat Scientific
Calibration Data Sheet

Customer:	Digiflow Systems
Sales Order #:	SO103006
Serial No:	14282
Model No:	M-500SLPM-D
Adder Codes:	5M,52T,GAS:Air,RANGE:400SLPM
Process Gas:	Selectable
Calibration Gas:	Air
Range:	400 SLPM
Environmental Cond.	Temperature: 23.8 Humidity: 58%
Calibration Procedure/Rev #:	CAL M, Rev. 4
Calibrated by:	JH
Date:	8/9/2002
Due 1 yr. after receipt by customer:	
Calibrator Used:	CGAUGE-8
Calibrator Due Date:	1/28/2003

Calibration:

Required Accuracy: +/- 1 % of Full Scale = +/- 4.00 SLPM
Calibration Pressure: 50 PSIG

Actual: SLPM	% Full Scale Error	Indicated: SLPM	Primary Output (Vdc)	Secondary Output (Vdc)
0		0.0	0.010	
96	-1.0	100.0	1.250	
'00	0.0	200.0	2.500	
397	-0.8	400.0	5.00	

Notes: Secondary output is 0-5V slaved to temperature (0-80C).

Test equipment used for calibration is NIST traceable.

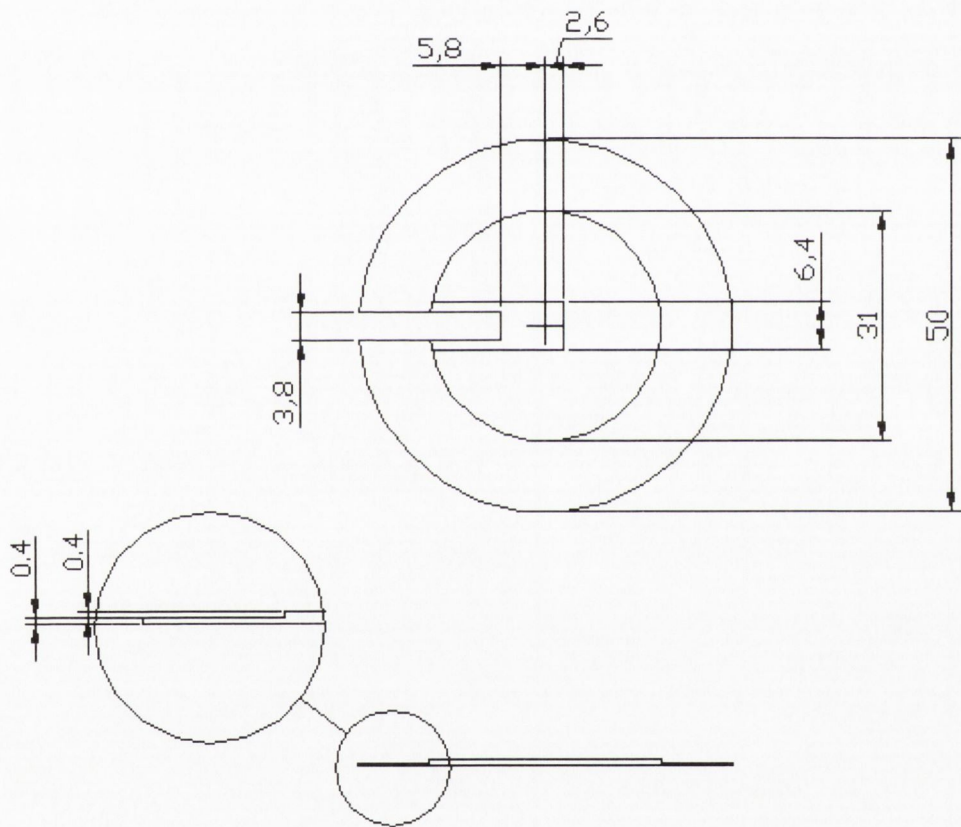CS1 Rev 4 Last Modified 6/26/02

Tech Signature:

QC Signature:

A 5. PROBE DIMENSIONS

All Dimensions in mm

Sectional view
through probe

| Not to scale | Blood Perfusion Probe | Initials : CN |
| | | Date : 4 Feb 01 |

A 6.PLATE DIMENSIONS

All Dimensions in mm

		Initials : CN
Not to scale	Copper base plate	Date ⡈ 4 Feb 01

170